Addis Ababa Institute of Technology

School of Gradute

Center of Energy Technology

Design and Development of low power output Solar Chimney Power Plant

By: ***Ashenafi Tesfaye***

Advisor: ***Dr. Solomon T/Mariam***

Co.Advisor: ***Tewodros walle(MSc)***

A thesis submitted to the school of graduate studies of Addis Ababa university institute of Technology in partial fulfillment for the degree of masters of science in Energy of technology

Addis Ababa, Ethiopia

July,2018

CERTIFICATION

I, the undersigned, certify that I read and hear by recommend for the acceptance by Addis Ababa University institute of Technology, center of Energy Technology a thesis entitled “Design and development of small scale solar chimney power plant.” This certificate used as a partial fulfillment of the requirement for the design of Masters of Science in Energy Technology.

Signature: _____

Date: _____

DECLARATION

I, Ashenafi Tesfaye, I declare that this thesis is the result of my own work and that all source or material used for this thesis have been duly acknowledged. This thesis is submitted in partial fulfillment of the requirement for Master's Degree in Energy Technology at Addis Ababa university and to be made available at the university's Library under the role of the Library. I confidently declare that this thesis has not been submitted to any other institutions anywhere for the award of any academic degree, diploma, or certificate.

Signature: _____

Date: _____

Ashenafi Tesfaye

Addis Ababa Institute of Technology

School of Graduate

Center of Energy Technology

Design and development of small scale solar chimney power plant

By:*Ashenafi Tesfaye*

Approved by board of Examiners

(Advisor)	Signature	Date
(Internal Examiner)	Signature	Date
(External Examiner)	Signature	Date
(Chairman)	Signature	Date

ACKNOWLEDGMENT

First of all I am very grateful to **God Almighty**,this study would not have been possible with out his **blessing** and **graces**.

Then I would like to express my deepest gratitude to my advisor Dr. Solomon T/Mariam**,** who have been supportive in the entire activity and works actively to the completion of this research with a continuous follow up ,guidance and also for sharing his knowledge and experience in thermal and energy concept, this project could not have been possible without his support and care.Then I would like to express my sincere gratitude to Mr. Tewodros Walle(MSc),for his continuous support,guidance and also provides the necessary material and measuring tool,this project could not be possible with out his care.Then I would like to express my appreciation to Mr. Fitsum Salehu (MSc)**,** for his constructive comment while developing the proposal and also provides related article and journals, his care and support made this project possible.I am also grateful to Dr. Kamil Dino, for his valuable comment, suggestion and for providing usefull measuring device.Then I would like to express my sincere appreciation to Mr. Kasay Negash, for his suggestion, valuable comment while developing the actual prototype, his support made this project possible.Last but not least, I would like to pass my deepest gratitude and appreciation for my friends and class mates for their peer review and guidance, without their comment and help this project could not be possible.

ABSTRACT

In order to convert solar energy resource into useful power source different technology has been used so far. SCPP is proposed to be a cost-effective sector for the production of electrical energy in a large scale for the future. In SCPP system solar air collector, chimney tower and turbine are the three essential main components. In this study a detail design and modeling of SCPP is investigated for maximum power output of $30\,kW$. The optimization of geometry for each component is modeled using MATLAB software, Moreover MATLAB is used to predict the performance of large scale electricity generation from the plant. ENERGY 2D software is used to study flow characteristics of air temperature inside the collector. As a result for 30 kW power output the selected optimized dimensions: chimney height, collector diameter, chimney diameter and collector height (distance between the edges of collector and the ground) are estimated to be 15m, 15m, 0.2m and 0.2m respectively. For a fixed chimney diameter and collector height, an increase in the height of the chimney rises the power output upto a certain optimum height, an increases in chimney height beyond the optimum point results an energy loss due to pressure drop along the chimney will start to dominate the energy rise due to the stack effect. The model developed is scaled down to a chimney height of $3\,m$ and collector diameter of $2\,m$ with maxmum power output of 32 W.

In the experiment under investigation the characteristics of the temperature inside the collector throughout the day was studied by varying height of the collector above the ground from 0.17 m upto 0.4 m. The temperature of the fluid is minimum when the collector height is 0.4 m and maximum at 0.17 m. The result obtained for a temperature difference between collector exit and collector inlet from the comparison of experimental and simulated modeled are in a good agreement under a certain condition. So, the implementation of solar chimney power plant as a rural electrification is feasible with the potential to provide electrical energy throughout the day for a desired potential.

Key Words: Solar energy, Solar chimney power plant, Optimum chimney height, Solar collector, natural convection.

A. NOMENCLATURE

Symbol	Description	units
A	Area	m^2
$A_{abs,surf}$	absorber surface area	m^2
Br	thermal expansion coefficient of pebble	--
Cp	specific heat capacity at constant pressure,	$J/kg.K$
C_{ps}	specific heat capacity of storage material	$kJ/kg\ K$
C	Compression temperature ratio	--
D_{chim}	chimney diameter	m
Dr	diffuse radiation	W/m^2
dh	Surface Diameter (hydraulic diameter)	m
D_{pebble}	pebble diameter	m
ε_p	$emmitance\ of\ plate$	--
ε_{abs}	$emissivity\ of\ absorber\ plate$	--
ϵ	pebble bed void	- -
ε_g	$emissivity\ of\ glass$	--
E_{eff}	effectiveness of coefficient	--
F_R	collector heat removal factor	--
F'	collector efficiency factor	--
Gr	global radiation	W/m^2
g	gravitational acceleration,	m/s^2

G	Global Solar irradiation	W/m^2
h_{c1}	Glazing height from ground at entrance	m
h_{c2}	Glazing height from ground at exit	m
$Hchim$	Chimney height,	m
h_w	wind heat transfer coefficient	$W/\ m^2\ k$
h	Enthalpy	J / kg
I	solar radiation	W/m^2
I_b	beam radiation	W/m^2
K	thermal conductivity	$W/m.K$
K_r	$thermal\ diffusivity$	m^2/s
M_s	$mass\ of\ storage\ material$	kg
$\dot{m}$	mass flow rate	kg/s
P_r	$Prandtl\ number$	--
P	pressure	Pascal
P_0	Atmospheric pressure	pascal
P_{output}	Power Output	W
Δp_{tot}	total pressure difference	Pascal
$Q_{usefull}$	useful heat gain	W/m^2
R	ideal gas constant,	$J/kg\ k$
R_d	diffused radiation factor	--
R_b	beam radiation factor	--
r	Cycle pressure ratio	--
T_a	Temperature of the air inside the collector	K
ΔT	Temperature rise between ambient and collector outlet	K

T	absolute temperature	K
$\boldsymbol{T_{pm}}$	mean plate temperature	K
Tp	average temperature of a plate	K
$t_{\,exposed\ to\ sun\ light}$	time pebble is exposed to sun light	$seconds$
$\Delta t_{req.}$	the time required to store heat	$seconds$
Δt_{disch}	the time required to store heat	$seconds$
U_t	over all heat transfer coefficient	$W/m^2\ K$
Vr	radial velocity of air flow	m/s
V	flow velocity,	m/s
V_{bed}	$volume\ of\ bed$	m^3
Δx	$thickness\ of\ the\ absorber\ plate$	m
ρ	density	kg/m^3
ρ_{pebble}	density of pebble	kg/m^3

B. GREEK SYMBOLS

α	absorption coefficient
β	coefficient of volumetric thermal expansion, 1/K
Δp	pressure drop, Pa
ɡ	specific heat ratio
η	Efficiency
μ	dynamic coefficient
f	friction factor
v	viscosity
τ:	transmittance
γ	isentropic constant

C. SUBSCRIPTS

1, 2, 3, 4:	Position along plant (as in Fig. 2.12)
$chim$	chimney
$Coll$	collector
hc1	height of the collector at the entrance
hc2	height of the collector at the exit
gz	glazing
g	ground
abs	absorber
pb	pebble
f	fluid(air)
tur	turbine
Sol	solar
$lift$	Power required to lift air in the chimney

Table of Contents

LIST OF FIGURES

LIST OF TABLES

CHAPTER ONE

1. Introduction

The cause for the serious environmental problem is the increase in global energy consumption and the rapid development of the global economy in both developed and developing countries(Wetstone *et al.*, 2016). Even today, fossil fuels are the primary fuel sources and are still widely used for major electricity generation around the world. According to the report of (Renewable and Agency, 2017),the energy consumption for electricity production worldwide is projected to increase up to 2040 G.C following the historical trend as shown in figure 1.1.

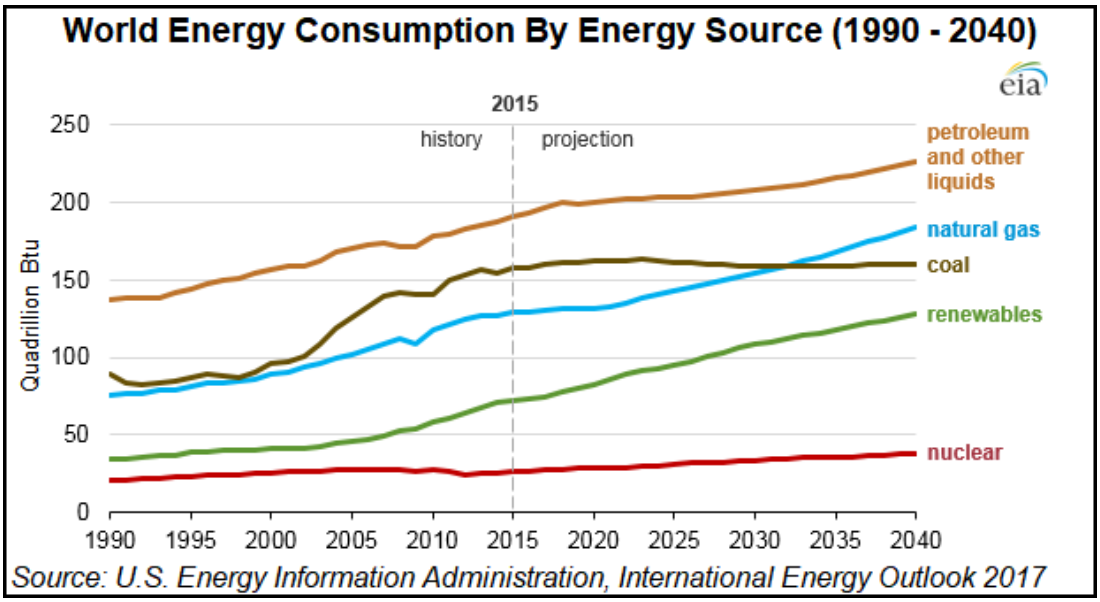

Figure 1-1:worldwide fossil fuel consumption for electricity generation (Wetstone et al., 2016)

Ethiopian is one of the developing countries with higher solar radiation resource(Wetstone *et al.*, 2016).However, Electricity generation is highly dependent on hydropower plant, Table 1.1 presents current and future electricity generation from 2015 G.C to 2030 G.C. Ethiopia's electricity generation composition from a renewable source in 2015 was 93.1% of the system generation capacity. The majority share (92.5%) comes from hydro generation. However, the produced electricity is not covering the entire energy demand of the country as a whole.

Table 1-1: Current and future generation composition of the power system(Renewable, Program and Final, 2012)

Type	Existing			2015			2030		
	MW	GWh	%	MW	GWh	%	MW	GWh	%
Thermal	79.2	563.6	6.90%	79.2	563.6	1.40%	79.2	563.6	0.57%
Non-Renewable Total	**79.2**	**563.6**	**6.90%**	**79.2**	**563.6**	**1.40%**	**79.2**	**563.6**	**0.57%**
Hydro	1,850.6	7574	92.50%	10,641.6	36506	90.80%	22,000.0	86,724.0	87.26%
Wind			0.00%	772.8	1,928.2	4.80%	2,000.0	4,029.6	4.05%
Geothermal	7.3	49	0.60%	77.3	571.0	1.40%	1,000.0	7,446.0	7.49%
Bagass			0.00%	103.5	626.7	1.60%	103.5	626.7	0.63%
Renewable Total	**1,857.9**	**7623**	**93.10%**	**11,595.2**	**39,631.9**	**98.60%**	**25103.5**	**98,826.3**	**99.43%**
Total	**1,937.1**	**8,186.6**	**100.00%**	**11,674.4**	**40,195.5**	**100.00%**	**25,182.7**	**99389.9**	**100.00%**

So, according to the reports('IEA - Report', 2015) and EEPCO harnessing the solar energy resource shown in figure 1.2, could solve the power demand totally as shown below.

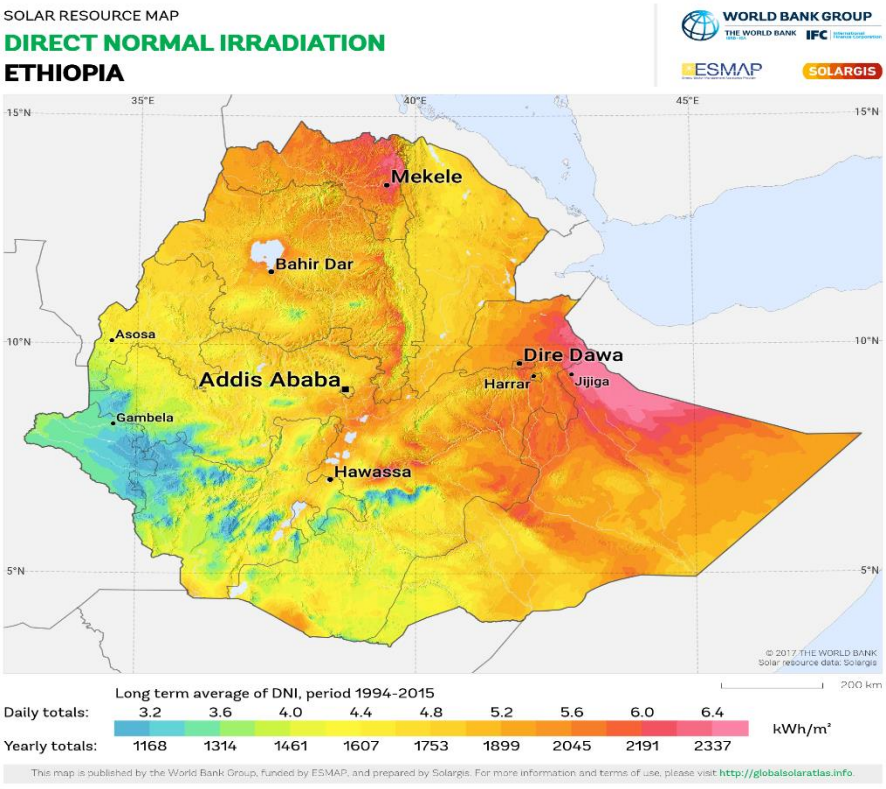

Figure 1-2**:** Ethiopian Solar resource map [(Renewable and Agency, 2017)]

Currently, renewable energy-related technologies are still in its primary stages even though they hold a great promise for the future. This is due to the fact that renewable energy is a cleaner and greener source of energy and is also available in abundance. Even though there are different types of mechanism to convert the sun into useful energy they have some technical and financial problem. On the other hand, another form of solar energy system like solar chimney power plant can provide high megawatt energy production with simple technical method and financial capacity if it is harnessed in a very well manner. The biggest problem with solar energy is that it is only available in the day, but technical advancements through research has made it possible to harness the solar energy at night by storing the solar energy available in the day.

The solar chimney power plant is a naturally driven power generating system. It can convert solar energy first into thermal energy then into kinetic energy finally into electrical energy. It combines the concept of solar air collectors and a central updraft chimney to generate a solar induced convective flow which drives turbines to generate electricity.

In this research small-scale solar chimney power is constructed and studied by aiming the development 30 kW electrical power output for Ethiopian rural area clinic with consideration of covering the main medical device load demand at the clinic. In this research, the potential of solar chimney power plant for different load demand has been studied in a detailed manner. The effective utilization of the solar power is studied by employing energy storage in the system Additionally, in this project the optimum geometrical size of each component is studied in order to get maximum power put from the system. Whenever employing the solar chimney system for the power production their major problem is that they only provide power during the daytime to avoid these placing the energy storage unit at the bottom of the collector roof are investigated carefully.

1.1 Statement of the Problem

Solar chimney power plant is considered to be the most economical renewable energy conversion technologies though their is efficiency is not significant.Lower in efficiency of the system will be the main obstacle on the development of the system as a result it does not attract potential investor and community interest in general.

Most research works have predicted **SCPP** performance by considering a uniform solar insolation through a day, this leads to a prediction of a constant hot air temperature at inlet of the turbine.Some of the literature also concluded their research result by mathematical model and simulation this may leads to overprediction of expacted power output .

Generally, for the development of large scale solar **SCPP**, this study is carried out by initially designing the main component of the system then modeling and simulation and finally to a development of small scale experiment for actual measurement of output.

In this study, the influence of main parameter on the performance of **SCPP** is investigated by combining result obtained from numerical model and experimental model developed.

1.2 Objectives

General objective

The main objective of this research is to design and develop technically feasible low power output solar chimney power plant.

Specific objectives

In order to attain the above main objective, the following specific objective are conducted

I. Designing and modeling of main geometrical components of the system.
II. Evaluate and optimize geometrical size of solar collector and chimney height for a maximum Power output from a system.
III. Manufacturing and testing of the SCPP model to evaluate the predicted power output of the designed system.

1.3 **Scope of the study**

This study focuses on the design and development of low power output solar chimney power plant. It will include the modeling of the solar chimney power plant system integration using the CATIA V5 software. The simulation of the optimum power output at a certain geometrical combination of the main component is simulated using MATLAB and the thermal transient analysis is simulated using ENERGY 2d software. Solar data that are used for the design of the SCPP are taken from Meteoblue and meteorological data so the accuracy of the design will depend on the obtained data. To design the appropriate thermal energy storage system, a different size of pebble is used randomly in order to investigate heat storage capacity but the size of the pebble may not be uniform in all test due to crashing equipment inaccuracy. The prototype is developed using locally available materials so the efficiency of the experiment may reduce due to the material used.National instrument(NI) data logger is used to log the reading of thermocouple, but only two thermocouples are available to read the data so temperature is taken only at collector exit and at mid-point of the collector by assuming the temperature at the collector inlet is equal to the ambient (25℃).Finally, the optimum geometrical combination to obtain maximum power output of 30 kW is selected by considering the temperature variation obtained throughout the day from the reading of simulation and experiment.

1.4 Significance of the Study

The contribution of this study is very significant in terms of introducing electricity generation from solar radiation by air convection. Electricity generation from solar radiation by air convection works when the air beneath the collector exposed to heat then tend to reduce its density and goes up and flows through axial flow turbine to generate shaft power and flow through chimney pipe by bouncy force and create a pressure difference between bottom and top of the chimney. So, this study combines three basic concepts GHG effect, collector effect and chimney effect to create electrical power. This system can generate in MW capacity of electrical energy at relatively less cost than other renewable energy resources like hydro, wind and Pv system. This system is also suitable for Ethiopia with lower wind speed resource areas like Gambela,Asosa, Metema and Somalia region. This system also powers many rural health care centers that require electrical load demand which directly save the lives of many women and children dying from birth-related problems.

Therefore, the impact of this study is clearly higher in solving the power demand of off-grid areas with a lower financial requirement. So, this may attract the attention of many researchers to go further in improving the efficiency of solar chimney power plant and the solar system in general. Additionally, reducing the hard currency expended for purchasing a material for same desired maximum power output compared to hydro, wind and Pv system.

CHAPTER TWO

2. Literature review

2.1 First steps and recent developments of solar chimney power plant

The concept of utilizing the air rising upward to create rotation was first used by Italian famous artist and genius Leonardo da Vinci (1452–1519). He used the hot air rising in a chimney to drive a windmill which rotates his roasting spit connected to the windmill above a fireplace as shown in Figure 2.

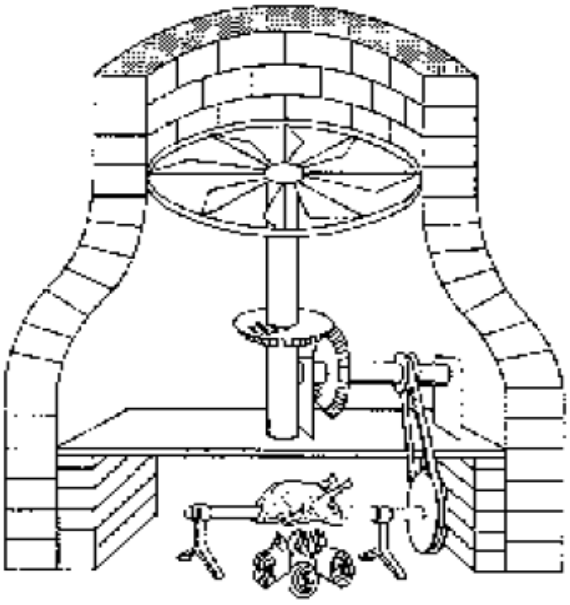

Figure 2-1:Spit of Leonardo da Vinci driven by rising hot air [Al-kayiem and Aja, 2016)

In 1926, the construction of a solar chimney power plant whose chimney will be positioned on the slope of a high mountain was proposed by Prof Engineer Bernard Dubos as shown in Figure 2-3. In 1931, a German author, Hanns Gunther demonstrated and published the concept of a solar chimney power plant technology developed by Dubos by performing a small experiment based on plate and a spirit lamp which acts as the heat from the Sahara Desert and the small wind wheel on top of the chimney represents the wind turbines as shown in Figure 2-2.

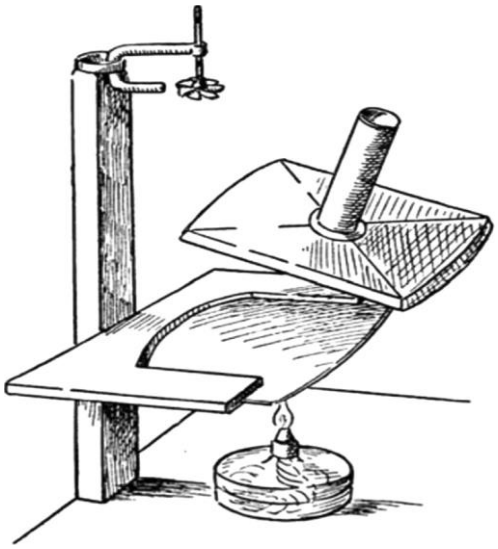

Figure 2-2: Solar chimney presented by Gunther(Al-kayiem and Aja, 2016)

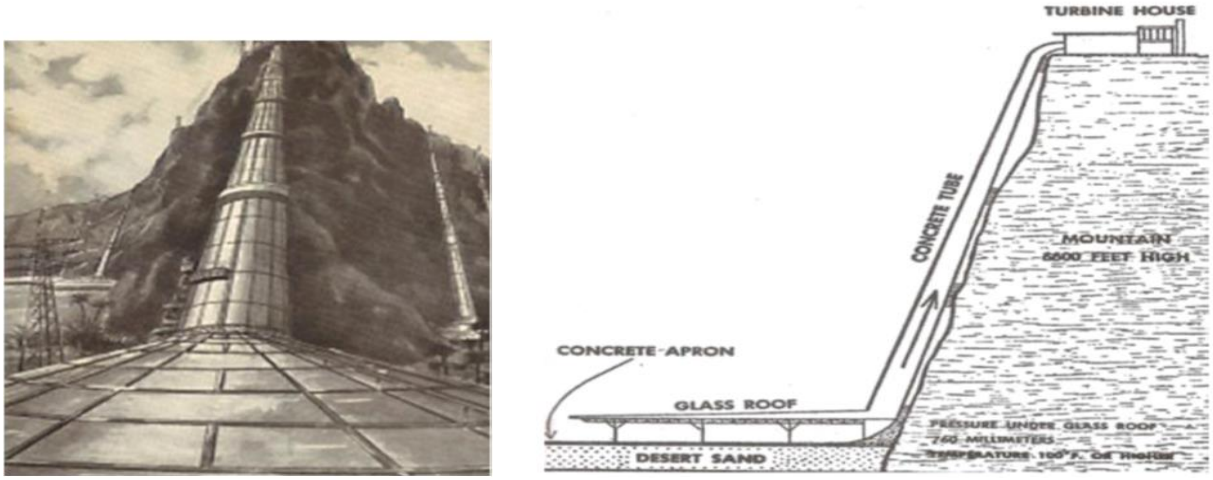

Figure 2-3:Prof Bernard Dubos's proposed solar aero-electric power plant [Al-kayiem and Aja, 2016)

(Ngala, Sulaiman and Garba, 2013),Many prototypes of the solar chimney power plant had been built by researchers in various countries but the first pilot plant of the SCPP was built in Spain in 1982 as shown in Figure 2.4. At the beginning the pilot power plant is designed to cover the total collector radius of 122m and a chimney height of 194.6m and produced a maximum updraft air velocity of 15m/s under no load conditions power plant.

Figure 2-4: The SCPP in Manzanares, Spain 1982[(Ngala, Sulaiman and Garba, 2013)]

(Al-kayiem and Aja, 2016),Currently Australian intends to construct the largest SCPP in the world at present with the generation capacity reaching up to 200 MW in New South Wales of Australia. A chimney in the plant will be 1000m in height and the collector is 7 km in diameter, the system would cover a ground area of 38 km2. Experimental work and numerical calculation method can be used to study on the performance of the SCPP, but the large-scale system is hard to establish. However, with the development of computer technology and commercial software techniques, both temperature and pressure distribution in the large system can easily be obtained by numerical calculation method [(Huang *et al.*, 2007)].

2.2 Solar chimney power plant

Solar chimney power plant is classified as a solar thermal energy system that utilizes solar energy to produce ventilation that drives air turbines to produce electric power (Zhou, Wang, *et al.*, 2010). solar thermal power plant generally classified as a high and low-temperature power plant. These classifications mainly depend on the operating temperature and process type. High-temperature power plants collect direct solar radiation and often use a closed cycle thermodynamic process. These plants have very high efficiency but also require high capital costs and operational costs.

Solar chimney power plants are classified as low temperature power plant since its working fluid is kept primarily in the free atmosphere(Ninic, 2006). Generally, solar chimney power plant comprised of a solar collector, solar chimney and turbine as shown in Figure 2.5 (Bernardes, Voß and Weinrebe, 2003).

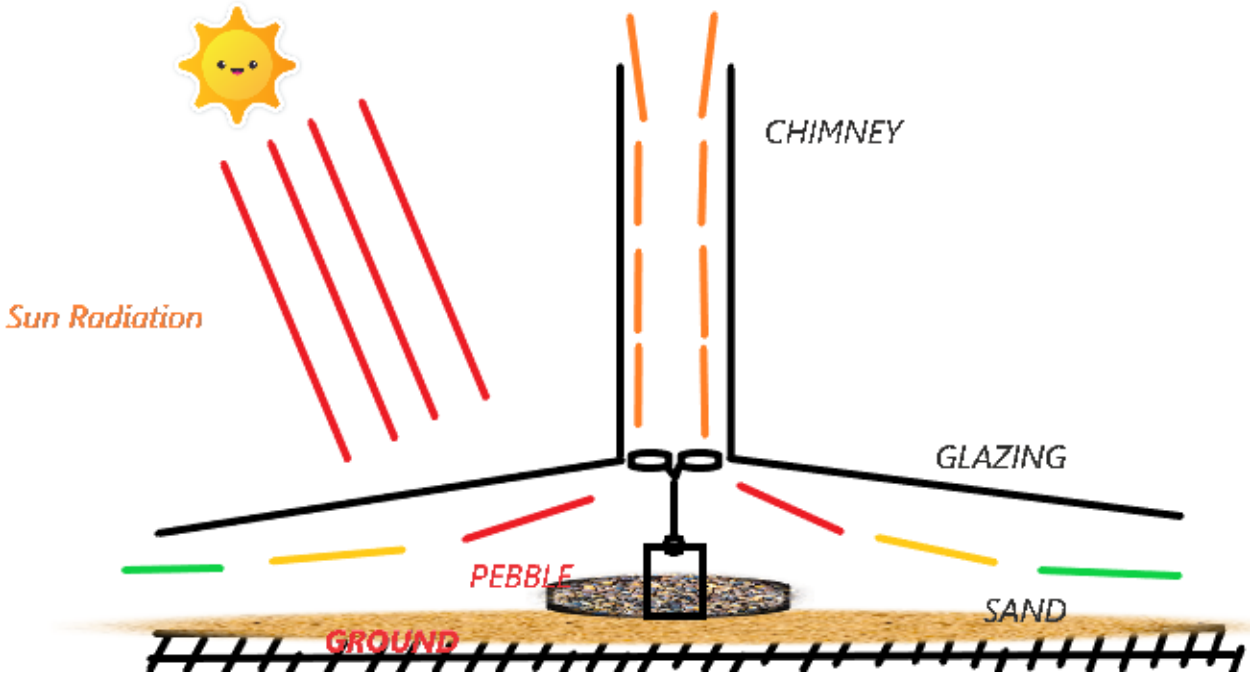

Figure 2-5: Solar chimney power plant layout [appendix].

2.2.1 Solar collector

In the solar chimney power plant system, a solar collector is the main component that allows the short-wave radiation to pass through it and block the long wave radiation from going back through it. This will result in the heating up of air under the collector which then flows radially towards the center where the chimney is positioned. The collector is usually made up of glass or plastic film which is stretched horizontally for designed meters above ground or supported close to the ground. In order to reduce eddy loss and air friction the collector height increases towards the center where the chimney is placed this will ensures a smooth transition of hot air flowing from the collector to the chimney as shown in Figure 2.6(Schlaich and Bergermann, 2002).

Figure 2-6: solar chimney collector(Amrutkar, Ghodke and Patil, 2012).

The area under the collector is covered by soil that will emit most of the solar radiation during the day and release small amount of heat during the night. Since the soil is not good enough to store the sun radiation black painted water-filled tube will be placed on each side of the collector underneath.

2.2.2 Chimney

A Chimney is a long cylindrical structure placed at the middle of collector and one or more turbo-generators are installed at its base for the purpose of power generation(Zhou *et al.*, 2014),it is usually called solar tower. The function of a chimney is to convert the thermal energy produced in the collector into a kinetic energy. The pressure difference is produced due to the density difference between the airflow at chimney base and chimney top(Kinan and Sidik, 2016).

Solar chimney can be installed using a different specific angle of inclination, often vertical orientation will be utilized as it is easier to build and operate. however, the vertical orientation is suitable also it can be constructed in through various like free-standing reinforced concrete tubes, steel sheet tubes supported by guy wires, or cable-net construction with a cladding of sheet metal or membranes as shown in Figure 2.7(Backström, Gannon and Backstro, 2000). Current technological progress has shown that 1,000 m chimney Height can be built without difficulty(Hanna *et al.*, 2016) .

Figure 2-7: solar chimney construction layout.(Kaledin *et al.*, 2009)]

2.2.3 Solar chimney Turbine

Turbine is the main component of SCPP which will be used as the power producing unit of the plant. The main purpose of the turbine is to convert the kinetic energy of heated air into mechanical energy using the turbine rotors. In order to have easier installation and maintenance turbine are usually placed at the base of the chimney. The turbine of SCPP is usually an axial flow type turbine as shown in Figure 2.8(Backström and Gannon, 2004).

The operation and design of modern wind turbines could be applied to the solar chimney but in comparisons solar chimney turbines have a much higher energy extraction per unit flow and are more a similar to gas turbines. Solar chimney turbines have a greater pressure drop than wind turbines and require more blades but not as many as gas turbines. It was found that wind turbine blades can be treated accurately as individual airfoils. This is not the case in the solar chimney turbine due to the higher blade solidity (blade chord to pitch ratio).The pitch angle of the blades can be adjusted like wind turbines but due to the flow being enclosed in a SCPP like a gas turbine, the turbine may have radial inflow guide vanes(Fluri, 2008).The blades required for the solar chimney turbine are of low solidity when compared to gas-turbine turbomachinery but they cannot be treated accurately as single blades like those of wind turbines.

Figure 2-8: Axial flow solar chimney blade, source(Hanna *et al.*, 2016)

2.3 Solar Chimney Power Plant Theoretical and Experimental Models

In 1998, (Pasumarthi & Sherif, 1998a) built a small-scale SCPP prototype to study the effect of various geometric parameters on the air temperature, air velocity, and power output of the solar chimney. Further studies conducted by (Pasumarthi & Sherif, 1998b) showed that the collector performance can be modified by extending the collector base and by introducing an intermediate absorber. Both modification help in increasing air temperature and mass flow rate inside the chimney resulting in higher power output.

In 2003, (Bernardes, Voß and Weinrebe, 2003) develop the first attempt to solve by CFD (Computational Fluid Dynamics) the convective flow in a SCPP. He presented a solution for Navier-Stokes and Energy Equations for the natural laminar convection in steady state, predicting its thermo-hydrodynamic behavior. The approach Finite Volumes Method in Generalized Coordinates was employed allowing a detailed visualization of the effects of geometric of optimal geometric and operational characteristics. According to results obtained, curved junctions initiates well distributed-temperature fields, recirculation free flow as well a higher mass flows compare to straight junctions at the center of the base of the collector.

In 2006,(Ninic, 2006),Studied and determined the dependence of the work potential on the air flowing into the air collector from the heat gained inside the collector, air humidity and atmospheric pressure as a function of elevation. In his study, various collector types using dry and humid air have been analyzed. The influence of various chimney heights on the air work potential are also established. He made a discussion on the possibly of higher utilization factors of the available hot air work potential without the use of high solid chimneys.

In 2014, (Zhou *et al.*, 2014), had studied the effect of the chimney height through varying different parameter by comparing their obtained result with the first pilot plant constructed in Manzanares, Spain. They showed that different atmospheric pressure changing at different sites will result in different maximum height of a chimney. The maximum chimney height for convection avoiding negative buoyancy at the chimney and the optimal chimney height for maximum power output are presented and analyzed using a theoretical model and validated with the measurements from the prototype in Manzanares. The result showed that as standard lapse rate of atmospheric temperature is used, the maximum power output of 102.2 kW is obtained for the optimal chimney height of 615 m, which is lower than the maximum chimney height with a power output of 92.3 kW. Sensitivity analyses are also performed to examine the influence of various lapse rates of atmospheric temperatures and collector radii on maximum height of chimney. The results show that maximum height gradually increases with the lapse rate increasing and go to infinity at a value of around 0.0098 K/m and that the maximum height for convection and optimal height for maximum power output increase with larger collector radius.

In 2013 ,(Koonsrisuk and Chitsomboon, 2013) presented the mathematical model that shows the ratio of the pressure drop across the turbine to the total available driving pressure of a system, so according to their analysis in order to achieve maximum power output the optimal ratio of the turbine extraction pressure has to be greater than and equal to 2/3 of the available driving pressure, the optimal pressure ratio of 2/3 is valid only for the constant-driving-pressure and temperature of the systems. They also presented the relationships between the pressure ratio and the mass flow rate and between the temperature rise across the collector and the power output.

In 2014,(Sakir, Piash and Akhter, 2014), they presented the performance of small scale solar chimney power plan by conducting an experiment. The small power plant is constructed at the top of apartment roof found in Bangladesh. The constructed solar chimney power plant has some similarity and variation in terms of power output, pressure, inlet temperature, density and mass flow rate compared to the calculated results. They also presented the variation of the temperature, pressure, mass flow rate and power output in all time of the day. Experimental result shows that the power output along with the parameters which are homogeneous to the power such as velocity at entrance, pressure difference, and mass flow rate approaches their peak almost always at mid-day approximately as expected because at that time sun radiation becomes maximum due to its position. The result shows that the average power output of 3 to 20 watts could be achieved from the from the particular chimney size of 0.15 meter.

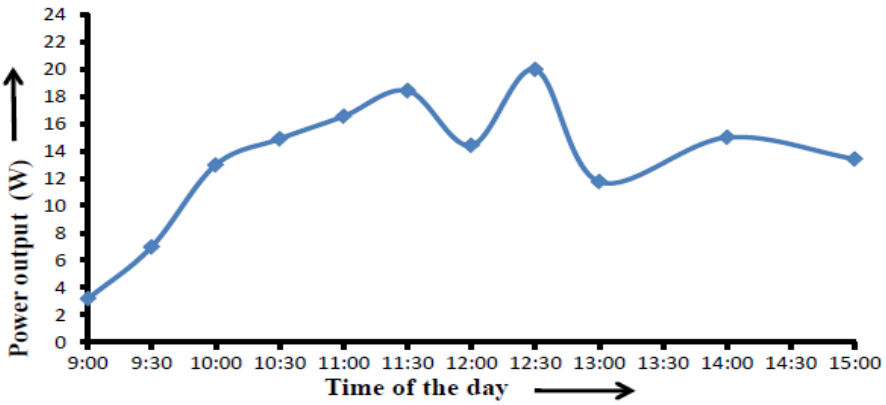

Figure 2-9: Power output vs time of a day(Sakir, Piash and Akhter, 2014)

The result in Figure2-9, shows that the power output was increasing with the time of the day at first from 3.75 watts at 9 am and then dropped suddenly. Then at 12:30 pm it peaked to 20.1 watts. Generally, the power production dropped down after the mid-day and declined after 15:00 pm following the sun radiation. Experimental result of this study shows that the power output along with the parameters which are homogeneous to the power such as velocity at entrance, pressure difference, and mass flow rate approaches their peak almost always at mid-day approximately because at that time sun radiation becomes maximum, after the mid-day curve of all parameter gradually drop down following the decrease in sun radiation.

In 2016,(El-ghonemy, 2016), carried out a case study in kingdom of Saudi Arabia particularly for Skaka site, by considering the chimney height 200 meter and collector diameter of 500-meter their study showed variation of power output ranging from 118 KW - 244 KW in all month of the year with respect to solar radiation and ambient temperature. According to the mathematical model developed in this study the power output is directly proportional to the chimney height and collector radius. The experimental result of this study showed that increasing the collector radius with decreasing the chimney height the same amount of useful energy. Additionally, they showed that the increased inlet velocity will directly increases the power output of the power plant.

In 2011,(Robera and Dr.abebayehu, 2011), presented the Modeling and Simulation of Solar Chimney Power Plant with and without the Effect of Thermal Energy Storage Systems. The main focus of their study was on the economic feasibility of installing energy storage unit in the system. The analysis showed that if the total project cost is $2,336,158.18 without the storage unit**,** levelized cost of electricity will be $0.56 per KWh^{-1} then adding an investment cost of $56857.57 on energy storage unit will result reduced cost of electricity to $0.24 per KWh^{-1} [22].

In 2010,(Koonsrisuk, Lorente and Bejan, 2010),Studied the effect of tower area change in a solar chimney power plant was using CFD technology. The results from their study showed that the tower area change affects the efficiency and the mass flow rate through the plant. It was found out from their study that although velocity increases at the top of a convergent tower, the mass flow rate remains similar as that of a constant area tower. For a divergent tower design, velocity increases near the base of the chimney and the maximum kinetic energy also occurs at the base of the chimney.

In 2016,(Ming *et al.,* 2016),performed further studies on the thermal performance of a solar chimney power plant. They established a simple analysis of the air flowing through the solar chimney power plant and also a thermodynamic cycle of the solar chimney power plant including the environment. They also produced mathematical model of ideal and actual cycle efficiencies for medium-sized and large-sized solar chimney power plant, accordingly the result of their study showed that the ideal cycle efficiency and actual efficiency of standard Brayton cycle corresponding to medium scale solar chimney power generation system are 1.33% and 0.3%

respectively, while the ideal efficiency of large scale SC system with chimney height 1000 m is 3.33%, while the maximum value of the actual efficiencies is 0.9%.The results from their work used as a theoretical guideline for designing and building a commercial-size solar chimney power plant in China. In 2000, (Backström, Gannon and Backstro, 2000),presented an air standard cycle analysis of the solar chimney power plant for the calculation of limiting performance, efficiency, and the relationship between the main variables, including chimney friction, system, turbine, and exit kinetic energy losses.

In 2010,(Hamdan, 2010),performed an analytical model and a thermodynamic study of steady airflow inside a solar chimney. He used a simplified Bernoulli's equation combined with fluid dynamics and ideal gas equation using EES solver to predict the performance of the solar chimney power plant. The analytical model was validated against an experimental and numerical data available and was also used to evaluate the effect of geometric parameters on the solar chimney power plant. From his analysis, it could be said that the height and diameter of the solar chimney are the most important variables for solar chimney power plant design and also the collector area has small effect on second-law efficiency but strong effect on harvested energy. Further studies were conducted by (Hamdan, 2013) to evaluate the use of constant density assumption and compare it with the more realistic chimney mathematical model. From the results obtained, it can be concluded that the constant density assumption simplifies the analytical model but it over predicts the power output. From the result it can also be concluded that maximum power output depends on the turbine head.

(Pretorius, 2007),Investigate the optimization and control of large scale solar chimney power plant by developing the numerical simulation model. The numerical simulation model is refined and used to perform a sensitivity analysis on the most prominent operating and technical plant specifications. In this study the effects of ambient wind, temperature lapse rates and night time energy storage system temperature variation on plant performance are examined. Results indicate that, through the modification of the collector roof reflectance, collector roof emissivity, ground surface absorptivity or ground surface emissivity, major improvements on plant performance are possible. Additionally, introducing thermal insulation or double glazing of the collector roof also improve on the power output yield.

(Pretorius *et al*,2006) evaluated the influence of a recently developed convective heat transfer equation, a more accurate turbine inlet loss coefficient, quality collector roof glass and various types of soil on the performance of a large-scale solar chimney power plant. Results from this study indicated that the new heat transfer equation reduces the power output of the solar chimney power plant significantly. Also, the effect of a more accurate turbine inlet loss coefficient is very minor and by using a better-quality glass can highly improve the efficiency of the solar chimney power plant. Models tested with Limestone and Sandstone soil produced virtually comparable results to a Granite-based model. Further study performed by (Pretorius and Kroger), showed that 24hrs power production is possible if appropriate thermal energy storage is place beneath the collector roof.

(Bernardes and Zhou, 2013),analyzed particularly the sensible heat storage physical process in a Solar chimney power plant collector taking into account the transient heat transfer in ground through conduction, convection and solar radiation and the use of water bags. Thicknesses of water bags were varied and simulated with and without insulations. From the results obtained, it can be concluded that thicker water bags reduce the daily temperature efficiently and the thermal stratification effect. Additionally, they showed that water bag storage unit alone is not enough to provide power throughout the night and the cannot achieve peak heat.

(Choi *et al.*, 2016),In this study, a new mathematical analysis model was developed considering realistic physical pressure drops throughout the whole SCPP system. This new analysis model was validated through comparison with the experimental data of a prototype plant in Manzanares, Spain. The pressure drop and mass flow rate were calculated through an iteration process using MATLAB. The final output power can be predicted from the pressure, density, temperate and pressure drop at each point. Additionally, the largescale solar chimney was evaluated according to dimension such as the collector radius and chimney height, among others. To determine the electricity generated at night, an analysis of the water stored under the collected was conducted. The power output with the water storage system was predicted based on the change in depth under the collector.

2.4 Cycle analysis of solar chimney power plant

In 2000, (Backström, Gannon and Backstro, 2000),analyzed the cycle of a chimney with the simple air standard cycle. Considering the simple air standard cycle as it determines the upper performance limits of the ideal solar chimney power plant. In 2002 (Backström, Gannon and Backstro, 2002),developed simple thermodynamic cycle analysis that includes system losses to obtain accurate predictions of the plant power output. In order to calculate the operating range of the solar chimney turbine, it is useful to perform a thermodynamic cycle analysis. According to Gannon and Von Backström (2000 & 2002) analysis and investigation, the two most important variables in terms of power output in the solar chimney power plant are the chimney height and the solar collector temperature rise, this fundamental relationship is found by developing simple complete air standard cycle.

2.4.1 Thermodynamic cycle

In order to understand the actual process operating range of solar chimney power plant thermodynamic cycle will be used as it simulate the actual process. The working fluid in a solar chimney power plant is air and it is assumed to behave as an ideal gas.

Assumption considered in the simple air standard air cycle(Gannon and Backstro, 2000).

i. The working fluid is dry air ,assumed to be behaving as an ideal gas with constant specific heat
ii. The mass flow rate of the system is constant
iii. The compression and expansion processes in the air standard cycle are adiabatic and reversible (isentropic)
iv. The inlet and exit atmospheric conditions are identical

2.4.2 Gas turbine cycle

Solar chimney power plant cycle is similar with ideal gas turbine (Brayton cycle). In gas turbine air standard cycle there are four basic process; isentropic compression, constant pressure heat addition, isentropic expansion and constant pressure heat removal(Backström and Gannon, 2004). Although there is some technical similarity between Solar chimney power plant cycle and gas turbine cycle there are also basic difference. One of the main practical differences is that the inlet

and the exit atmospheric conditions are assumed to be identical in the gas turbine cycle, however this is not true for the solar chimney power plant cycle since the exhaust is at the altitude of the chimney top, and the atmosphere has the additional function of recompressing the exhaust air to the ground inlet conditions. This compression doesn't have to be isentropic; it can be approximated by a polytropic expression of the form:

$$\frac{P}{\rho^n} = constant \quad \text{or} \quad PV^n = constant$$

Where p is the pressure, V is volume, ρ is density and n some exponent that is not necessarily equal to the specific heat ratio γ but less.

Note: isentropic process only work transfer no heat transfer. but in a Polytropic heat and work both can be transfer. The following T-S diagram is taken from the analysis of(Backström,Gannon and Backstro, 2000; Ming *et al.*, 2010)

In order to study and understand the solar chimney power plant cycle, it is very important to simulate the solar chimney power plant cycle as a gas turbine air standard cycle where the chimney is eliminated and an isentropic compressor is added. To better simulate the environmental conditions of the solar chimney power plant, assume that the gas turbine plant is placed at the altitude of the chimney top.

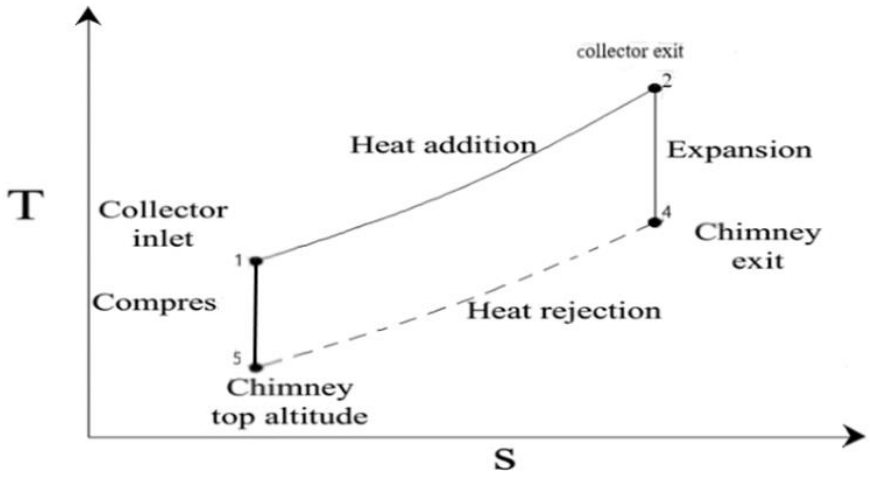

Figure 2-10: T-S, diagram for air standard gas turbine cycle in the solar chimney power plant.

The pressure ratio chosen for the solar chimney power plant is the ratio of the atmospheric pressure on the ground level to the atmospheric pressure at the solar chimney top.

The cycle pressure ratio is defined as(Ming *et al.*, 2016)

$$r = \frac{P_1}{P_5} = \frac{P_2}{P_4} \qquad \boldsymbol{eq(2.1)}$$

The compression temperature ratio is defined as(Ming *et al.*, 2016)

$$C = \frac{T_1}{T_5} = \frac{T_2}{T_4} = r^{\gamma-1/\gamma} \qquad \boldsymbol{eq(2.2)}$$

Then the cycle efficiency is defined as the turbine shaft power out divided by the thermal power or the solar energy transferred to the air moving across the solar the solar collector:

$$\eta = \frac{shaft\ power\ out\ put}{thermal\ power\ \ in} \qquad \boldsymbol{eq(2.3)}$$

The turbine output power or the shaft power out is defined as:

$$\text{Pshaft} = \dot{m} \times Cp \times (T_2 - T_4) - \dot{m} \times Cp \times (T_1 - T_5) \qquad eq(\mathbf{2.4})$$

But it is assumed that the power consumed in the process 1-2 is relatively low it as assumed zero Solar energy transferred to the air:

$$\Delta P_{23} = \dot{m} \times Cp \times (T_2 - T_1) = \dot{m} \times (h_2 - h_1) \qquad eq(\mathbf{2.5})$$

Then the efficiency of the cycle can be re written(Backström, Gannon and Backstro, 2000)

$$\eta = 1 - 1/C = 1 - \frac{1}{r^{\gamma-1/\gamma}} \qquad eq(\mathbf{2.6})$$

From the above relation it is observed that the system efficiency is dependent on the pressure ratio.

2.5 Air standard cycle for Solar chimney power cycle

SCPP operates in the same principle with gas turbine air standard cycle except for some practical difference. In the SCPP cycle analysis compression takes place in the environment this makes the cycle different from gas turbine cycle where the compression takes place in the system. The other difference is that when analyzing the gas turbine of solar chimney in the above section ,analysis of compressor inlet temperature T1 is at the top altitude of the chimney, Instead T1 will be used as collector (glazing beneath) inlet temperature due to the fact that it is easy to measure from the

ground (Ming *et al.*, 2016).The temperature T5 will be assigned and placed at the intersection between the constant pressure line through point 4 and the isentropic line through point 1 as shown below.

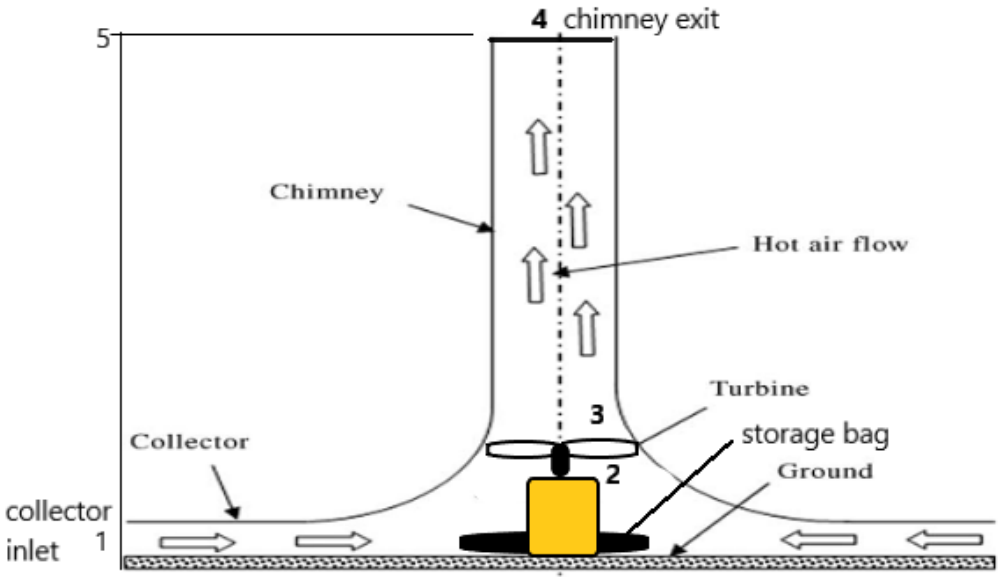

Figure 2-11: Schematic showing nomenclature of solar chimney power plant

In an ideal gas turbine cycle where there is a reversible process all the power could be extracted as the gas expands from process P_2 to P_4 to obtain the shaft power of $(\dot{m} \times Cp \times (T_2 - T_4)$. In this solar chimney power plant cycle the power required to lift the air up the chimney must be taken into account.

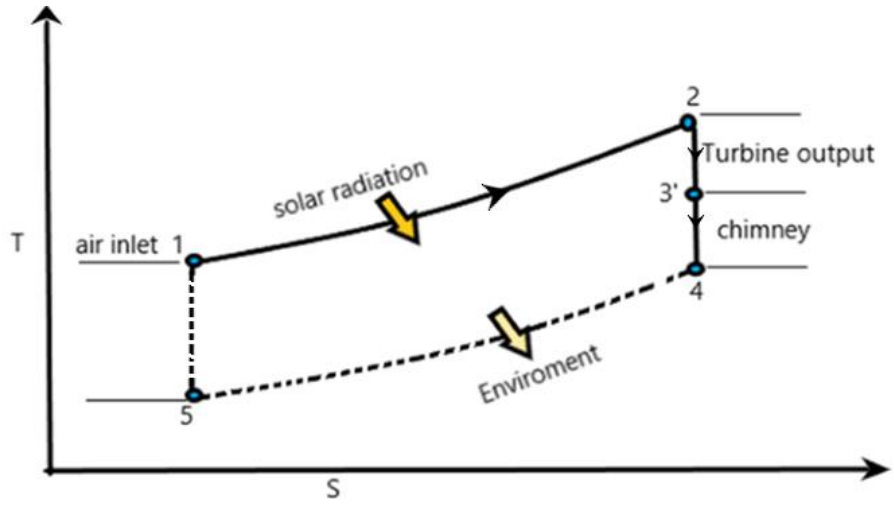

Figure 2-12:T-S diagram of solar chimney power plant air standard cycle.

i. From the above T-s diagram **the significant state of air** is:

a) State 1: the state of the collector inlet
b) State 2: the state of the collector outlet, which is also the state of turbine inlet
c) State 3: the state of the chimney inlet, which is also the state of the turbine outlet
d) State 4: the state of the chimney outlet
e) State 5: the state of the environment at the same height of the chimney outlet.

ii. **The four-basic process of the thermodynamics cycle** are:

a) Process 1-2: heat addition from solar radiation
b) Process 2-4': isentropic expansion (turbine shaft power but no shaft power from chimney)
c) Process 4'-5: heat rejection(environment)
d) Process 5-1: isentropic compression(open to the enviroment)

Note: From the above process two of them takes place in the environment this makes it different from gas turbine.

The total power available;

$$Pavalible = \dot{m} \times Cp \times (T_2 - T_4{}') \qquad \boldsymbol{eq(2.7)}$$

The power required to lift the air up the chimney;

$$P_{lift} = \dot{m} \times g \times H_{chim} \qquad \boldsymbol{eq(2.8)}$$

Since there is no heat loss and shaft work along the chimney height.

So, the enthalpy change in the chimney becomes:

$$\Delta h = g \times \Delta H_{chim} \qquad \boldsymbol{eq(2.9)}$$

The energy exchange is isentropic, since the friction and heat transfer are negligible. Then the value of Δh can be equated to the amount of air that has descended again in the atmosphere after having been cooled to.

The amount of enthalpy gained is defined as:

$$\Delta h = g \times \Delta H_{chim} = Cp \times (T_1 - T_5) \qquad eq(\mathbf{2.10})$$

Then the turbine shaft power becomes

$$P_{shaft} = \dot{m} \times Cp \times (T2 - T3) - \dot{m} \times Cp \times (T_1 - T_5) \qquad eq(\mathbf{2.11})$$

Then the T-S diagram will be changed onto the following form

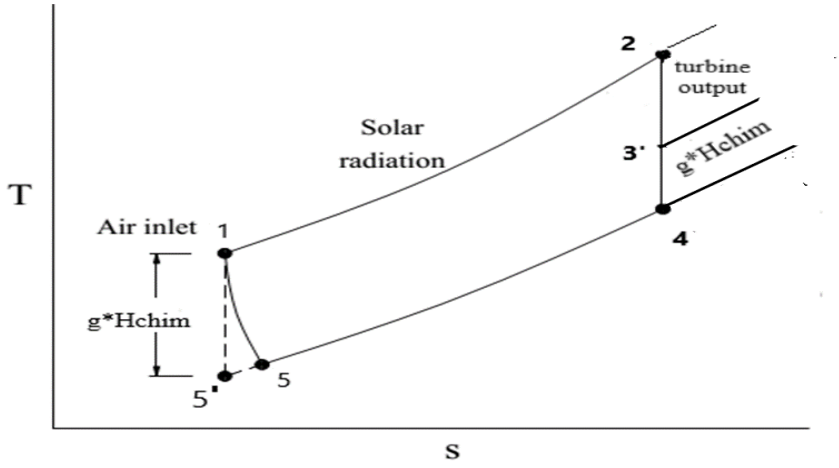

Figure 2-13: T-S diagram of SCPP with no heat loss and friction in the system.

The temperature T5 is assumed to be the temperature that has less temperature than T4, this will be helpful to consider as an isentropic compression in agreement with the air standard assumptions.

In the solar chimney an internal exchange between the enthalpy and geopotential energy takes place in the chimney and the process is reversed in the external environment (Backström and Gannon, 2004).

The pressure ratio is defined as the collector exit pressure over the chimney exit pressure;

$$r = \frac{P_1}{P_5} = \frac{P_2}{P_4} \qquad eq(\mathbf{2.12})$$

The temperature ratio becomes:

$$C = \frac{T_1}{T_5} = \frac{T_2}{T_4} \qquad eq(\mathbf{2.13})$$

The **cycle efficiency** becomes :

$$\eta = \frac{shaft\ power\ out\ put}{thermal\ power\ \ in} = \frac{W_{shaft}}{q_{12}} \qquad \boldsymbol{eq(2.14)}$$

The thermal power transferred to the air in the collector is;

$$P12 = \dot{m} \times C_P \times (T_2 - T_1) \qquad eq(\mathbf{2.15})$$

Then the shaft power output is re written ;

$$W_{shaft} = C_P \times (T_2 - T_3) = h_2 - h_3 \qquad eq(\mathbf{2.16})$$

Then thermal power can be given as;

$$q_{12} = h_2 - h_1 = C_P \times (T_2 - T_1) \qquad eq(\mathbf{2.17})$$

2.6 Efficiency of the Cycle

Then substituting $eq(2.16)\ and\ eq(2.17)$ the efficiency of the cycle can be re-written as;

$$\eta = \frac{T_2}{T_2 - T_1}(1 - (P_3/P_2)^{\gamma-1/\gamma}) \qquad \boldsymbol{eq(2.18)}$$

When the hot air flows from the bottom through the chimney to the environment, the same mass of cold air comes from the environment at the same height of chimney outlet to the collector inlet.

The energy transfer equation can be written as(Ming *et al.*, 2016).

$$C_P \times \partial T = g \times \partial \times H_{chim} \qquad eq(\mathbf{2.19})$$

The by integrating these equations the following result can be obtained:

$$C_P \times (T_1 - T_5) = g \times H_{chim} \qquad eq(\mathbf{2.20})$$

Then the efficiency of the cycle can be modified by equating the temperature drop with the potential energy:

$$\eta = \mathrm{g} \times \frac{H_{chim}}{C_P \times T_1} \qquad \boldsymbol{eq(2.21)}$$

From the above equation efficiency is proportional to the chimney height, inversely proportional to collector inlet temperature.so this showed that the system efficiency is independent of the collector temperature rise.

2.7 Variation of atmospheric air pressure and temperature with elevation

Now consider the atmospheric air surrounding the SCPP as unsaturated medium, assume the air obeys the ideal gas eqn. Then the air expands slowly as shown in equation below. The atmospheric pressure and temperature variation with respect to elevation is shown below;

$$P(z) = P_0(e^{g \times z / R_{air} \times T}) \qquad eq(\mathbf{2.22})$$

Then using the above equation and basic ideal gas equation, the dry adiabatic lapse rate will be formulated ((Koonsrisuk and Chitsomboon, 2013))

$$\frac{dT}{dz} = -\frac{g}{C_P} \qquad \boldsymbol{eq}(\mathbf{2.23})$$

2.8 Research gap

In this research, comprehensive study is under taken by assessing more than 20 articles from different journals, those reviewed article carried their study based on more than 100 studies and literature over the past 90 years. Most of the reviewed article make a conclusion based on the CFD result and mathematical model. Among the reviewed article only 24 % of studies develop an experimental model to generate a comprehensive and sound result.

In the literature, while making a conclusion based on only a mathematical and simulation their results like power output, temperature at collector exit and electrical generation per day from the plant tends to be over predicted. Sometimes, the actual influence of solar radiation data and environmental condition on the actual project site may not be included while using mathematical and numerical model.

On the other hand some of the article with experimental model has errors while making a prediction on the power output due to the fact that their experimental test site is in a laboratory with a controlled condition. However, some study built an actual experiment but they do not study the influence of solar collector height from the ground on the collector exit temperature through adjusting the height of the collector inlet gap.

Generally, from a reviewed article some gaps are identified. So, for high reliance on the development of large scale commercial solar chimney power plant, it is suggested to develop chain projects from feasibility (technical design), numerical modeling and simulation,to a small-scale, finally scale up to the large-scale solar chimney power plants.Therefore,in this study the above methodology is used following the identified gap in the influence of collector height from the ground a long side with integrating a thermal energy storage unit in the system.

CHAPTER THREE

3. Solar Energy Resource Data

Ethiopia is categorized as a part of the world where the solar radiation source is maximum. It is, therefore, a matter of interest to assess the significance of solar energy and its utilization in different fields of applications.

The study of solar energy resource at a particular site is a very important aspect for a design of the solar energy conversion system. One of the most important requirements in the design of any solar energy conversion equipment is the intensity of the solar radiation. Direct radiation and diffuse radiation are the two main components of radiation reaching the ground. This data is collected using solarimeter but most of this meter usually measure the global (or total) solar radiation on a horizontal surface. However, in other applications knowledge of diffuse radiation is also essential. Solar radiation can be measured experimentally using instruments such as pyranometers and radiometers

The amount of solar radiation which reaches the earth's surface varies from one place to another place, due to climatic condition and geographical appearance of sites. Hence the detailed study of solar radiation under local climate conditions is essential. In Ethiopia, there is lack of measuring instruments for solar radiation in many sites, the data for desired location will be taken from the nearby site of a data center.

In this study, the experimental design will be constructed inside 5 kilo campus, so the data are taken from Ethiopian metrological data agency. However, the study will be conducted inside 5 kilo campuses, the data will be taken from ENTOTO site, due to the fact that ENTOTO is the nearby site with measuring instrument installed by the agency. Global Solar radiation data is used from meteoblue and metrological agency.

3.1 Incident Solar Radiation

The total incident solar radiation on earth surface is consists of direct solar radiation(beam), diffuse and reflected solar radiation from the ground and surrounding as shown in figure 4.

The total incident solar radiation can be written as;

$$I_T = R_b I_b + R_d D_r + \rho R_r G_r \qquad \boldsymbol{eq}(\mathbf{3.1})$$

The heat flux incident beam radiation transferred through the glazing of solar collector per unit time is given by;

$$q'' = I_T(\tau\alpha) \qquad \boldsymbol{eq}(\mathbf{3.2})$$

Table 3-1: Monthly Averaged Insolation Incident on A Horizontal Surface at Indicated GMT Times (kW/m^2) at addis ababa 5 kilo campus.

Time	Jan	Feb	Mar	Apr	May	Jun	Jul	Aug	Sep	Oct	Nov	Dec
6:00	0.01	0.01	0.01	0.02	0.03	0.03	0.02	0.02	0.02	0.03	0.02	0.01
9:00	0.43	0.44	0.47	0.51	0.52	0.45	0.34	0.34	0.47	0.55	0.53	0.47
12:00	0.85	0.9	0.89	0.88	0.86	0.78	0.69	0.72	0.81	0.88	0.87	0.85
15:00	0.64	0.67	0.64	0.6	0.56	0.55	0.54	0.52	0.53	0.56	0.56	0.59
18:00	0.08	0.1	0.09	0.09	0.08	0.08	0.08	0.08	0.06	0.05	0.04	0.06

The monthly average amount of the total solar radiation incident on a horizontal surface at the surface of the earth for a given month, averaged for that month over the 22-year period (Jul 1983 - Jun 2005). Each monthly averaged value is evaluated as the numerical average of 3-hourly values for the given month.

The graphical expression of Monthly Averaged Insolation Incident on A Horizontal Surface at Addis Ababa institute of technology is shown below;

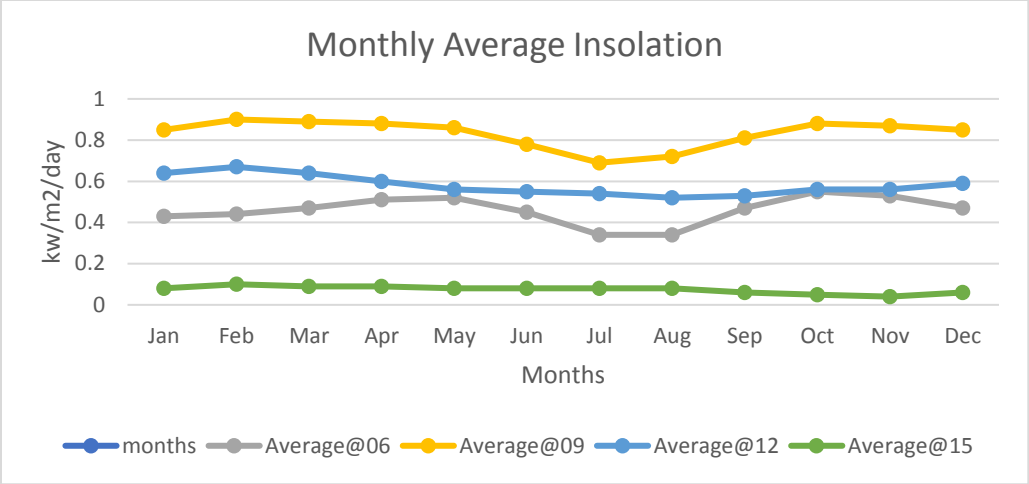

Figure 3-1: Monthly averaged insolation incident solar radiation

3.1.1 Global solar radiation(Gr)

Global solar radiation is the sum of beam radiation and diffuse radiation. The total Global radiation available at Addis Ababa institute of technology at @**Latitude 9.038 / Longitude 38.763** is taken from; NASA Surface meteorology and Solar Energy - Available Tables.html; the data are recorded for 22 years separately for diffused and direct beam radiation.

a) Diffused Radiation (D_r)

The monthly average amount of solar radiation incident on a horizontal surface at the surface of the earth under all-sky conditions with the direct radiation from the sun's beam blocked by a shadow band or tracking disk for a given month, averaged for that month over the 22-year period (Jul 1983 - Jun 2005)

Table 3-2: Monthly Averaged Diffuse Radiation Incident on A Horizontal Surface (kWh/m^2/day)

	Jan	Feb	Mar	Apr	May	Jun	Jul	Aug	Sep	Oct	Nov	Dec	Average
22-year Average	1.23	1.43	1.82	2.01	1.91	2	2.18	2.25	2.08	1.61	1.25	1.12	1.74

The graphical Expression for Monthly Averaged Diffuse Radiation Incident on A Horizontal Surface is shown in figure 3.2.

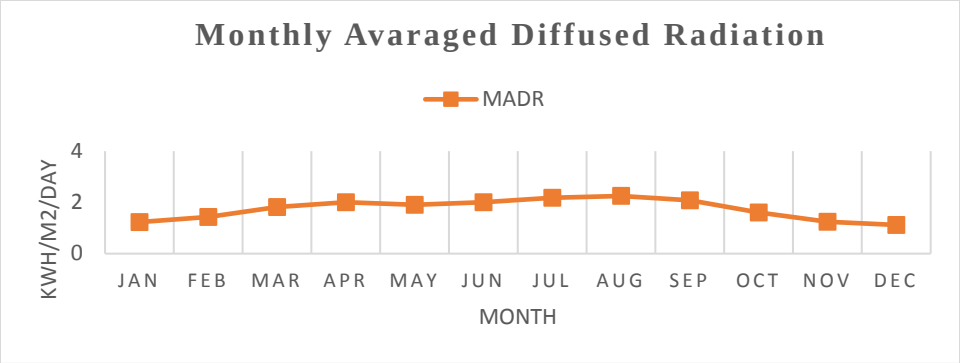

Figure 3-2 : Monthly average diffused radiation.

b) Monthly Averaged Direct Normal Radiation (Beam radiation)(I_b)

Beam radiation is the solar radiation received by the earth surface without being scattered by the atmosphere. The monthly average amount of solar radiation incident on a surface oriented normal to the solar radiation for a given month, averaged for that month over the 22-year period (Jul 1983 - Jun 2005) is listed in the table 3.3 as shown below:

Table 3-3: Monthly Averaged Direct Normal Radiation (kWh/m^2/day)

	Jan	Feb	Mar	Apr	May	Jun	Jul	Aug	Sep	Oct	Nov	Dec	Annual Average
22-year Average	8.03	7.83	6.76	6.32	6.48	5.64	4.31	4.16	5.35	7.13	8.05	8.26	6.52

The graphical expression of monthly average direct normal radiation is shown below;

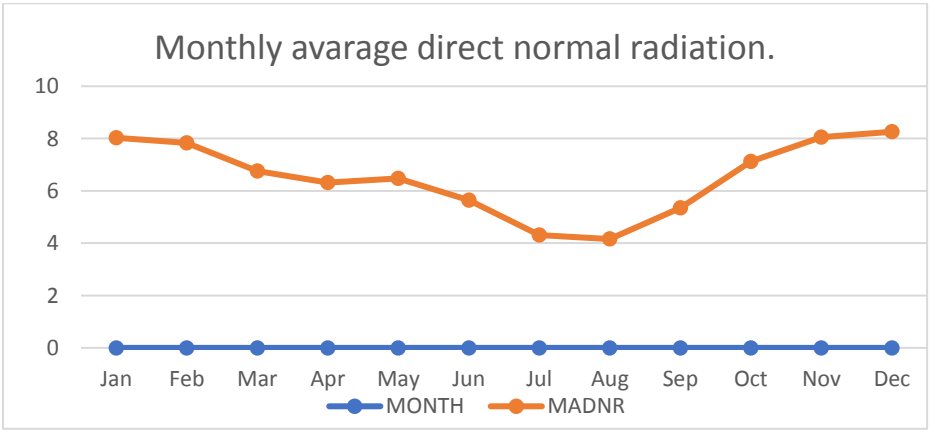

Figure 3-3: Monthly average direct normal radiation

3.2 Radiation factor

3.2.1 Beam radiation factor (R_b)

Beam radiation factor is ratio of the average daily beam radiation on a tilted surface to that on a horizontal surface(Duffie, Beckman and Worek, 2003)

According to (Duffie, Beckman and Worek, 2003) the horizontal and inclined incident radiation can be written as follow;

The flux beam radiation incident on horizontal surface is given as;

$$I_{bz} = I_N COS(\theta_Z) \qquad \boldsymbol{eq(3.3)}$$

The flux beam radiation on inclined surface is given as;

$$I_{bi} = I_N COS(\theta_i) \qquad \boldsymbol{eq(3.4)}$$

Therefore, the Radiation factor(Rb) can be written as;

$$R_b = \frac{I_N COS(\theta_i)}{I_N COS(\theta_Z)} = \frac{COS(\theta_i)}{COS(\theta_Z)} \qquad \boldsymbol{eq(3.5)}$$

3.2.2 Diffused radiation factor(Rd)

Diffused radiation factor is the ratio of the flux of diffuse radiation falling on the titled surface to the horizontal surface.Then according to (Duffie, Beckman and Worek, 2003) ,it can be calculated as;

$$R_d = \frac{(1+\cos(\beta)}{2} \qquad \boldsymbol{eq(3.6)}$$

4.2.3 Reflectivity factor (R_r)

Reflectivity factor is the component that comes mainly from ground and other surrounding objects.

$$R_r = \frac{(1-\cos(\beta))}{2} \qquad \boldsymbol{eq(3.7)}$$

3.3 Basic Sun Angle

3.3.1 Angle of incidence (θ_i)

Angle of incidence is the angle which an incident line or ray makes with a perpendicular to the surface at the point of incidence.

It can be found from (Duffie, Beckman and Worek, 2003);

$$\cos(\boldsymbol{\theta_i}) = cos(\emptyset)\cos(\beta) + \sin(\emptyset)\sin(\beta)\cos(\delta)\cos(\omega) + \sin(\delta)((\sin(\emptyset)\cos(\beta) - (\sin(\beta)\cos(\emptyset) \qquad \boldsymbol{eq(3.8)}$$

3.3.2 Zenith angle (θ_z)

Zenith angle is the angle between sun's ray and the perpendicular line to the horizontal plane,

Zenith angle can be found from (Duffie, Beckman and Worek, 2003);

$$\cos(\boldsymbol{\theta_z}) = cos(\emptyset)\cos(\delta)\cos(\omega) + \sin(\delta)\sin(\emptyset) \qquad \boldsymbol{eq(3.9)}$$

Monthly Averaged daylight average of hourly cosine Solar Zenith Angles can be found from NASA data base in the following table;

The determination of monthly averaged daylight average of hourly cosine solar zenith angles for each month is based on the "monthly average day".

Table 3-4**:** Monthly Averaged daylight average of hourly cosine Solar Zenith Angles

Lat 9.038 Lon 38.763	Jan	Feb	Mar	Apr	May	Jun	Jul	Aug	Sep	Oct	Nov	Dec
Average	0.53	0.58	0.62	0.64	0.64	0.64	0.64	0.64	0.63	0.59	0.59	0.51

3.3.3 Latitude (∅)

Latitude is a geographic coordinate that specifies the north–south position of a point on the Earth's surface as shown in figure 3-4.so,the coordinate of current project site is 9.038, 38.763.

Location = latitude 9.038 north facing , Longitude 38.763

3.3.4 Declination angle (δ)

The angular distance of the sun north (positive) or south (negative) of the equator. Declination varies through the year from 23.45° north to 23.45° south and reaches the minimum/maximum at the southern/northern summer solstices. The determination of monthly averaged declination for each month is based on the "monthly average day,

From (Duffie, Beckman and Worek, 2003) it can be calculated as;

$$\delta = 23.45 sin\left[\frac{360}{365}\,(284 + N)\right] \qquad \boldsymbol{eq}(\mathbf{3.11})$$

According to 22 years NASA Surface meteorology and Solar Energy data, the Monthly Averaged Declination (degrees) is listed in the Table 3-5.

Table 3-5 : Monthly Averaged Declination (degrees)

	Jan	Feb	Mar	Apr	May	Jun	Jul	Aug	Sep	Oct	Nov	Dec
Average	-20.7	-12.3	-1.81	9.70	18.8	23.0	21.2	13.7	3.09	-8.44	-18.1	-22.8

CHAPTER FOUR

4. Methodology

In this project detail study of SCPP is performed through combining, a theoretical design of technical parameters and simulation of the possible system main component using CFD tools. In order to reach to the final decision for desired 30 kW power out MATLAB simulation is used as an optimization tool. For the analysis of temperature and thermal characteristics inside the collector, ENERGY 2d is used as computational fluid dynamics (CFD) tool, it is also used to simulates the temperature variation in all dimension of Collector sides.

The actual prototype of the project is designed and developed to generate power out of 30 $watt$ maximum due to to the fact that it is constructed inside the campus workshop, so there is a geometrical constraint and also going beyond geometry selected for prototypes is not a feasible task to the machining equipment. So, after theoretical design, the geometry of the prototype is modeled using CATIA V5 and simulated using MATLAB.

4.1 Technical design

In the technical design of the solar chimney power plant, equation is developed by considering the basic concept of conservation of energy, thermodynamic, momentum and continuity equation. Figure 4.1 show the overall flow diagram of the technical design for the design of desired shaft power output .The following figure 4.1 show the instantaneous fluid flow through the collector beneath.

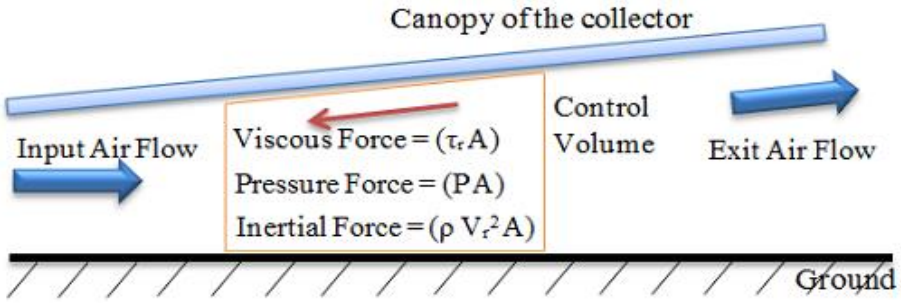

Figure 4-1: The force that acts inside the bottom of the collector(Mustafa, Al-kayiem and Gilani, 2015)

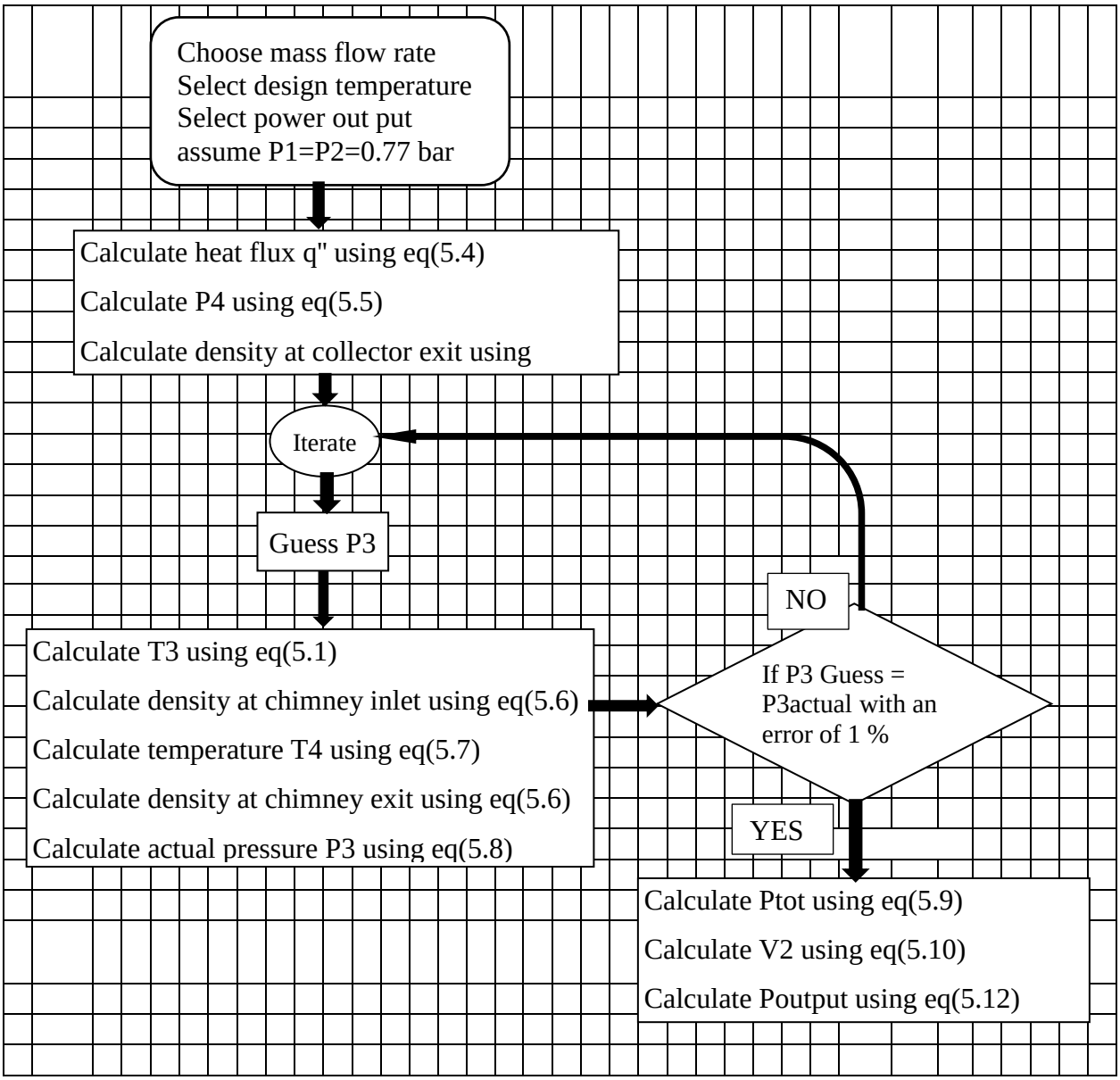

Figure 4-2:Flow diagram for technical calculation of power output

4.2 Numerical work

ENERGY 2D uses unsteady Navier-Stokes equation in their conservation form to solve set of equations. The instantaneous equation of mass (continuity), momentum, and energy conservation are presented below((Mustafa, Al-kayiem and Gilani, 2015)).

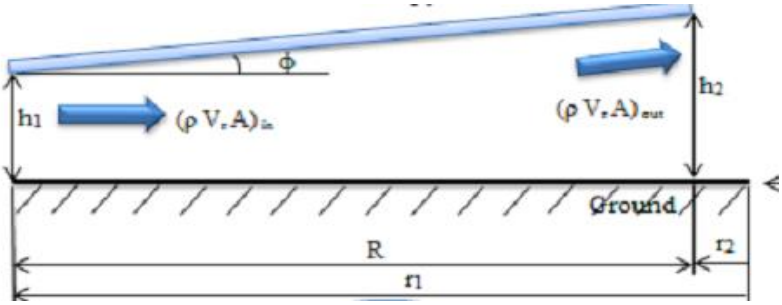

Figure 4-3: Radial section of collector

i. Continuity equation

Following figure 4.3, the continuity equation of the glazing written as;

$$(\rho_1 V_r A_{COLL})in = (\rho_2 V_r A_{COLL})out \qquad \boldsymbol{eq(4.1)}$$

ii. Momentum equation

From figure 4.1, Balance of forces of air flow inside the collector can obtain by applying Newton's second law for partial control volume:

$$\frac{\partial(\rho V_r^2)}{\partial r} = -\frac{\partial P}{\partial r} + \frac{\partial \tau_r}{\partial r} + \rho g \qquad \boldsymbol{eq(4.2)}$$

$\frac{\partial P}{\partial r}$:is the free streams of pressure gradient and shear stress, $\tau = \mu \frac{\partial V}{\partial r}$

iii. Energy conservation

The total energy per area of the collector is the sum of;

a. Heat gain into the glazing = heat lost from the glazing
b. Heat gain into the absorber = heat lost from the absorber
c. Heat gain into the fluid = heat lost from the fluid
d. Heat gain into the ground = heat lost from the ground

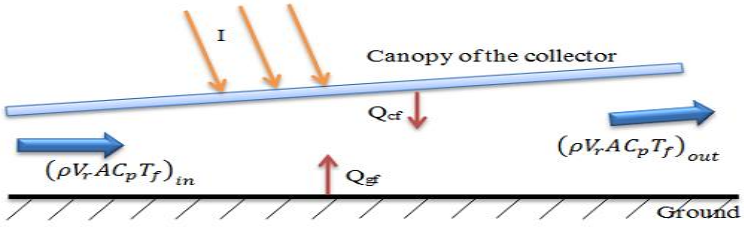

Figure 4-4:Energy balance diagram for solar chimney power plant system.

In this study, the flow of the fluid is due to natural convection. In the meanwhile, ENERGY 2D can model SCPP as a natural and mixed convection by considering buoyancy source term. Natural convection is when the fluid is driven by local density difference while mixed convection flows occurs when the convection of a fluid is driven by both a pressure gradient and buoyancy forces(Kaledin *et al.*, 2009)

4.2.1 Buoyancy forces

In this research, the flow is assumed to be single phase flow, then the fluid density is directly affected when there is temperature and pressure variations. These include all ideal gases and real fluids and when a multicomponent fluid is used. For Eulerian multiphase or particle tracking, it is also set even if all phases have constant density. In most gases, temperature variations significantly affect densities. A buoyancy reference temperature must be specified as an approximate average value of the expected domain density. For multiphase simulations, other factors must be considered(Kaledin *et al.*, 2009).

Buoyancy is normally driven by variations in density and this can arise from a number of sources. Some of the sources are:

- ✓ Variations in local temperature causing change in density; this is natural convection.
- ✓ Variations in the mass fraction cause density variations because each component usually has a different density. This occurs in multicomponent flows.
- ✓ Local pressure variations also cause changes in density in case of ideal gases and real fluids. These changes are often small and the buoyancy effect is usually not important in the flow. Buoyancy does not necessarily need to be modelled if there are no other sources of buoyancy.

Temperature variations which causes buoyancy forces in a mixed convection flow can be estimated by using the ratio of Grashoff and Reynolds Numbers

4.3 Geometry generation and modeling

The geometrical modeling of the SCPP is performed using CATIA V5 3D modeling and ENERGY 2D software. All the main component is designed and modeled separately as a part design in Catia 3d modeling. After the completion of each component the model is created using CATIA assembly interface is used as shown in Figure 4.5. The overall height of the plant is about 3.5 m above the ground and the collector diameter is 2 m horizontally. For this study straight chimney is used with constant diameter of 160 mm and collector height from ground is varied from 170 – 400 mm above the ground.

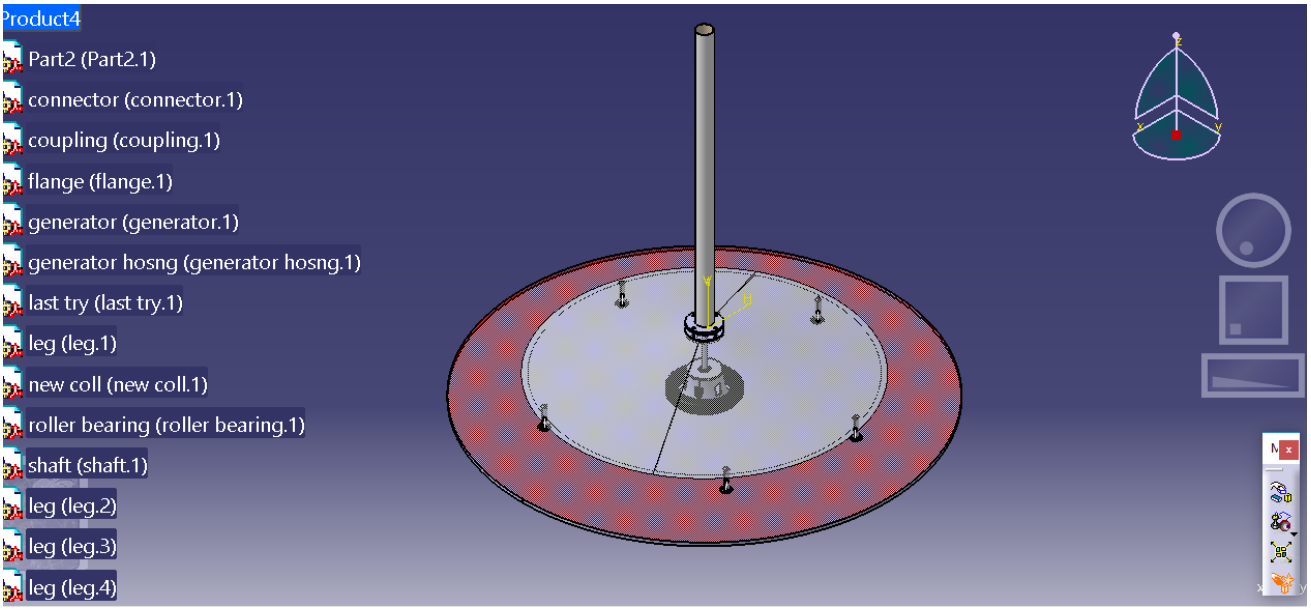

Figure 4-5: Catia modeling of solar chimney power plant

4.4 Transient analysis

After modeling of the SCPP, ENERGY 2D is to investigate the characteristics of the fluid flow inside the collector. For the simulations, steady state analysis is selected by creating an environment of updraft solar chimney power plant environment in the interface of ENERGY 2D. Draw or import the geometrical set of the SCPP in the front interface of the software as shown in the Figure 4.9. The air is used as a working fluid and gravity is set as 9.8 m/s^2.so the background condition is set as follow in the Figure 4.6. The heat source is set as sun and the mode of heat transfer is also set as convective as shown in Figure 4.7. The optical property of the glazing is set as follow in the Figure 4.8.

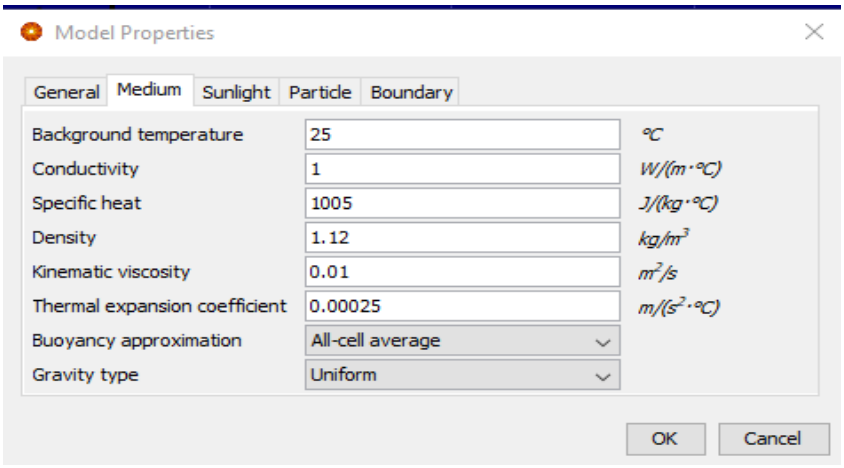

Figure 4-6 : Air background property

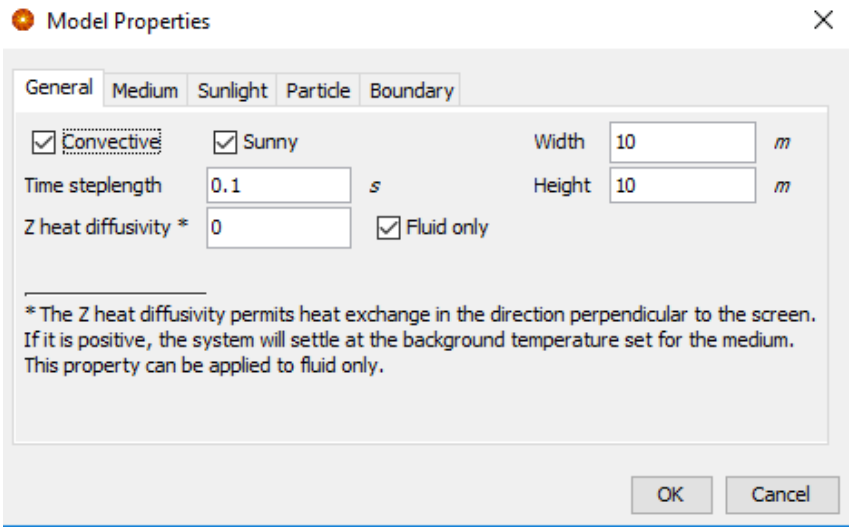

Figure 4-7: general properties of the SCPP.

In the figure 4.9, The thermal boundary condition for every side of the system is set as 25℃ and the Dirichlet constant temperature is selected for study.

After inserting all the boundary condition and thermal property of the system, insert all the thermocouple and heat flux sensor at each state in the system.

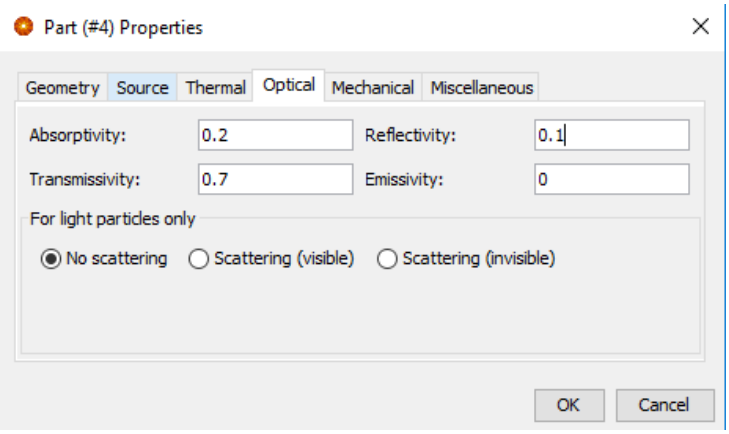

Figure 4-8: optical property of the glazing

Finally, the simulation will run for 6 *hours* a day in order to study the variation of temperature throughout the day, by varying the solar radiation data for every hour. Then sort the data using excel for further investigation.

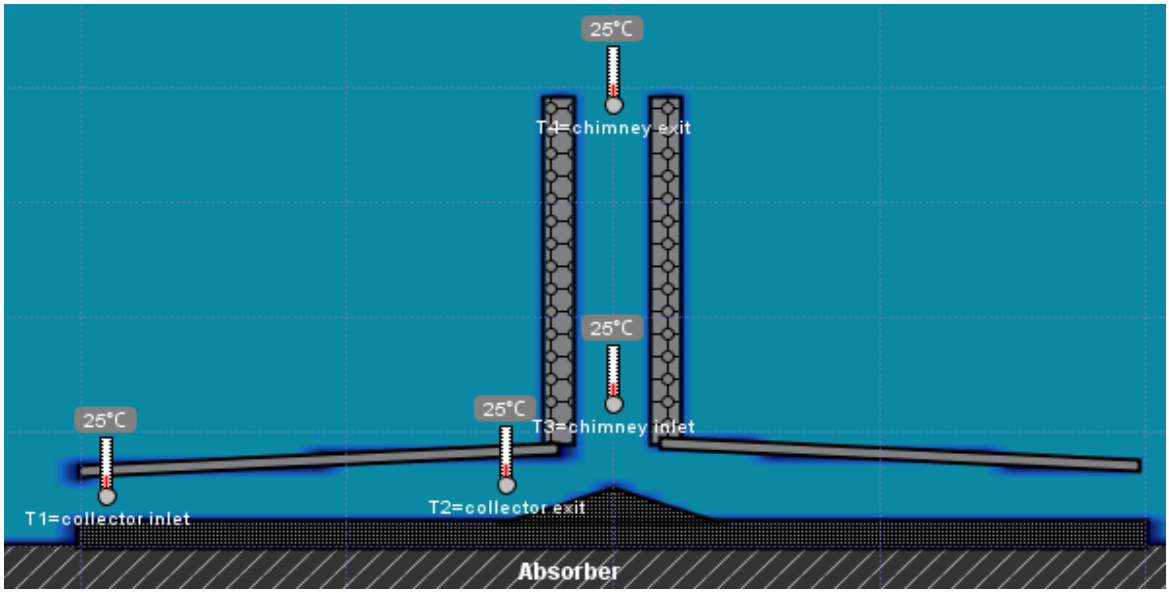

Figure 4-9: Thermal boundary condition

4.5 Experimental setup

The prototype development of solar chimney power plant is completely done in AAiT mechanical workshop, however due to the manufacturing machine equipment capacity there has been some changes from the initial geometrical dimension and structure.; in the following section the development of each component will be separately shown.

4.5.1 Support Leg Preparations and rolling of RHS pipe

For this particular prototype the total number of legs are three as shown in the picture below, this is selected so as to reduce air obstacle incoming to the collector beneath.

The three legs are welded perpendicular to the RHS steel at equidistance from the circumference of 2-meter RHS steel so that they can firmly hold the circular steel structure;

Material =20*30 RHS steel, adjustable leg Hight =0.4 meter(max) upto 0.17meter(min)

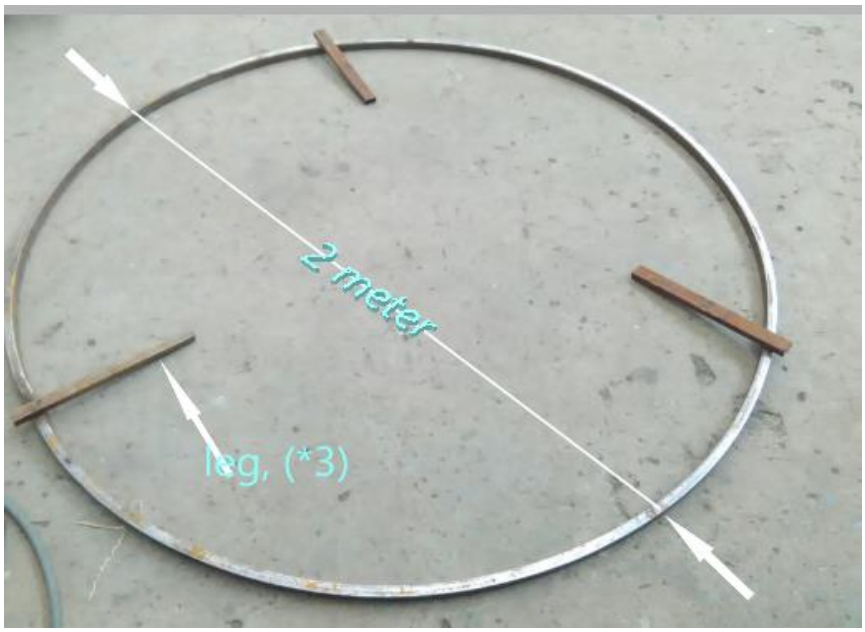

Figure 4-10: Rolled RHS Steel with leg

After final construction of the solar chimney power plant the height of the leg from the ground will be adjusted from its maximum height of $0.4\,meter$ to minimum height of $0.1\,meter$ accordingly on the requirement of the test.

4.5.2 Chimney load support

Chimney load support structure is constructed on the top of 2-meter circular RHS steel structure. Its basic function is to hold and distribute the load of the Pvc chimney pipe the will be connected on the top of the Circular RHS as shown on figure below;

Figure 4-11: chimney load support structure construction

4.5.3 Glazing support structure (glazing roof construction)

In this particular study the glazing of the solar chimney power plant is plastic thin film with higher transmittance property, so the support structure for this glazing is made of flat iron as shown below;

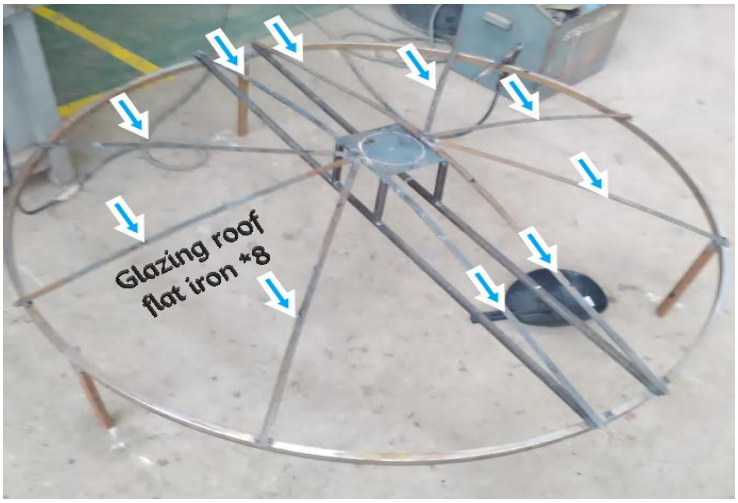

Figure 4-12: glazing roof steel structure

4.5.4 Collector air outlet preparation

In order to allow the air with less dense to escape through the middle of the glazing, $0.16-meter$ hole will be prepared as shown below,

Figure 4-13: Hole preparation as a collector exit

4.5.5 Chimney guiding

Due the height of the chimney ,4 wire guide has been used so as to keep the Pvc pipe Perpendicular to the roof. So, ring is hinged on the middle of the chimney and one side of wires are attached to it.

Figure 4-14: chimney guide hinged ring

4.5.6 Flange preparation

Flange in the system is used to connect the collector roof structure with the chimney(Pvc's); in this case four flange are used to connect the two main components (Steel roof and chimney).

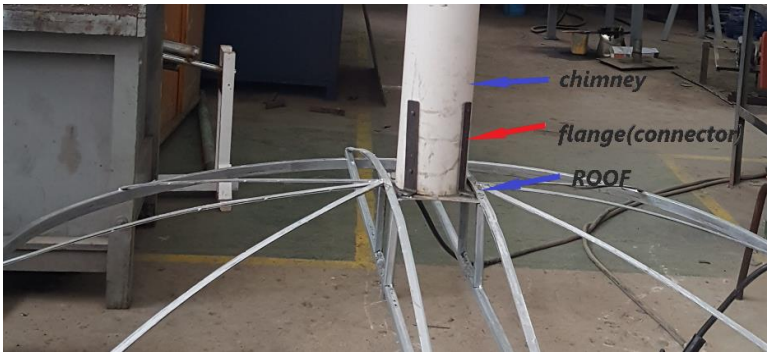

Figure 4-15: Flange(connector)

4.5.7 Covering the roof with Glazing material

After the completion of the entire mechanical work the roof is covered with the prepared plastic thin film.CM-43 glue is used to bind the plastic thin film with the flat iron as shown figure 4.16.

Table 4-1: optical property of plastic thin film(Diathermanous). [sun borne energy, Inc]

No	Optical property	Intensity	symbols	value
1	Transmittance	High	τ	0.82
2	Absorptance	Low	α	0.11
3	Reflectivity	Low for short wave	ρ	0.07

Figure 4-16: plastic thin cover glazing

4.5.8 Runner installation

The runner is installed in throat between the collector exit and the chimney inlet a shown below

Figure 4-17: Runner installation

4.5.9 Preparation of plant in the Testing site

Figure 4-18: plant at testing site

4.5.10 Sand placement at the collector beneath

Figure 4-19: sand placed beneath the collector

4.5.11 Storage bag placement beneath the collector

The thermal property of the selected dry earth surface is listed in the table 4.2.

Table 4-2: thermal property of earth dry absorber surface. [sun borne energy, Inc]

No	Property	Values
1	Density (kg/m^3)	1260
2	Thermal conductivity($W/m.K$)	2.51
3	Specific heat capacity ($kJ/kg.K$)	2.093
4	Thermal diffusivity(m^2/s)	0.705
5	Heat capacity ($J/m^3.K$)	3.5581

The storage bag place beneath the collector is black painted body that contain pebble enclosed inside in it.

Figure 4-20: thermal energy storage bag placement.

4.5.12 Data acquisition on experimental set up

Three **k-type thermocouple** temperature (PT -100) sensors are fitted at the inlet of the collector, middle of the collector and the exit of the collector. **National instrument** data logger is used to log the temperature obtained at all terminal.

Figure 4-21:Data acquisition of experimental set up.

4.5.13 K- Type Thermo Couple

In order to take the temperature measurement obtained across all three terminal, K-type thermo couple(three) wire is used as shown in figure below. The detail specification of the thermocouple is shown in the table below;

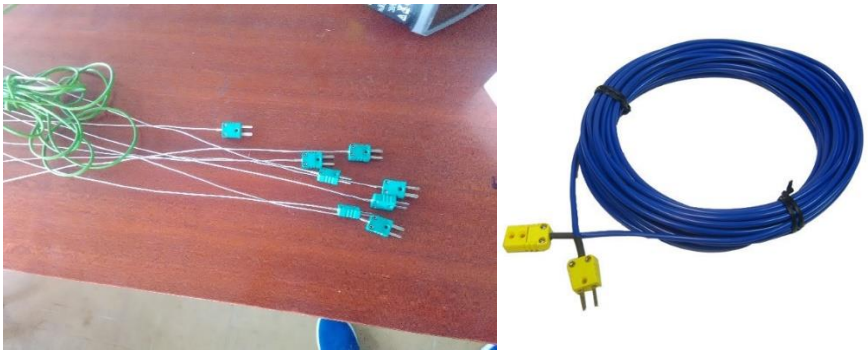

Figure 4-22: K- type thermocouple

Table 4-3: specification of k-type thermocouple

Standard range

Thermocouple type						Sheath						
Type	Working temperature	Mean sensitivity µV/°C	Thermoelectric wires			Material	Diameter in mm						
			Material		Code		0.25	0.34	0.5	1	1.5	2	3
							Code						
K	-200 up to 800°C -200 up to + 1000°C 1250°- 1370°C	41	NiCr (+) NiAl (-)	KP KN	2 AB	Ac I Special alloys	025 025 -	034 034 -	05 05 -	10 10 10	15 15 15	20 20 20	30 30 30
J	-40 up to + 750°C	55	Fe (+) Constantan® (-)	JP JN	2 FK	Ac	-	-	-	10	15	20	30
N	-40 up to + 1200°C - 40 up to + 1300°C	37	NiCrSi (+) NiSi (-)	NP NN	2 LM	I Nm Ig If	- - - -	- - - -	05 05 - -	10 10 10 10	15 15 15 15	20 20 20 20	30 30 30 30
E	-200 up to + 900°C	68	NiCr (+) Constantan® (-)	EP EN	2 AK	Ac	-	-	05	10	15	20	-
T	-200 up to + 350°C	51	Cu (+) Constantan® (-)	TP TN	2 CK	Ac	-	-	-	10	15	20	30

4.5.14 National instrument data logger (NI instrument)

In order to log the temperature reading from the thermo couple, NI instrument is used as shown in the figure below. The instrument has five slot, each capable of logging four different thermocouple temperature at a time. The data logger is capable power through electric cable with 25V voltage power input. The detail specification of the logger is listed in table below.

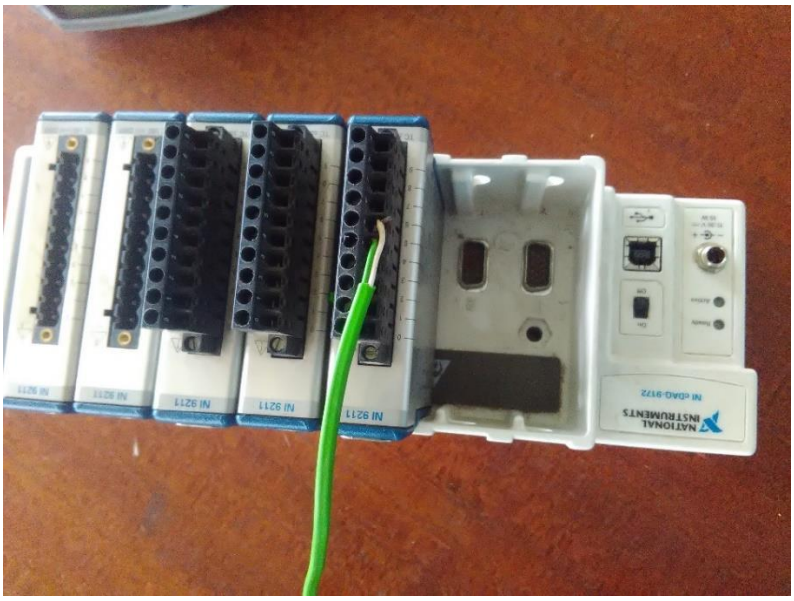

Figure 4-23: NI instrument data logger

Table 4-4: National instrument data logger specification

4.5.15 infrared-thermo couple

Infrared thermocouple is used to measure surface temperature of glazing, absorber, ground(sand) and pebble.

Figure 4-24:Infrared thermocouple

CHAPTER FIVE

5. Design of Solar Chimney Power Plant: A case study

In this chapter the design of solar chimney power plant will be studied theoretically and technically using the literature as a guide line. The designed power plant is expected to deliver shaft power output of 30 kW.The main factor that are considered as a design concern are;

i. The material selected for design is conducted by considering the availability of the manufacturing equipment in the campus.
ii. The whole component of the SCPP is considered based on the availability of material on local market with good efficiency.
iii. Most importantly cost of the material are also taken into consideration.

I. Initial design parameters

In this thesis the design power output is initially assumed to fulfil the power demand of particular application, since the experiment is conducted in Addis Ababa at latitude of 9.038N, 38.76E. However, this study is carried out in Addis Ababa with lower solar radiation capabilities, the actual plant is considered to be developed, for rural area around Gambela, Asosa, Adwa and Metema that are expected to have higher solar radiation intensity than Addis Ababa, thus recording the primary data at the experimental site is expected to match the actual site result.

In order to achieve the desire shaft power output from the system some assumption has been made as shown in the table 5.1.

Table 5-1:Design initial assumed parameters

No	Parameters	Symbol	Assumed
1	Turbine Shaft Power output	$Poutput$	30 kW
2	Mass flow rate	$\dot{m}$	0.08 kg/s
3	Temperature inside the collector	T_2	315 K

Following $eq(2.22)$ and $eq(2.23)$ an assumption can be made initially for pressure extraction ratio P_3/P_2 to be 0.82. The collector inlet pressure P1 is assumed as Patm=0.77 bar (atmospheric pressure at inlet @$T_1 = 25$℃).

5.1 Temperature of air at the entrance of chimney or turbine exit (T_3)

Since the work extraction process at the turbine is assumed to be an isentropic process T_3 can be calculated from the equation below;

$$T_3 = T_2\left(P_3/P_2\right)^{\frac{\gamma-1}{\gamma}} \qquad eq(\mathbf{5.1})$$

5.2 Heat Flux (q'') incident on a collector glazing

From the energy equation:

$$q''A_{gz} = \frac{1}{2}\dot{m} \times ({v_2}^2 - {v_1}^2) + \dot{m} \times Cp(T_2 - T_1) \qquad eq(\mathbf{5.2})$$

According to (Koonsrisuk and Chitsomboon, 2013) frictional effect is ignored since the velocity in this region is quite low. Because the flow is in the very low Mach number regime, the kinetic energy contribution can be safely neglected.

Then the above equation will be re-written as:

$$q''A_{gz} = \dot{m}Cp(T_2 - T_1) \qquad eq(\mathbf{5.2})$$

This shows that the mass flow rate is inversely proportional to the collector temperature rise, Since the mass flow rate is assumed to be constant, then collector area can be found from (Koonsrisuk and Chitsomboon, 2013) equation.

$$T_2 = T_1 + \frac{q''A_{gz}}{\dot{m}Cp} \qquad eq(\mathbf{5.3})$$

Assuming the overall heat loss coefficient of the collector $U_t = 5\ W/m2\ \ K$ and taking the average global radiation of 600 W/m^2.

$$q'' = (\alpha \times \tau) \times G_r - U_t \times \Delta T \qquad eq(\mathbf{5.4})$$

The heat flux q'' incident on the surface of the glazing is equal to 335 W/m^2.Now select chimney height of $H_{chim} = 17$ meter initially as a design input.

5.3 Pressure at The Chimney Exit (P_4)

Then the pressure P_4 at the chimney exit can be found from the following equation;

$$P_4 = P_1(1 - (\frac{g*H_{chim}}{Cp*T_1})^{Cp/R})) \qquad eq(\mathbf{5.5})$$

5.4 Pressure at the turbine exit (P_3)

The from previous assumption:

$P_3 = 0.82 \times P_2$

This result shows that the pressure P_3 is less than the pressure P_4 which violates the above solar chimney air standard cycle. This finally gives the idea that the initially assumed pressure ratio has to be greater than 0.82. Therefore, a new pressure ratio will be taken, this procedure will continue until P_3 is greater than the P_4.so, by considering the pressure ratio of $P_3 = 0.97 \times P_2$,the new Temperature T_3 at chimney inlet using $eq(4.1)$ is equal to $312.5K$.The assumed pressure will not directly have taken as it stands rather it will be compared with actual pressure P_3 in $eq(5.8)$.

From ideal gas constant the density of each state can be written as;

$$\rho_2 = \frac{P_2}{RT_2}, \rho_3 = \frac{P_3}{RT_3}, \rho_4 = \frac{P_4}{RT_4} \qquad eq(\mathbf{5.6})$$

5.4 Density of air at collector exit (ρ_2)

Using $eq(5.6)$, the density of air at the collector outlet can be found as;

$$\rho_2 = \frac{P_2}{RT_2} = 1.09\ kg/m3$$

5.5 Density of air at chimney inlet, (ρ_3)

Using $eq(5.6)$, the density of air at the chimney inlet or turbine exit can be written as follows;

$$\rho_3 = \frac{P_3}{RT_3} = 1.05\ kg/m3$$

5.6 Temperature of air at the chimney outlet (T_4)

In order to determine the density at the chimney outlet the temperature at that state should be known; According to the (Backström, Gannon and Backstro, 2000) equation of temperature $T4$ becomes;

$$T_4 = T_3 - g \times \frac{H_{chim}}{Cp} \qquad eq(\mathbf{5.7})$$

5.7 Density of air at the chimney outlet (ρ_4)

Then density at chimney exit is calculated as follow using eq (5.6)

$$\rho_4 = \frac{P_4}{RT_4}$$

5.8 Actual pressure at the turbine exit ($P_{3actual}$)

Now recall that the above parameter are computed by the assumed value of pressure P_3,so this result has to be validated by equation developed by (Backström, Gannon and Backstro, 2000) for actual P_3.

Pressure at the chimney inlet or turbine outlet;

$$P_{3actual} = P_4 + 0.5 \times (\rho_3 + \rho_4) \times g \times H_{chim} + \left(\frac{\dot{m}}{A_{gz}}\right)\left(\frac{1}{\rho_4} - \frac{1}{\rho_3}\right) \qquad eq(\mathbf{5.8})$$

Then from the above equation the pressure P_3 is found to be $0.964 \times 10^5 pascal$ from this result we can say that the assumed value of P_3 and calculated result are nearly the same. so, the assumed pressure ratio is taken as it is because of its good agreement with 1% error.

The tower (chimney) converts the heat-flow produced by the collector into kinetic energy (convection current) and potential energy (pressure drop at the turbine). Thus, the density difference of the air caused by the temperature rise in the collector works as driving force.

The theoretical power extracted by the turbine can be determined from the energy equation and Gibbs relation from classical thermodynamics:

5.9 Total pressure difference (Δp_{tot})

The lighter column of air in the tower is connected with the surrounding atmosphere at the base (inside the collector) and at the top of the tower, and thus acquires lift. The pressure difference Δp_{tot} is produced between tower base (collector outlet) and the ambient;

Pressure difference can be written as;

$$\Delta p_{tot} = g \times \int_0^{Hchim} (\rho_2 - \rho_4) dH$$

The **pressure difference** can be re-written as;

$$\Delta p_{tot} = g \times (\rho_2 - \rho_4) \times H_{chim} \qquad eq(\mathbf{5.9})$$

5.10 Air Velocity at The Collector Exit (V_2)

Then the velocity at the chimney entrance V_2 can be found from (Zhou, Xiao, *et al.*, 2010);

$$V_2 = \frac{G(\tau \times \alpha) \times A_{gz} - \beta(\Delta T_a \times A_{gz})}{\rho_{air} A_{chim} c_p (\Delta T)} \qquad eq(\mathbf{5.10})$$

Then, $\Delta T_a = (T_{pm} - T_1)$

I. Mean plate temperature (T_{pm})

$$T_{pm} = T_1 - \frac{Q_{useful}}{A_{gz} \times \beta \times F_R} \times (1 - F_R) \qquad eq(\mathbf{5.11})$$

II. Collector Heat removal factor (F_R)

$$F_R = \frac{\dot{m} \times C_P}{A_{gz} \times \beta} \left(1 - \exp\left(\frac{A_{gz} \times \beta \times F'}{\dot{m} \times C_P}\right)\right) \qquad eq(\mathbf{5.12})$$

5.11 Power output of the plant

The final shaft power output of the plant by considering the turbine efficiency of 85% is found as follows;

$$P_{out} = \eta_{tur} \times \Delta p_{tot} \times V_2 \times A_{gz} \qquad eq(\mathbf{5.13})$$

In the meanwhile, the desired power output is achieved at a certain height of a chimney and collector diameter, but in the last section of this study the optimum geometrical set will be investigated so that it can provide the same desired power output at minimized cost.

5.12 Design of thermal Storage Material

Thermal energy storage material is the material that stores the heat energy gained from sun radiation during the day and release it when there is no sun radiation(night).

Specifiactions:

Material: pebbles (stone granite)

Initial Design requirements(assumption);

- ✓ Pebble is assumed to store 70% solar energy transferred from the absorber plate.
- ✓ Pebble Charging time is assumed to be 6 hours per day and
- ✓ Discharging time of 5 hours per day.

Table 5-2. Thermal property of pebble. [Y. cengel]

No	Property	Symbol	Values
1	Density (kg/m^3)	δ	3300
2	Thermal conductivity($W/m.K$)	K	2.4-2.6
3	Specific heat capacity ($kJ/kg.K$)	C_P	0.88
4	Thermal diffusivity(m^2/s)	K_r	0.799-1.84

CHAPTER SIX

6. Transient analysis of solar chimney power plant

6.1 Heat transfer analysis in the SCPP system.

In order to do the heat transfer analysis in the system some assumption will be made as shown below.

i. Steady state condition.
ii. The air under the glazing roof is heated by the convective heat transfer between glazing, absorber plate and ground.
iii. Assume the system obeys the ideal gas law.
iv. Temperature is uniform in the vertical direction along the glazing beneath.
v. Radiation heat transfer between the glazing and the sky is neglected.
vi. Radiation heat transfer between the absorber plate and glazing is only during the day.
vii. Conduction Heat transfer between ground and pebble is neglected.
viii. Conduction heat transfer between pebble to absorber is neglected.

6.1.1 Partial layout of the SCPP system for the heat transfer analysis.

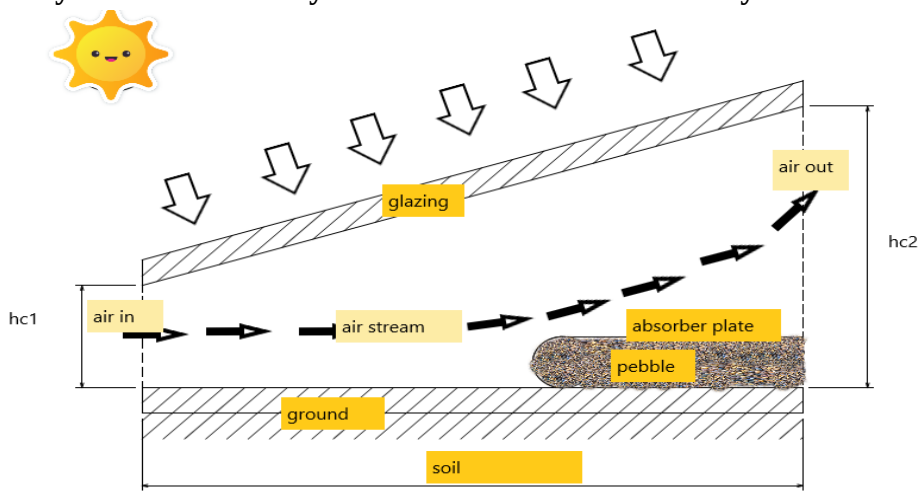

Figure 6-1: Solar chimney thermal analysis boundary layers. [appendix]

In the designed solar chimney power plant system, the heat transfer takes place between glazing and airstream, ground to airstream and storage system to air stream;

- Q_{cf} =convection heat transfer from glazing to air(fluid)
- Q_{gf} =convection heat transfer from ground to air
- Q_{ca} =covection heat transfer from glazing to ambient
- Q_{gc} =radiation heat transfer from ground to collector

So, from the above heat transfer mode we can now draw the heat balance at glazing, storage unit and airstream.

6.2 Theoretical analysis of the experiment

The analysis of the experiment is conducted by following the literature parameters that are developed by the different authors on the same basis.

6.2.1 Theoretical analysis of the collectors

i. Temperature of the air inside the collector during the night (T_a)

The temperature of the air inside the collector can be written as follows;

$$T_a = T_{pm} - T_1 \qquad eq(6.1)$$

ii. Collector efficiency factor(F')

Collector efficiency factor is the ratio of the actual thermal collector power to the power of an ideal collector whose absorber temperature is equal to the fluid temperature so this factor is found using $eq(5.12)$

6.2.2 The amount of heat stored by the pebble

The amount of heat stored from pebble is found from (Antia and Etuk, 2017)

$$Q_s = M_s \times C_{ps} \times T_{pb} \qquad eq(6.2)$$

The from the design specification the heat stored by the pebble is equal to 70% heat from the sun radiation incident on the absorber plate.

Again using the equation of (Antia and Etuk, 2017) the heat stored can be rewritten as;

$$Q_s = qq^{\cdot\cdot} \times A_{abs,surf} \times 0.7 \times t_{\,exposed\ to\ sun\ light} \qquad eq(6.3)$$

The re arranging $eq(6.2)$ and $eq(6.3)$,the **temperature of the pebble** can be found as;

$$T_{pb} = \frac{qq^{\cdot\cdot} \times A_{abs,surf} \times 0.7 \times t_{\,exposed\ to\ sun\ light}}{M_s \times C_{ps}} \qquad eq(6.4)$$

Solar intensity reaching the pebble is written as;

$$qq'' = G(\tau\alpha) \qquad eq(6.5)$$

6.2.3 The amount of heat gain by the pebble(Antia and Etuk, 2017)

$$Q_{gain} = M_s \times C_{ps} \times (T_{pb} - T_1) \qquad eq(6.6)$$

A. Heat gain per second

The amount of heat gain per second for the storage material is found from the following equation(Antia and Etuk, 2017);

$$Q_{charged} = \frac{heat\ gain\ by\ the\ pebble\ (Q_{gain}, kJ)}{avarage\ sunshine\ hour(sec)} = \frac{M_s \times C_{ps} \times (T_{pb} - T_1)}{t_{sunshine\ hour}} \qquad eq(6.7)$$

B. Heat discharged per second

The amount of heat discharged to the air from heat stored in the pebble is found from (Antia and Etuk, 2017)

$$Q_{discharged} = \frac{heat\ stored\ in\ a\ pebble(Q_s, kJ)}{required\ discharged\ time(sec)} = \frac{M_s \times C_{ps} \times T_{pb}}{t_{req.}} \qquad eq(6.8)$$

Note: for this design the rate of heat discharge only occurs during the night time when the ambient temperature drops down drastically following the sun radiation.

C. **Heat gain by the air from the thermal storage during night**.

Then the heat gain by the pebble is calculated using**,** $eq(6.9)$ (Antia and Etuk, 2017)

$$Q_{air} = \dot{m} c_p (T_a - T_1) \qquad eq(6.9)$$

6.3 Design of the Area under the Glazing as an Absorber surface.

The area under the collector glazing is ground but some of the area of the Ground is covered with thermal energy storage bag. The area which is not covered by the thermal storage bag act as the energy absorbing units for the solar chimney power plant.

Specifications:

Surface type: earth dry

Selection criteria:

Have relatively desired thermal property than other material like concrete, brick floor and black granite stone at lower cost,

The thermal property of the selected dry earth surface is listed in the table below.

Table 6-1: thermal property of earth dry absorber surface. [sun borne energy, Inc]

No	Property	Symbol	Values
1	Density (kg/m^3)	δ	1260
2	Thermal conductivity ($W/m.K$)	K	2.51
3	Specific heat capacity ($kJ/kg.K$)	Cp	2.093
4	Thermal diffusivity (m^2/s)	Kr	0.705

6.4 Energy Balance of the Partial Section of the SCPP

6.4.1 Heat balance for glazing

In the glazing the heat transfer modes are shown below

i. Radiation heat transfer from glazing to ambient**,**
ii. Convection heat transfer from glazing to air stream;
iii. Radiation heat transfer from ground to glazing**,**
iv. Radiation heat transfer from absorber plate to glazing,

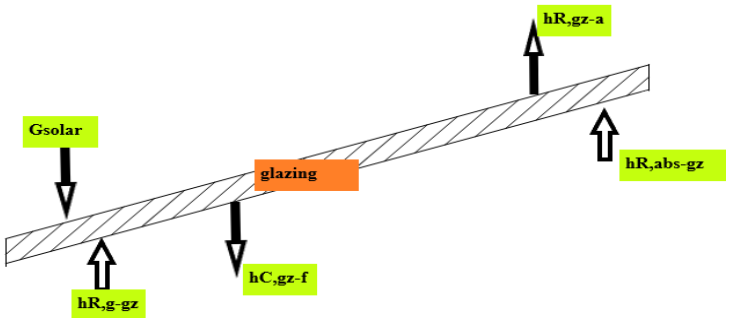

Figure 6-2: Heat balance of glazing(collector)

The from conservation of energy;

Heat gain into the glazing = heat lost from the glazing

$$\left(G_{sol}\,\alpha_{gz} + h_{R,g-gz}(T_g - T_{gz}) + h_{R,abs-gz}(T_{abs} - T_{gz})\right) \times A_{gz} =$$

$$(h_{C,gz-f}(\mathrm{T}_{gz} - T_f) + h_{R,gz-a}(T_{gz} - T_a) \times A_{gz} \qquad eq(6.10)$$

6.4.2 Heat balance for air stream

The rate of heat transfer into the fluid (air stream) from the glazing, ground and absorber by radiation and convection is balanced in the figure 6.3 as shown below.

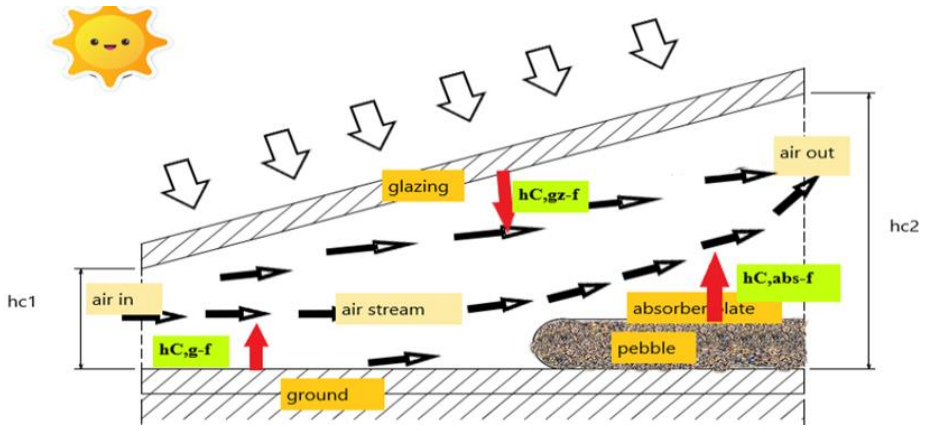

Figure 6-3: heat balance of the airstream [source: appendix]

$$h_{C,g-f}(T_g - T_f)(A_{gz} - A_{abs}) + (h_{C,gz-f})(T_{gz} - T_f) \times (A_{gz}) +$$

$$(h_{C,abs-f}(T_{abs} - T_f) \times (A_{abs,surf}) = \dot{m}C_P(T_{f,out} - T_{f,in}) \times (A_{out} - A_{in}) \qquad \boldsymbol{eq(6.11)}$$

Note: $A_{gz} = (r_{gz}^2 - r_{chim}^2)$ and $A_{abs,sur} = \pi \times r_{storage\ bag}^2$

$A_{out} = 2 \times \pi \times r_{gz} \times h_{c2}$ and $A_{in} = 2 \times \pi \times r_{gz} \times h_{c1}$

6.4.3 Heat balance of absorber plate (or storage bag)

Assumption considered in heat balance of absorber plate

- ✓ During the day there is no heat transfer by conduction from pebble to absorber
- ✓ No radiation heat transfer heat transfer from absorber to the glazing during day.

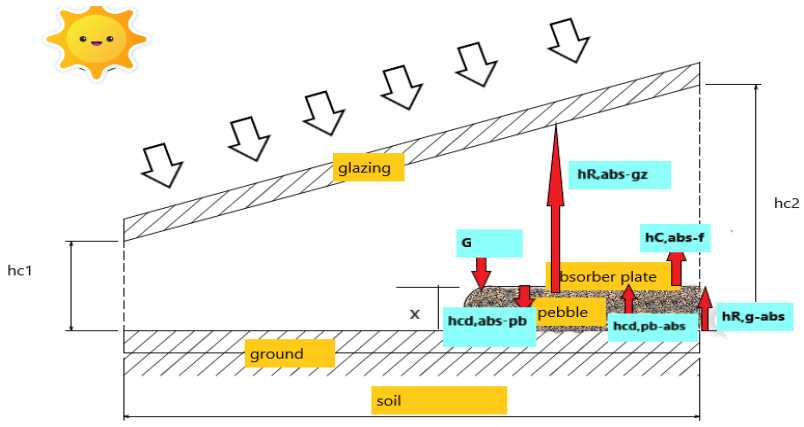

Figure 6-4: heat balance of absorber plate

$$\left(G_{sol} \times (\tau\alpha) + E_{eff}\sigma \times \left(T_g^4 - T_{abs}^4\right)\right) \times \left(A_{strg,crosssect}\right) =$$

$$\left(\left(-\frac{kA_{stor,sur}\left(T_{abs}-T_{pebble}\right)}{x} + \left(h_{C,abs-Tf}\right) \times \left(T_{abs} - T_f\right)\right) \times \left(A_{abs}\right)\right. \qquad \boldsymbol{eq(6.12)}$$

The absorber material property that are available on the market are show in the table below

Table 6-2 : Absorber material property

Material	Absorptivity (α)	Reflectivity (τ)	Emittance (Ɛ)	Transmittance/ absorptance (τα)
Red, Brick	0.55	0.45	0.9	0.6
concreate	0.6	0.4	0.92	0.6
Flat black	0.96	0.04	0.88	1.09
Granite	0.55	0.45	0.44	1.25

So flat black absorber plate is selected due to its higher amount of absorptance property and low reflective property.

6.4.4 Pebble heat balance

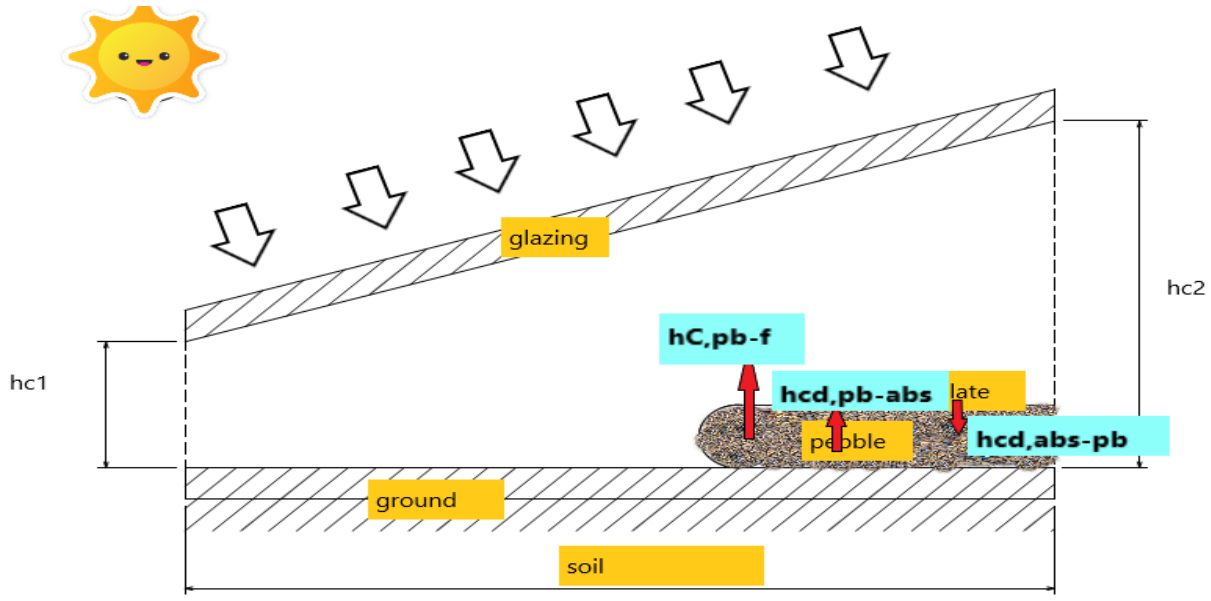

Figure 6-5: heat balance of pebble (thermal storage)

The heat gained by the pebble by conduction from absorber plate to pebble is equal to the heat loss from the pebble to the absorber plate.

$$\frac{-k_{abs}\times A_{abs,surf}\times(T_{abs}-T_{pebble})}{(\Delta x)} = V_{bed}(1-\epsilon)\rho_{pebble}\times C_{p,pebble}\frac{(T_{pebble}-T_{abs})}{\Delta t} \qquad \boldsymbol{eq(6.13)}$$

Table 6-3 : Natural heat absorbing material

Material	Density (kg/m^3)	Thermal conductivity (W/mK)	Specific heat capacity $(J/kg.k)$
Concreate stone	1900-2500	2-3.5	900-1000
Black granite stone	3000	2-2.2	800
Pebble stone	3300	2.4-.26	880

For the study under the research pebble stone is selected due to its availability and good thermal storage property.

6.4.5 Ground heat balance

$$Heat\ gained\ from\ the\ ground\ =\ heat\ loss\ from\ the\ ground$$

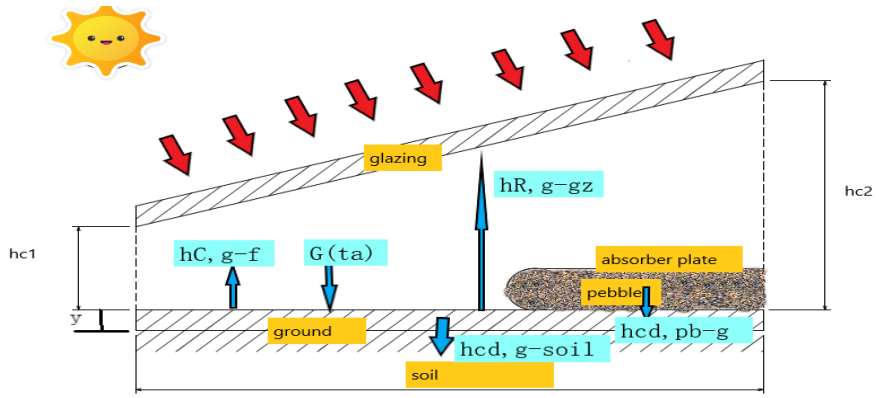

Figure 6-6: Heat balance of ground energy balance

Now assume the conduction heat transfer from the ground the to the soil is assumed to be zero due to the change in temperature is approximately zero.

$$G(\tau\alpha)\left(A_{gz} - A_{stor,surf}\right) + \left(\frac{-K\,A_{sur,strg}\left(T_{pebble} - T_g\right)}{\Delta x}\right) = h_{C,g-f}\left(T_g - T_f\right) + \varepsilon_{eff}\sigma\left(T_g^4 - T_{gz}^4\right) \qquad \boldsymbol{eq(6.13)}$$

Table 6-4: thermal property of ground

Material	Density (kg/m^3)	Specific heat capacity $(J/kg.K)$	Heat capacity (kJ/m^3K)	Thermal conductivity (W/mK)	Thermal diffusivity(m^2/s)
Earth dry	1260	2093	3.5581	2.51	0.705
Earth wet	1700	795	1.0017	0.25	0.25
Stone, granite	2640	820	2.1648	1.73-3.98	0.799-1.84
Stone, limestone	2500	900	2.25	1.26-1.33	0.56-0.591
Stone, marble	2600	800	2.08	2.07-1.33	0.995-1.493
Stone, sandstone	2200	710	1.56	1.83	1.172

For the thermal analysis of the ground the earth is considered as dry in the particular construction site.

6.5 Heat loss coefficients

The energy loss through the component in solar chimney power plant system is due to radiation, convection and conduction. In Some component heat loss through different mode is assumed to be zero due to its neglected temperature difference.

The heat loss coefficient in all components are;

i. heat loss coefficient by Radiation from glazing to ambient($\boldsymbol{h_{R,gz-a}}$),
ii. Convection heat transfer from glazing to air stream($\boldsymbol{h_{C,gz-f}}$),;
iii. Radiation heat transfer from ground to glazing($\boldsymbol{h_{R,g-gz}}$),
iv. Radiation heat transfer from absorber plate to glazing($\boldsymbol{h_{R,abs-gz}}$),

6.5.1 From glazing to the ambient

In this study the heat loss coefficient from glazing to the ambient is considered thermal loss from by radiation and convection but the amount of heat transfer by convection is neglected due to its low temperature exchange on the top of the glazing with the air above it.

a. Heat loss coefficient by Radiation from glazing to ambient,(Kumar and Mullick, 2012)

$$h_{R,gz-a} = \sigma \varepsilon_g (T_{gz}^4 - T_a^4)(T_{gz} + T_a) \qquad \boldsymbol{eq(6.14)}$$

Temperature of glazing can be found from (Aurélio, 2010)

$$T_{gz} = T_a + h_w^{-0.42}(0.61\varepsilon_p + \frac{T_P}{505} - 0.27)(T_P - T_a) \qquad \boldsymbol{eq(6.15)}$$

The wind heat transfer coefficient can be found from (Rabadiya and Kirar, 2012),

For wind direction ranging from $0°, 45°, 90°$ they obtained by the following relations

$$h_w(\text{W/m2-K}) = \left\{ \begin{array}{c} when\ i = 0° \\ 8.3 + 2.2\,\text{V} \quad \text{for } 0.8 < \text{V} < 6.7\frac{\text{m}}{\text{s}}. \\ when\ i = 45° \\ 7.9 + 2.6\,\text{V} \text{ for } 0.6 < \text{V} < 6.2\frac{\text{m}}{\text{s}} \\ \text{i} = 90 \\ 6.5 + 3.3\,\text{V} \quad 0.8 < \text{V} < 6.2\,\text{m/s} \end{array} \right\}$$

Now assume that the wind direction is in the range of 0° and low wind speed range the select

$$h_w = 8.3 + 2.2\,V \qquad \boldsymbol{eq(6.16)}$$

b. heat loss coefficient by convection from glazing to ambient ($h_{c,gz-a}$)

$$hc, gz - a = \frac{0.243+0.0015 \times V1(\rho 1\, Tm/\mu g \Delta T)^{1/3}}{(\mu\, Tm/g\Delta T\, Cp\, k^2 \rho 1^2)^{1/3}} \qquad \boldsymbol{eq(6.17)}$$

where $\Delta T = T_{gz} - T_a$

6.5.2 From glazing to the air stream

The thermal loss between the glazing and air stream beneath the collector is through radiation and convection, thus the heat loss coefficient through radiation and convection can be found (Mustafa, Al-kayiem and Gilani, 2015),

a. Heat loss coefficient by convective from glazing to airs stream

Then the convective heat transfer coefficient will be calculated from Gnietinski's eqn. of turbulent flow;

$$hc, gz - f = \frac{(f/8)(Re-1000)Pr}{1+12.7(f/8)^{\frac{1}{2}}(pr^{\frac{2}{3}}-1)}(kair/dh) \qquad \boldsymbol{eq(6.18)}$$

Take: $pr = 0.71$,for dry fluid

Reynold number can found from the equation of (Rabadiya and Kirar, 2012)

$$Re = \rho V_2 Dchim/\mu \qquad \boldsymbol{eq(6.19)}$$

Friction factor is found from(Kumar and Mullick, 2012)

$$f = (1.82 log_{10} Re - 1.64)^{-2}$$

6.5.3 From glazing to the ground

From the glazing to the ground heat is lost through radiation, however its loss is low then it is assumed to be zero/neglected.

6.5.4 From absorber plate to fluid

The heat transfer mode from the absorber plate to the air stream is by convection. Thus, the convection heat loss coefficient is found from,

a. The convection heat loss coefficient from absorber plate to the fluid

The convection heat loss coefficient from absorber plate to the air steam is calculated using Gnietinski's eqn.

$$hc,abs-f=\frac{(f/8)(Re-1000)Pr}{1+12.7(f/8)^{\frac{1}{2}}(pr^{\frac{2}{3}}-1)}\left(\frac{kabs}{dh}\right) \qquad \boldsymbol{eq(6.20)}$$

b. Heat loss coefficient by radiation from absorber to the glazing

The radiation heat loss coefficient from absorber plate to the plastic glazing is found as;

$$h_{R,abs-gz}=\sigma\varepsilon_{abs}\left(T_{abs}^4-T_{gz}^4\right)\left(T_{abs}+T_{gz}\right) \qquad \boldsymbol{eq(6.21)}$$

c. Heat loss coefficient by conduction between absorber plate and pebble

The heat loss by conduction through pebble to the pebble is modeled by conduction heat loss coefficient as follows;

$$h_{cd,abs-pb}=\frac{-k_{abs}\times(T_{abs}-T_{pebble})}{(\Delta x)} \qquad \boldsymbol{eq(6.22)}$$

6.5.5 Ground heat loss coefficient

From ground heat is transferred to the fluid by convection, heat by radiation to the glazing and heat transfer by radiation to the absorber plate. But the radiation heat transfer coefficient from the ground are neglected

a. Convection Heat transfer coefficient from ground to the air stream

The convection heat transfer coefficient from the ground and the air stream beneath the collector is found by;

$$hc,g-f=\frac{(f/8)(Re-1000)Pr}{1+12.7(f/8)^{\frac{1}{2}}(pr^{\frac{2}{3}}-1)}(kgr/dh) \qquad \boldsymbol{eq(6.23)}$$

6.5.6 Pebble heat loss coefficient

Heat is transferred in the pebble to the absorber plate by conduction and to the air through convection.

a. Convection heat loss coefficient

$$hc,pb-f=\frac{k\times Nu}{\delta} \qquad \boldsymbol{eq(6.24)}$$

where:$\delta=\pi\times Dpebble/2$

The Nusselt's number can be found from equation $\boldsymbol{eq(6.25)}$

$$Nu = 2 + \frac{0.589\ Ra^{1/4}}{(1+(0.469/Pr)^{9/16})^{4/9}} \qquad \boldsymbol{eq(6.25)}$$

Rayleigh numbers: A measure of the instability of a layer of fluid due to differences of temperature and density at the top and bottom;

$$Ra = \frac{g \times Br}{vKr}[T_{pb} - T_{amb}] \times \delta^3 \qquad \boldsymbol{eq(6.26)}$$

b. Conduction heat loss coefficient

Heat is loss by conduction to the absorber plate shown in $\boldsymbol{eq(6.27)}$. But this transfer can occur only during the night.

$$h_{cd,abs-pb} = \frac{-k_{abs} \times (T_{pb} - T_{abs})}{(\Delta x)} \qquad \boldsymbol{eq(6.27)}$$

6.6 Over all heat Loss Coefficient (U_t)

The overall heat loss coefficient of SCPP system is written as shown in the $\boldsymbol{eq(6.28)}$ below:

$$\boldsymbol{U_t} = \left\{\frac{1}{h_{c,gl-f} + h_{r,gl-g} + h_w + h_{r,gl-a}} + \frac{1}{\boldsymbol{h_{c,g-f} + h_{r,g-gl} + h_{cd,g-abs}}} + \frac{1}{\boldsymbol{h_{c,abs-f} + h_{r,abs-gl} + h_{cd,abs-pb}}}\right\}$$

$$\boldsymbol{eq(6.28)}$$

6.7 Total efficiency of the plant.

The total efficiency of the plant is the product of collector efficiency, chimney efficiency and turbine efficiency(El-ghonemy, 2016)

$$\eta_{tot} = \eta_{coll} \times \eta_{chim} \times \eta_{turb} \qquad \boldsymbol{eq(6.29)}$$

Where;

η_{coll}= the effectiveness of the collector to convert solar radiation into heat.

η_{chim}=effectiveness of the chimney to convert heat delivered by the collector into flow energy

η_{turb}=effectiveness of the wind turbine to convert kinetic energy of the flow into mechanical energy

6.7.1 collector efficiency

The collector efficiency is the ratio of heat output from the collector per solar radiation(G) received per unit area of a collector and expressed as shown below;

$$\eta_{coll} = \frac{\dot{Q}}{G \times A_{COLL}} = \frac{\dot{m} \times Cp \times (\Delta T)}{G \times A_{COLL}} \qquad \boldsymbol{eq(6.30)}$$

According to(Koonsrisuk and Chitsomboon, 2013),the Heat output $\dot{Q}$ under steady conditions can be expressed as a product of the mass flow rate $\dot{m}$, the specific heat capacity Cp of the air and the temperature difference between collector inflow and outflow ($\Delta T = Tout - Tin$)

6.7.2 Efficiency of Chimney

Chimney efficiency means the conversion of heat into kinetic energy is determined by the ambient temperature at the ground level and the height of the chimney. Whenever talking about the efficiency of the chimney it should be noted that it has extremely lower value. For example, according to (Mullett LB,1987) with a chimney height of 1000 m and standard conditions for temperature and pressure, the chimney efficiency achieves the maximal value of 3%.it can be expressed as shown below in $\boldsymbol{eq(6.31)}$.

$$\eta_{chim} = \frac{g \times H_{chim}}{Cp \times Tamb} \qquad \boldsymbol{eq(6.31)}$$

Following equation $\boldsymbol{eq(6.31)}$ it is clear seen that the chimney efficiency is dependent on chimney height than flow speed and collector temperature rise.

6.7.3 Efficiency of the turbine

The role of the turbine is the efficient power transformation of air current in the system into mechanical output in the form of rotational energy.

It can be expressed as shown in $\boldsymbol{eq(6.32)}$;(Hanna *et al.*, 2016)

$$\eta_{turb} = \frac{V_2^2}{2 \times Cp \times T_{23} \times \eta_{chim}} \qquad \boldsymbol{eq(6.32)}$$

CHAPTER SEVEN

7. Result and discussion

7.1 MATLAB result for solar chimney power plant

In this study, MATLAB is used to study the optimum geometrical size of main component of SCPP that provides maximum power put. In the analysis the influence of different parameter on the power output has been investigated as shown in the following sections.

7.1.1 Power output vs diameter of glazing(collector)

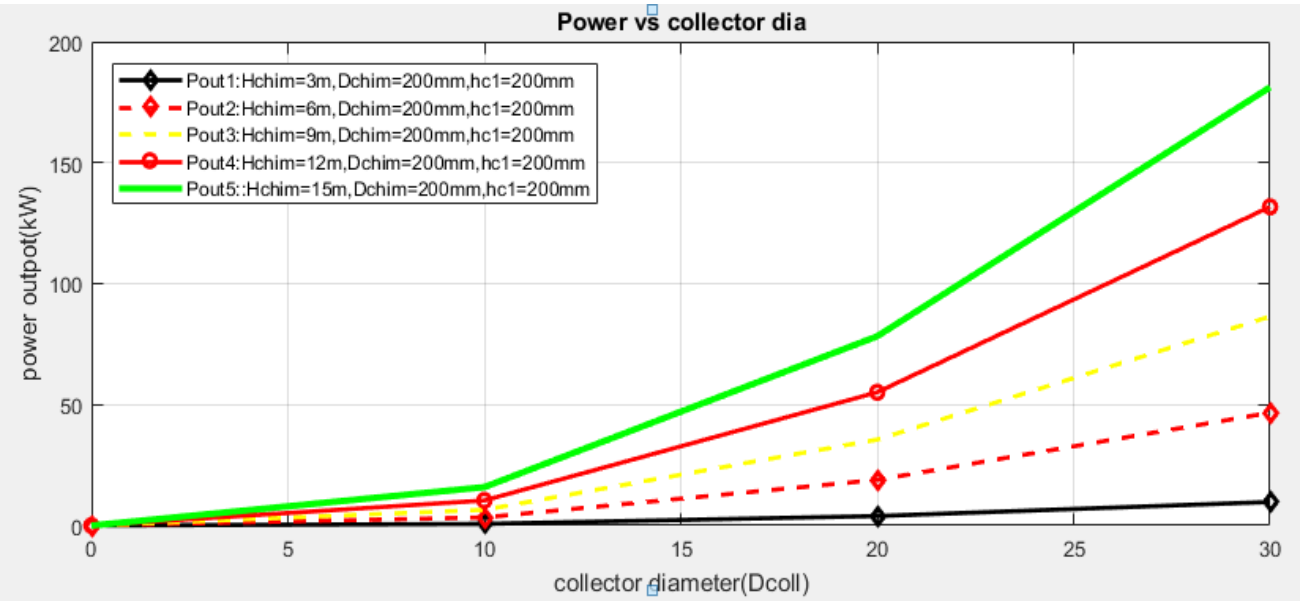

Figure 7-1:Power output vs diameter of glazing(collector)

From the above simulation it is observed that increasing the diameter of a chimney will results an increase in total power output at a fixed- parameters of chimney diameter, height of collector from the ground and chimney height.

According to figure 7.1, in order to achieve the designed power output of 30 kW from the plant, a chimney height must be more than 10 meters.

Following the above simulation, table 7.1 is drawn for the possible geometrical configuration of the plant that provides 30 kW power output.

Table 7-1: Geometry selection for 30kW for power output

Options	Geometry					
	Hchim	*hc1*	*Dcoll*	*Dchim*	*Power(kW)*	*Remark*
1	3 meters	200 mm	30 meters	200mm	15 kW	Less
2	6 meters	200 mm	28 meters	200mm	30 kW	
3	9 meters	200 mm	22 meters	200mm	30 kW	
4	12 meters	200 mm	16 meters	200mm	30kW	
5	15 meters	200 mm	13 meters	200mm	30kW	

7.1.1 Height of chimney versus power output

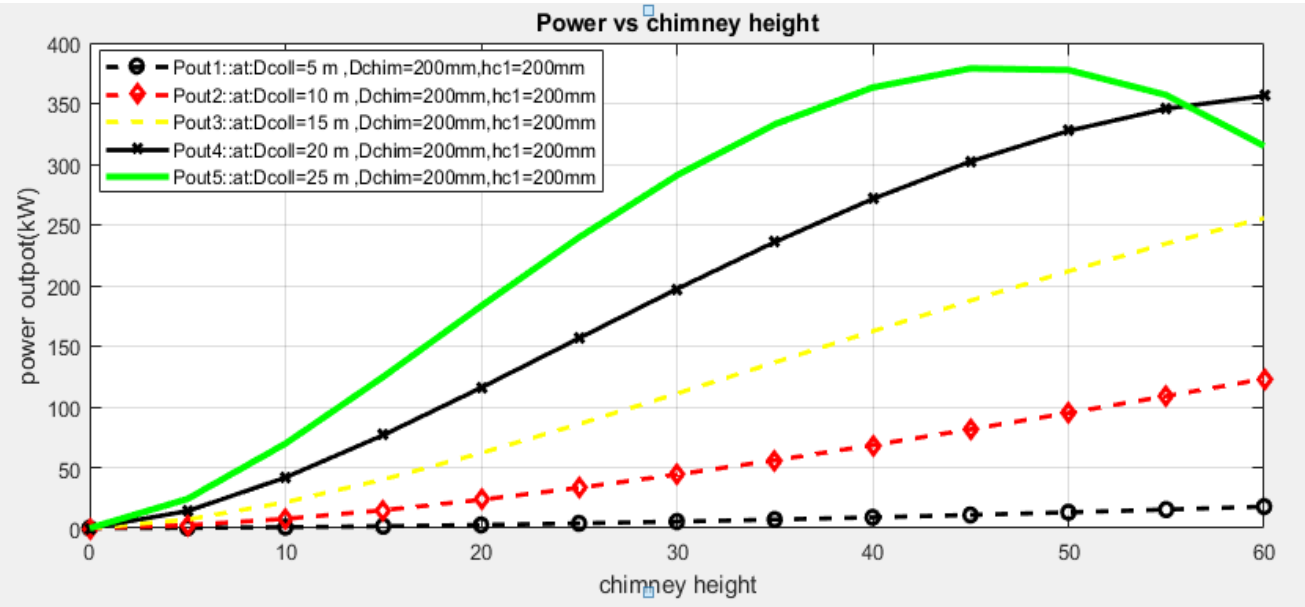

Figure 7-2: height of a chimney vs power output

The simulation in the figure 7.2 was conducted by varying the height of chimney and diameter of collector while fixing the indicated parameters. This simulation is useful so as to show the optimum chimney height that provides the maximum power output for a certain collector diameter, chimney height and collector height from the ground.

Table 7-2: Chimney height selection for $30kW$.

	Geometry					Remark
Option	$Dchim$	$Dcoll$	$Hchim$	$hc1$	Power (kW)	
1	200mm	5 meters	60 meters	200 mm	21 kW	less
2	200mm	10 meters	28 meters	200mm	30 kW	
3	200mm	17 meters	17 meters	200mm	30 kW	selected
4	200mm	20 meters	9 meters	200mm	30 kW	
5	200mm	25 meters	7 meters	200mm	30 kW	

So, using table 7.1 and table 7.2, conclusion has been made on the selection of the geometrical size of chimney height and collector diameter for the desired power output of 30 kW based on the factor like, cost of construction, construction simplicity and site area coverage for the plant.

It is concluded that option three (3) is the best option for the application of 30 kW power output, with chimney height of 17 $meters$ and 17 $meter$ of collector diameter. The selected collector diameter is relatively less compared to the other option as the same time by keeping the height of chimney which also require less cost for construction and for ease of simplicity as well.

However, by modifying the chimney height to 45 $meters$ and the collector diameter of 25 meter more than $350kW$ power output can be achieved by keeping the indicated fixed parameters.

On the other hand, using the selected geometry of chimney height and collector diameter as a fixed parameter and making a change on the fixed parameters will result more power output. In the figure 7.3, it clearly seen that increasing the chimney diameter from 0.2 meter up to 1 meter will result in increase more than 4 KW from the designed.

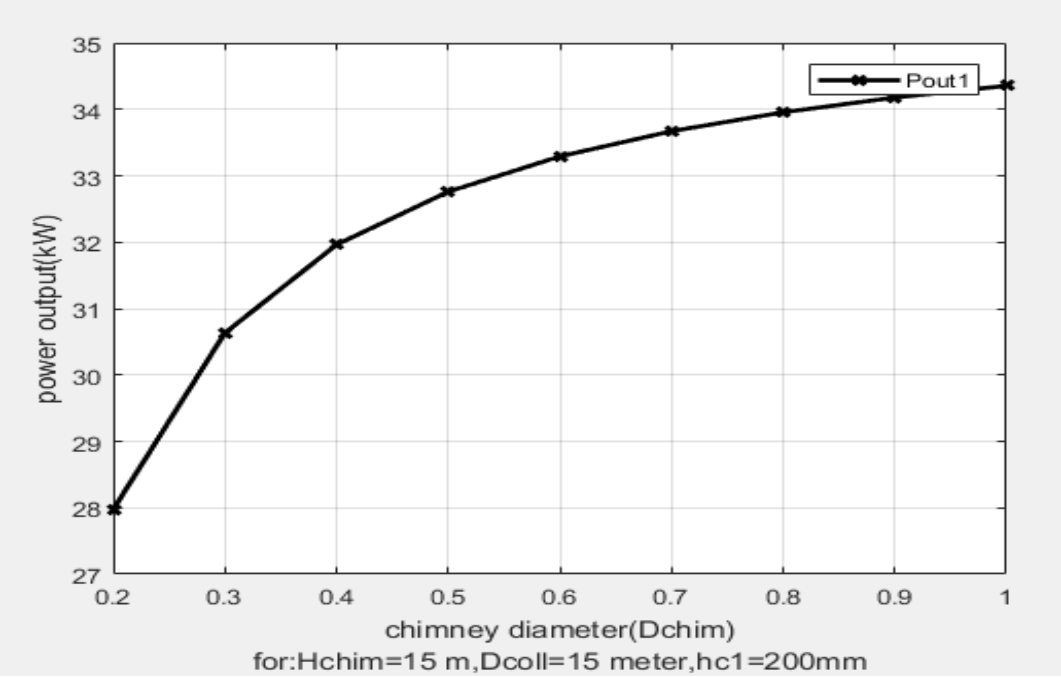

Figure 7-3: chimney height vs power at various chimney diameter

Figure 7.4, shows the optimum chimney height that provides optimum power output at fixed height of the collector from the ground at the same time with varying chimney diameter and collector diameter. The investigation was carried out by running the chimney height up-to 600 $meter$.In the table 7.3, the optimum chimney height for selected geometrical set are listed as shown below.

Table 7-3:optimum chimney height for different chimney diameter and collector diameter.

options	$Dcoll$	$Dchim$	hc1	Optimum chimney height	Max.Pout.
1	5 meters	0.2 meters	200 mm	600 meters	800 kW
2	10 meters	0.4 meters	200 mm	500meters	2 MW
3	15 meters	0.6 meters	200 mm	370 meters	4.7 MW
4	20 meters	0.8 meters	200 mm	370 meters	8 MW
5	25 meters	1.0 meters	200 mm	370 meters	14 MW

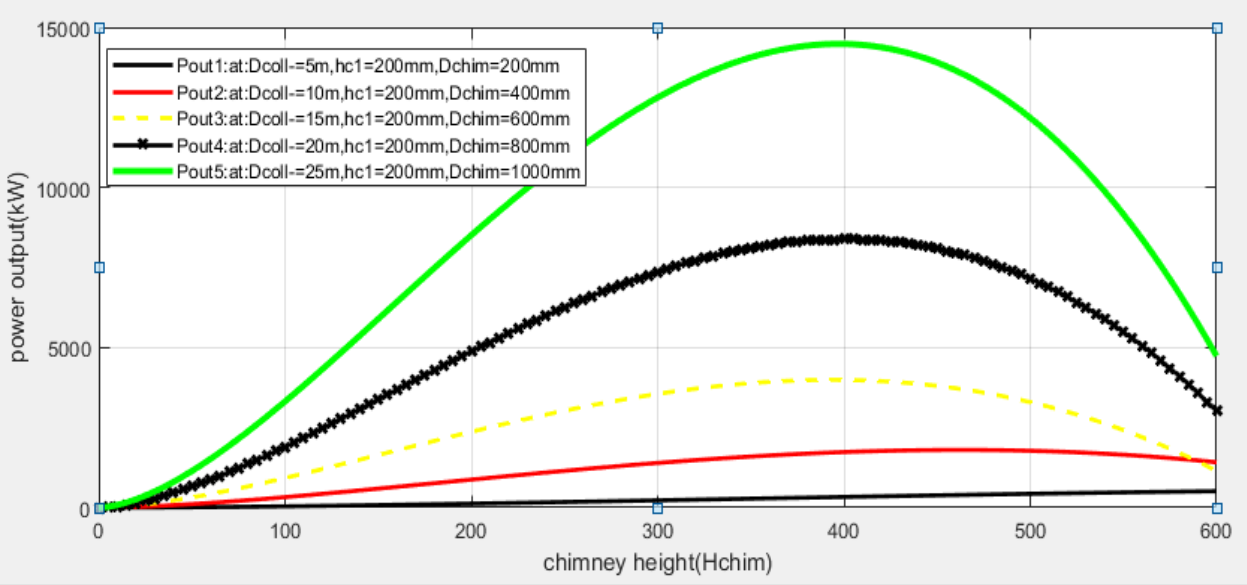

Figure 7-4:optimum chimney height for various

Therefore, Table 7.3, shows, increasing the chimney height greater than the indicated value results in a reduction of power output at the indicated fixed parameters, this is caused by the total frictional pressure drop in the chimney (draft tube) system.

7.2 Experimental set up MATLAB result.

7.2.1 Height of chimney versus power output

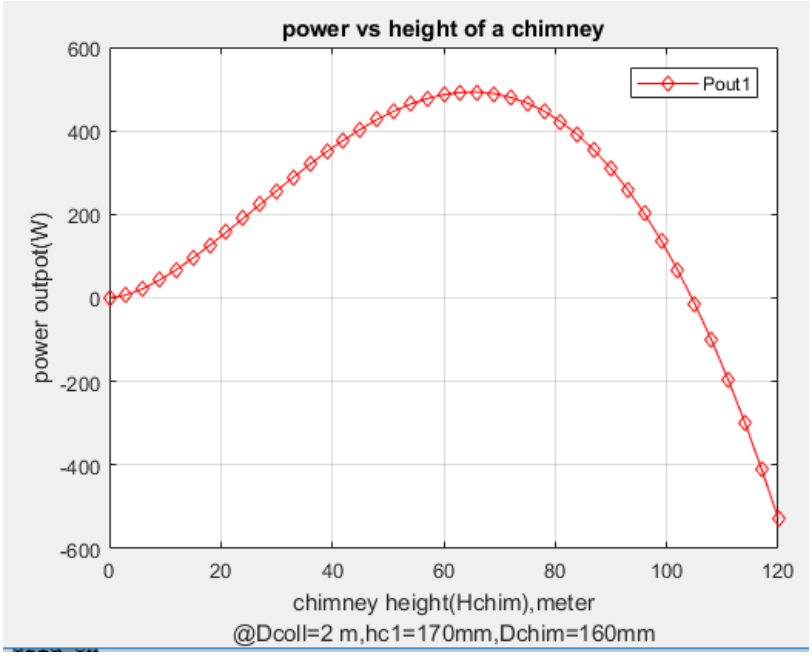

Figure 7-5: Power versus chimney height

According to the analysis performed in the figure 7-5, increasing the height of the chimney above 62 meters at fixed collector height from the ground ($hc1 = 170mm$), diameter of the chimney ($Dchim = 160mm$), diameter of the collector ($Dcoll = 2\ m$) will result power output reduction, the decrease in the power is caused by domination of a frictional pressure along the chimney(draft tube). when a chimney height reaches 107 m the power output equal to zero means frictional pressure loss is equal to useful driving pressure.Therefore,for the indicated fixed parameters shown the optimum chimney height for useful energy production is $58\ meters$.

For this particular study under consideration, the developed experimental solar chimney power plant is constructed with 3-meter chimney height and 2 meter collector diameter which provides a maximum power output of $32\ W$ as shown in the figure 7.5.

7.2.2 Collector area vs power output

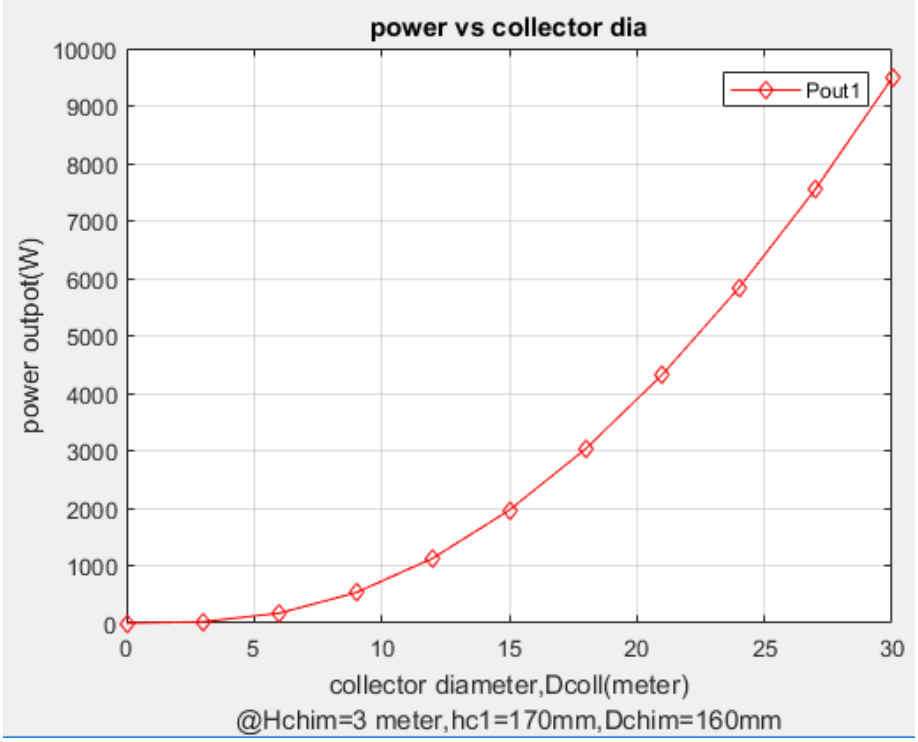

Figure 7-6 : power output versus collector diameter

According to the analysis increasing the diameter of the collector will directly increase the power output of the plant at fixed parameter of collector height from the ground (hc1=170mm), diameter of the chimney ($Dchim = 160mm$) and height of chimney ($Hchim = 3\ meter$).

7.2.3 Pressure (Pt) versus height of the chimney

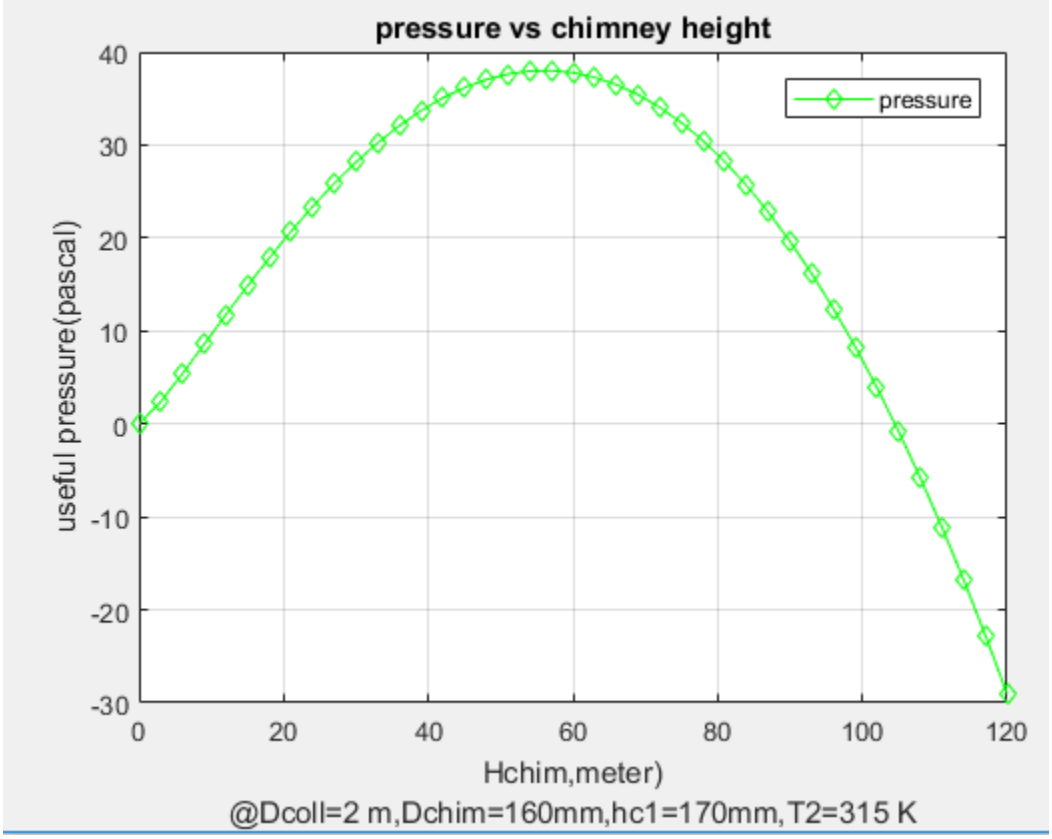

Figure 7-7:Pressure versus chimney height

Figure 7-7, shows the pressure variation with respect to chimney height, the result shows that at a fixed parameter of chimney diameter of 150 mm, collector diameter of 2-meter, collector exit temperature 315 K and 170 mm, height of the collector from the ground the total pressure(Pt) increases until the chimney height reaches 58 meters, beyond this height of the chimney the pressure tend to dramatically dropdown due to the cumulative effect of frictional pressure loss.

Therefore, at a fixed parameter total pressure that is useful for power production is zero when the chimney height reaches 103 meter this result in zero power output of the solar chimney power plant. So, the maximum allowable chimney height for this designed solar chimney power plant is 58-meter unless if the is no change in the fixed parameter.

7.2.4 Height of a chimney ($Hchim$) vs velocity ($V2$)

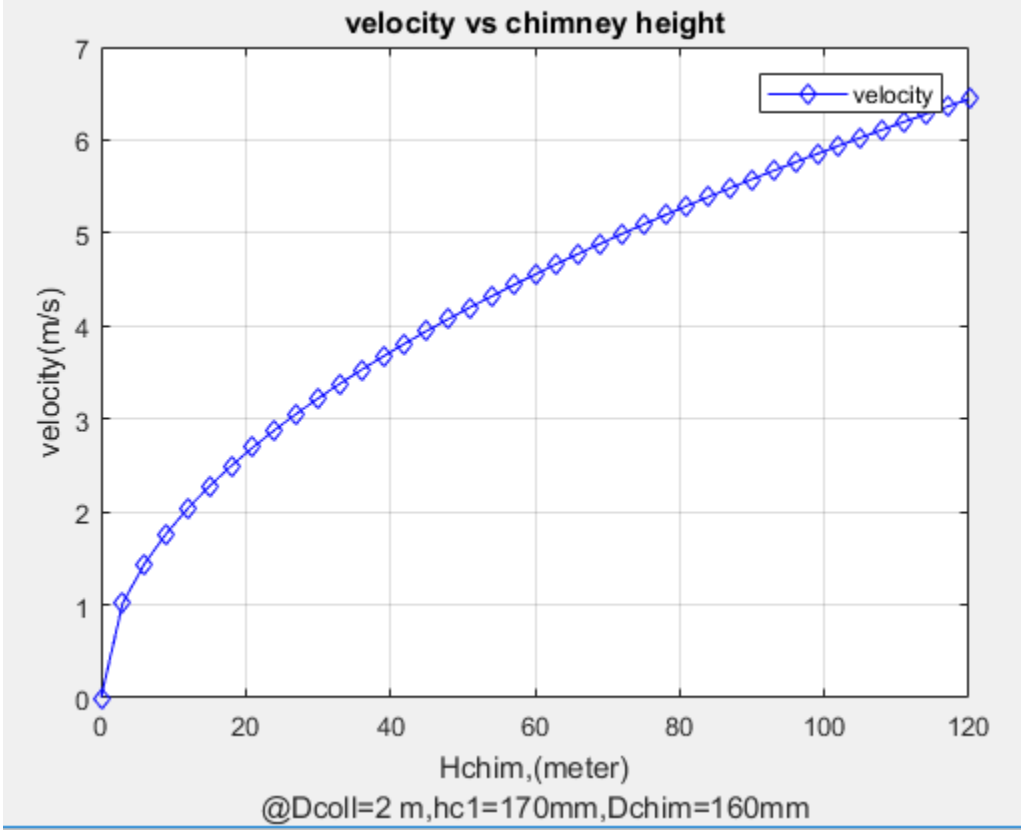

Figure 7-8: velocity versus chimney height

In the figure7-8, the relationship between chimney height and velocity has been studied under some fixed parameters. So, for fixed parameters shown in the graph the velocity at the collector exit reaches up to 6.5 m/s for a chimney height of 120 m.Making any modification on diameter of a collector will certainly increases the velocity of the collector exit by increasing the temperature T_2, an increase in velocity is directly increases the output power of the plant.

7.3 Temperature simulation using ENERGY 2D

For this study, the boundary condition for the temperature simulation is shown in the figure 7-9. Background temperature of working fluid is 25℃.In the figure 7-10, the variation of working fluid temperature throughout the day at collector inlet, collector exit, chimney inlet and chimney exit are simulated as shown.

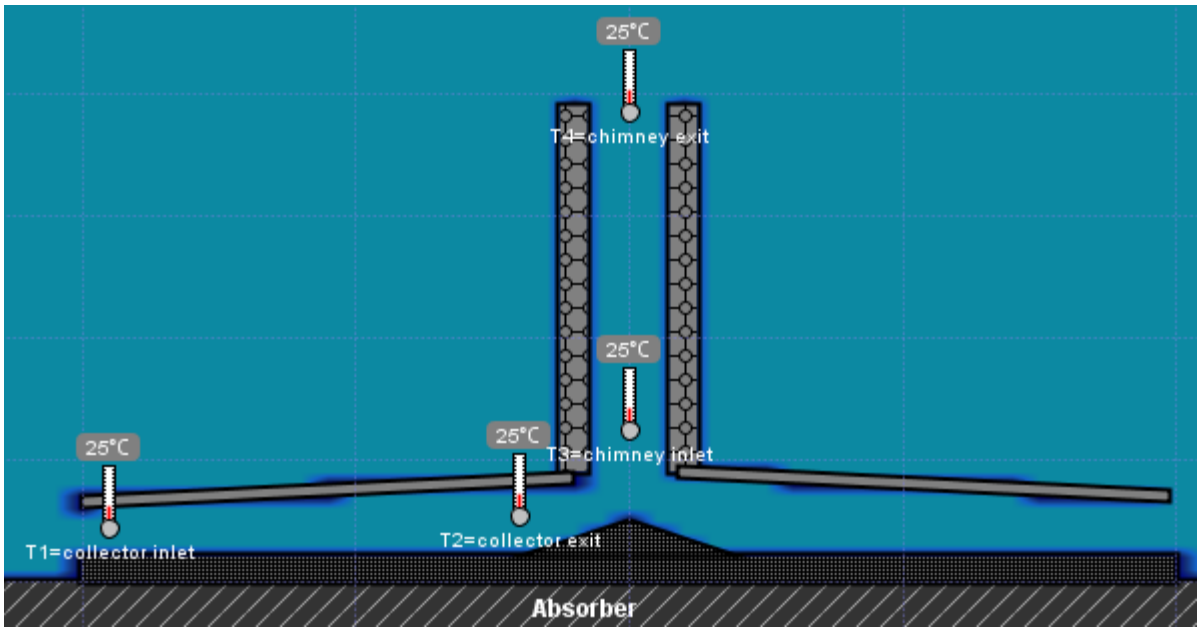

Figure 7-9: Temperature boundary condition

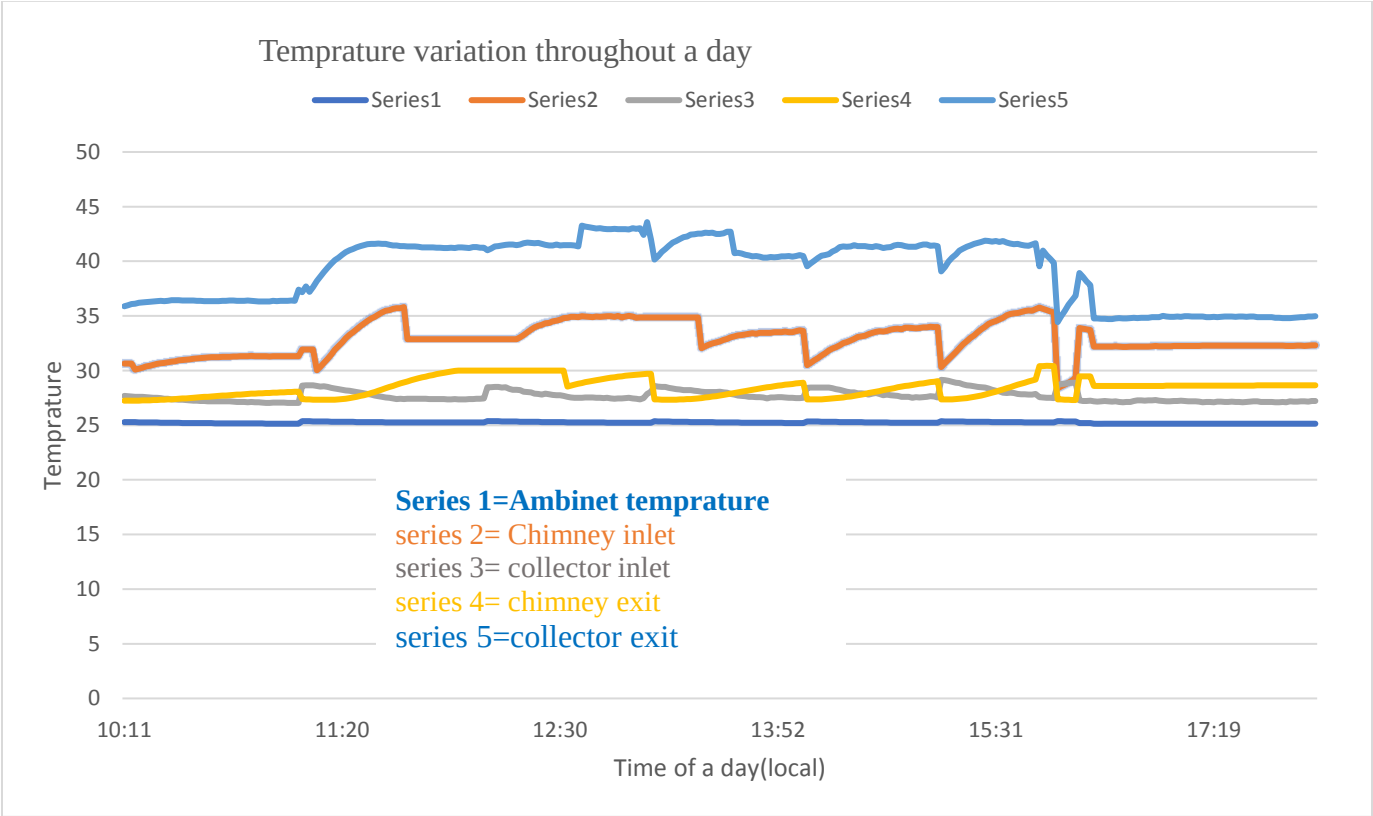

Figure 7-10: Temperature variation throughout the day

In simulation computed using ENERGY 2D tool, solar-radiation data and sun angle is influenced following the data obtained from source. So, according to the simulation conducted in the figure 7-10 Throughout the day the temperature of collector exit varies from 31℃ – 43℃ ,the minimum temperature reading was recording during morning time of 16:00 PM and maximum temperature was recorded during the mid-day at 12:38 PM.

7.4 Actual prototype temperature test result

7.4.1 Temperature throughout the day at height of the collector, hc1=170 mm

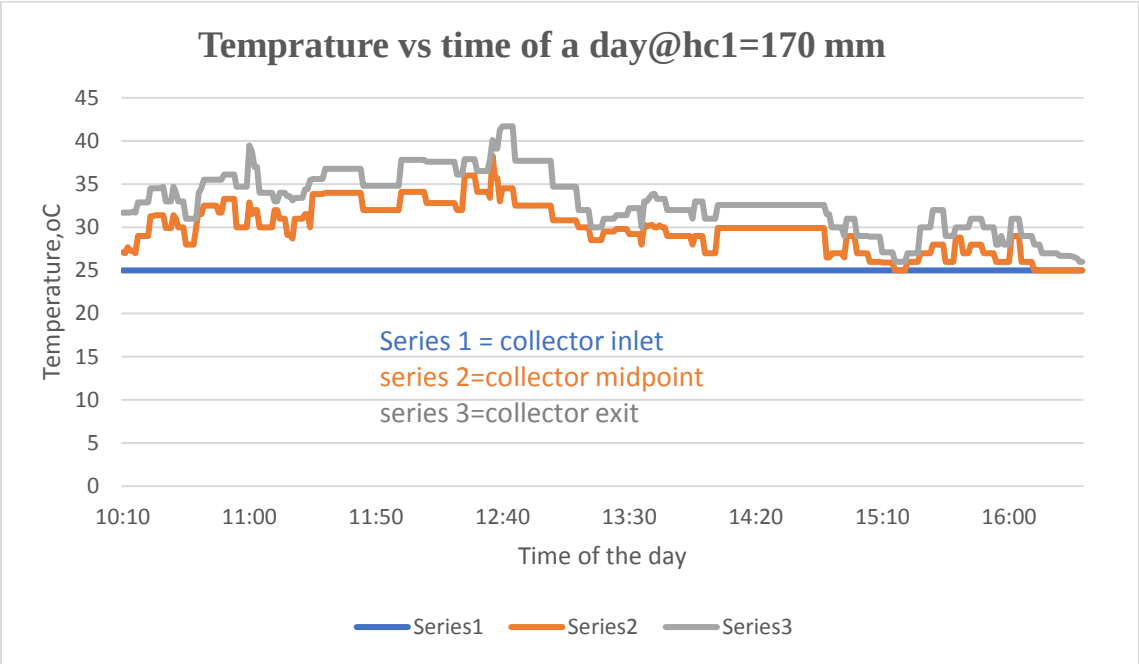

Figure 7-11: Actual prototype temperature result throughout a day at@hc1=170mm

In the experiment test result shown in figure 7-11, the temperature variation through the day was taken for three days in May 16/18, May 22/18 and May 23/18. The data was recorded for more than 6 hours per day for three different days, an average was taken for every 5-minute recording due to the instability of the weather condition.

In the meanwhile, the maximum collector exit temperature reading of 41.7℃ was recorded at mid-day at $12{:}44{:}00\ PM$.

7.4.2 Temperature at collector height from the ground $hc1 = 400mm$ in a day

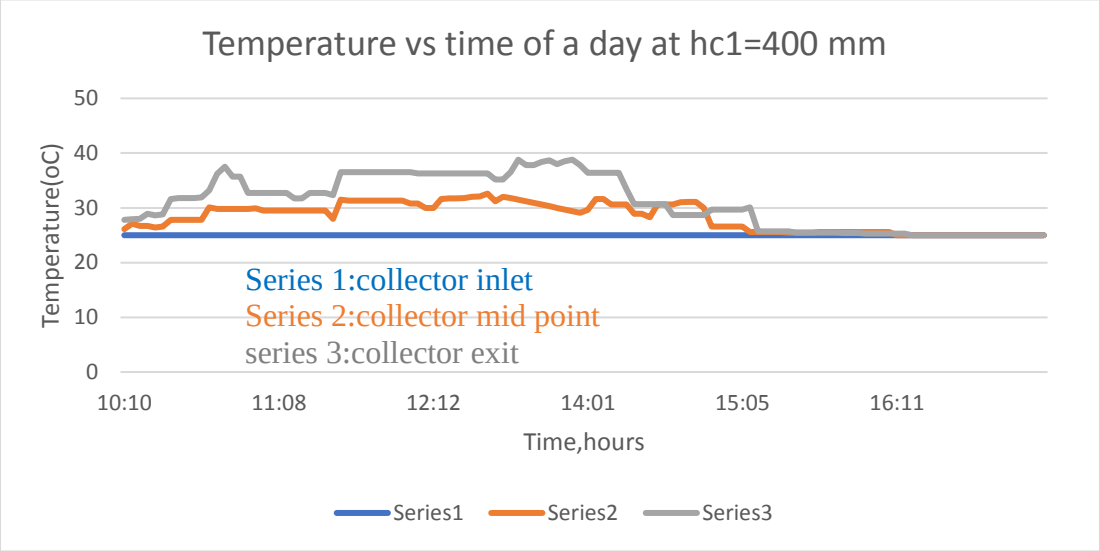

Figure 7-12: Actual prototype temperature result throughout a day at@hc1=400mm

The temperature result shown in the figure 7-12 is recorded by increasing the height of the collector from the ground to 400 mm. The maximum collector exit temperature 38.8℃ is recorded during 13:04 PM and minimum collector exit temperature of 25℃ is recorded during 16:10 PM.

7.4.3 Comparison between temperature at different collector height from Ground($hc1$)

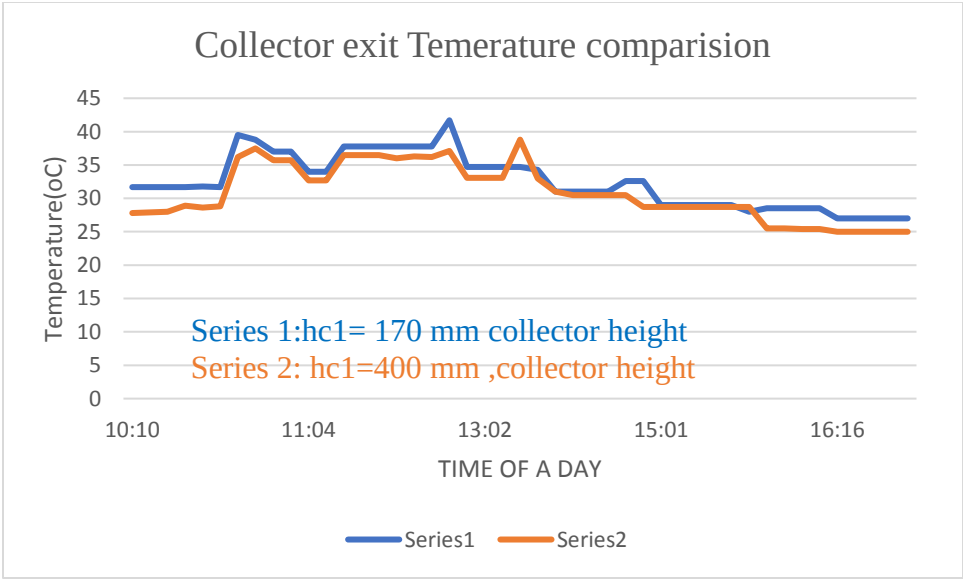

Figure 7-13:collector exit temperature comparison for different collector height from ground

In the experiment the collector exit temperature reading is taken for collector height of the 170 mm and 400 mm from the ground. In figure 7-13 it is clearly seen that the collector exit temperature is lower throughout the day for collector height of 400 mm and higher for a 170 mm collector height.so, it can be concluded that whenever the height of the collector from the ground is higher, the collector exit temperature will be lower for some fixed main geometrical configurations.

7.5 Validation of experimental result with simulated result

7.5.1 Temperature difference vs Time of the day

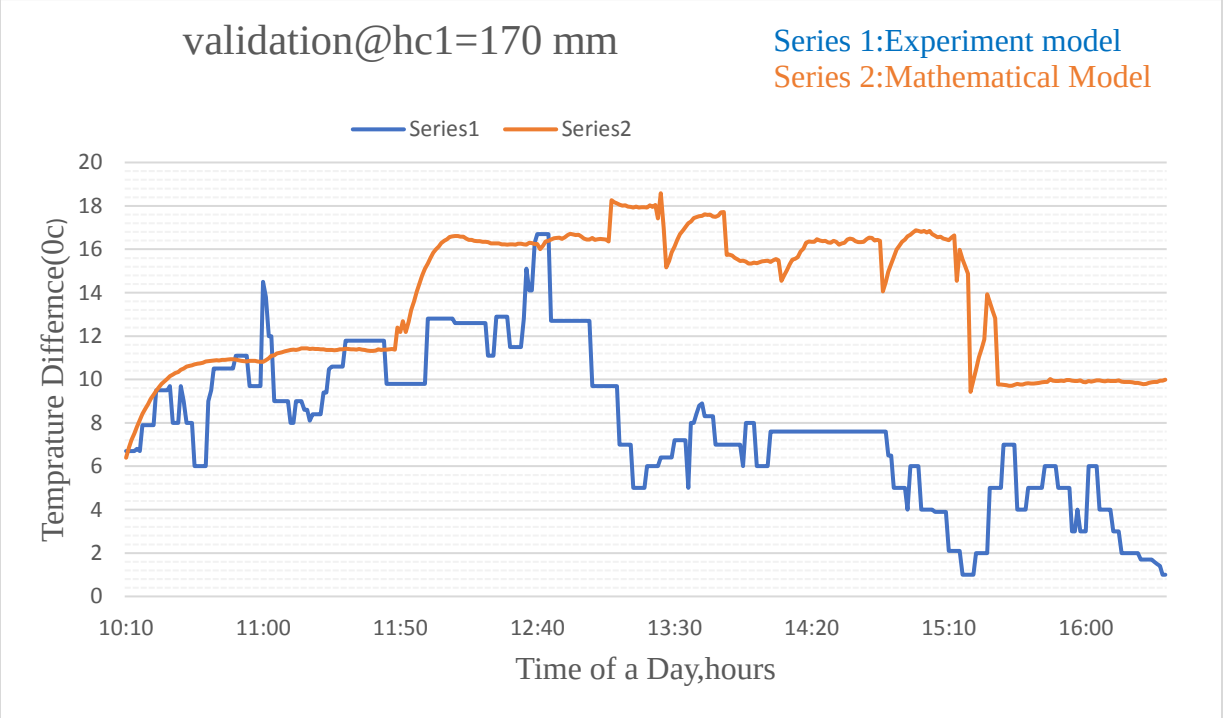

Figure 7-14: temperature difference for experiment vs simulation model

In the figure 7.14, the data comparison of experimental model and mathematical model are conducted by taking temperature difference of collector exit and collector inlet throughout the day. So, the temperature difference of the experimental model increases from 10:00 AM up to 12:44 PM resulting minimum and maximum temperature difference of 6℃ upto 17 ℃ respectively, then the temperature difference drops down from 12:50 PM up to 13:00 PM. On the other hand, the mathematical model temperature difference increases from 10:00 AM up to 15:00 PM, then it starts to drop down up to 15:10 PM.

Generally, the results show that after 12:44 PM the characteristics of the two model has a variation in temperature difference. For the actual experiment, while three days of testing the temperature of the collector exit was minimum during the afternoon as a result of the cloudiness in the sky, in the simulation this factor was not considered following historical data collected.

7.5.2 Power output vs time of the day

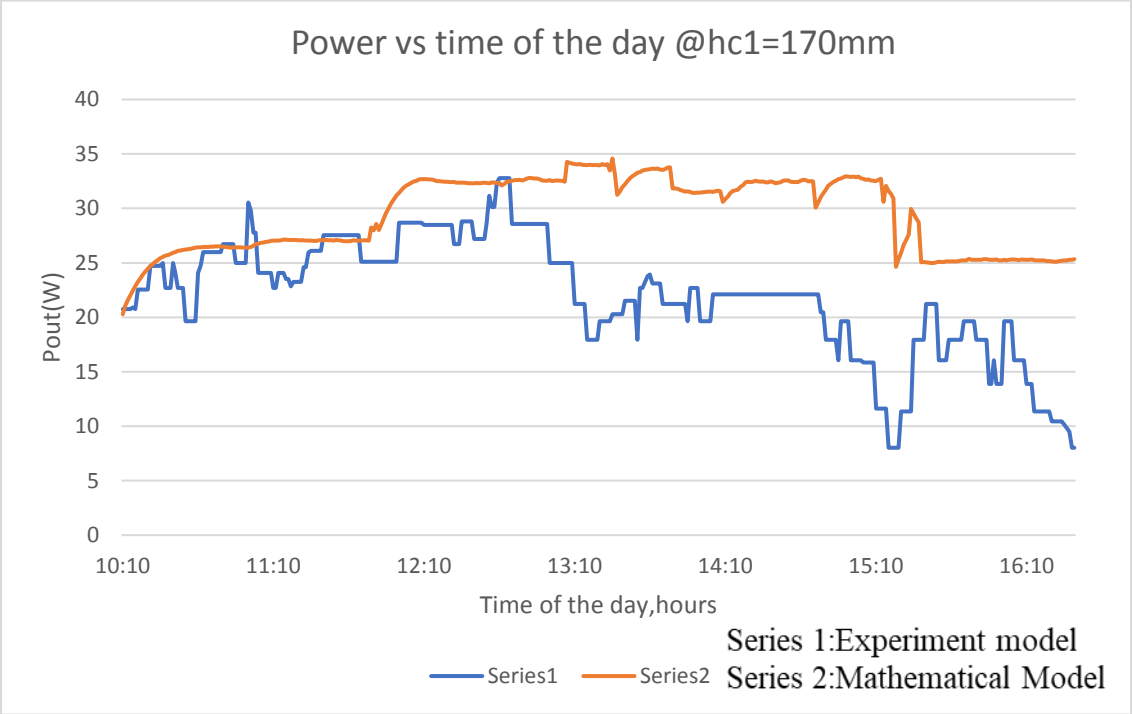

Figure 7-15:power output for actual experiment vs mathematical model

The power output for both model depends on the temperature difference throughout the day. So, the power output of the actual experiment varies from $8\,watt - 32\,Watt$,maximum power output was during the mid-day at $12{:}44\,PM$ and minimum at $15{:}19\,PM$. While, the simulated power output varies from $20\,Watt - 34\,watt$,maximum at $13{:}20\,PM$ and minimum at $10{:}10\,AM$.

Generally,for the actual experiment, the flow characteristics of power output in figure 7-15 is unstable as a result of collector exit temperature variation throughout the day, this is as a result of environmental and geographical condition of test site.

7.5.3 Efficiency of the collector

Using equation $\boldsymbol{eq(6.30)}$ collector efficiency throughout the day is computed as shown in figure 7.16. The curve shown in the figure below represent characteristics of efficiency with respect to solar radiation input through a day.

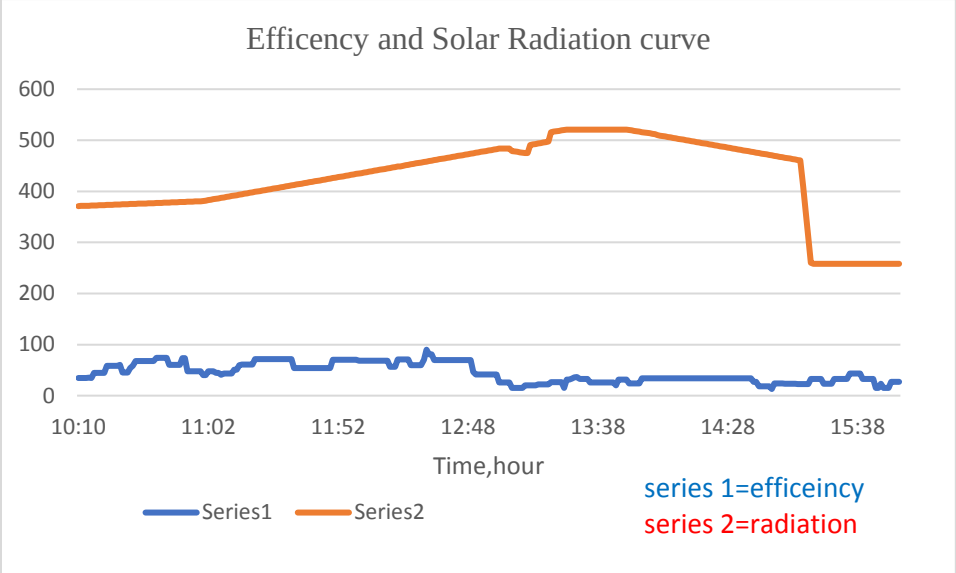

Figure 7-16: Efficiency and Solar radiation curve

The efficiency in the above figure is analyzed at a collector area of 3.14 m^2 ,0.17 meter collector height from the ground and chimney diameter of 0.16 meter the efficiency of collector.

According to this study the efficiency of the collector cannot be certainly concluded that whenever solar radiation increases the efficiency increases or vice versa. So, it is concluded that efficiency of the collector is dependent of temperature difference throughout the day.

On the other hand, $\boldsymbol{eq(6.30)}$ can be re-written;

$$Q = \tau\alpha \times G \times A_{COLL} - \beta(\Delta Ta) \times A_{COLL} \qquad \boldsymbol{eq(7.1)}$$

$$\eta_{coll} = \tau\alpha - \frac{\beta(\Delta Ta)}{G} \qquad \boldsymbol{eq(7.2)}$$

In $\boldsymbol{eq}(\mathbf{7.2})$, it is clearly seen that whenever solar radiation(G) increases the fraction of efficiency certainly increases for a constant ΔTa.This equation also gives the idea that however solar radiation increases the efficiency of the collector does not exceed a collector optical property of transmittance-absorptance. So, increases an in efficiency of the collector does not always mean there is high solar radiation in the site.

The average efficiency of the collector is found as;

$\eta_{coll} = 0.08 * \frac{1005*(315-298)}{3.15*700}$= 67.4%

CHAPTER EIGHT

8.1 Conclusion

Following the mathematical model developed by different authors as a guidance a, mathematical model was developed for this study. MATLAB software is used to obtain the solution of the model developed. In order to measure real time data Scaled down solar chimney power plant with concentric circle is designed, modeled and manufactured. CATIA V5 is used for geometrical modeling of the prototype.

ENERGY 2D is used to model the scaled down experiment temperature flow characteristics beneath the collector. The result of ENERGY 2D simulation and the actual experiment data was used to validate the project. Following the result of the simulation and experiment the following conclusion are drawn.

i. Increasing the collector height from 0.17m upto 0.4 m above the ground reduce the collector exit temperature, resulting reduced power output. The higher the height of the collector above the ground the lower the temperature inside collector.
ii. Increasing the height of the chimney upto 45 m increases the power output of the system for a 0.2 meter chimney diameter and collector height above the ground therefore an increase in the chimney height above 45 meter causes frictional pressure drop to be higher than the driving pressure difference resulting in negative total pressure, so, optimum chimney height has been determined to be 45 meter for a fixed geometrical configuration.
iii. Increasing the collector diameter increases collector exit temperature resulting in an increased power output of the plant due to the fact that the longer air takes to reach the collector exit the more it gains heat.
iv. For the design of 30 *kw* power output optimum chimney height of 17 m and collector diameter of 17 m is selected at a 0.2 m chimney diameter and height of the collector from the ground following the economical aspect and engineering criteria. However, making any modification on the fixed parameters results in a new optimum chimney height and collector diameter.
v. The experimental data and simulated data collected has a similarities and variation throughout, the variation is a result of instability of the weather condition of the actual test site.

vi. Solar chimney power plant is not economical for low power electrical power generation.

8.2 Recommendation for future work

In the future, in order to increase the efficiency of solar chimney power plant the following basic recommendation are made;

i. In the design of the solar chimney main component, divergent inlet and convergent exit chimney profile can be used so that the pressure at the exit of the chimney could be recovered.

ii. For thermal energy storage material, the mixture of pebble and water sealed with black painted body can be used.

iii. The solar chimney system can be used for water distillation around rural area that require pure water.

REFERENCES

Al-kayiem, H. H. and Aja, O. C. (2016) 'Historic and recent progress in solar chimney power plant enhancing technologies', *Renewable and Sustainable Energy Reviews*. Elsevier, 58(January), pp. 1269–1292. doi: 10.1016/j.rser.2015.12.331.

Amrutkar, S. K., Ghodke, S. and Patil, K. N. (2012) 'Solar Flat Plate Collector Analysis', 2(2), pp. 207–213.

Antia, O. O. and Etuk, D. J. (2017) 'Study of Thermal Storage Ability of Some Selected Pebbles (Marble and Granite) For Solar Incubation', 4(10), pp. 8293–8297.

Aurélio, M. (no date) 'Convective Heat Transfer Coefficients for Solar Chimney Power Plant Collectors', (Bernardes 2010).

Backström, T. W. Von and Gannon, A. J. (2004) 'Solar chimney turbine characteristics', (March). doi: 10.1016/j.solener.2003.08.009.

Backström, T. W. Von, Gannon, A. J. and Backstro, T. W. Von (2000) 'Solar Chimney Cycle Analysis With System Loss and Solar Collector Performance With System Loss and Solar', (August). doi: 10.1115/1.1314379.

Bernardes, M. A. dos S. and Zhou, X. (2013) 'On the heat storage in Solar Updraft Tower collectors - Water bags', *Solar Energy*, 91, pp. 22–31. doi: 10.1016/j.solener.2012.11.025.
Bernardes, M. A. S., Voß, A. and Weinrebe, G. (2003) 'Thermal and technical analyses of solar chimneys', 75, pp. 511–524. doi: 10.1016/j.solener.2003.09.012.

Chimney, T. S. and Bergermann, S. (2002) 'The Solar Chimney', pp. 1–14.
Choi, Y. J., Kam, D. H., Park, Y. W. and Jeong, Y. H. (2016) 'Development of analytical model for solar chimney power plant with and without water storage system', *Energy*. Elsevier Ltd, 112, pp. 200–207. doi: 10.1016/j.energy.2016.06.023.

Duffie, J. a., Beckman, W. a. and Worek, W. M. (2003) *Solar Engineering of Thermal Processes, 4nd ed., Journal of Solar Energy Engineering*. doi: 10.1115/1.2930068.

El-ghonemy, A. (2016) 'Solar Chimney Power Plant with Collector', 11(2), pp. 28–35. doi: 10.9790/2834-1102012835.

'Ethiopia's electric power coverage surpasses 57 pct - Xinhua English' (no date).
Factors, S. (no date) 'Success Factors for Women ' s and Children ' s Health Et h iopi a'.

Fluri, T. P. (2008) 'Turbine Layout for and Optimization of Solar Chimney Power Conversion Units .

Hamdan, M. O. (2010) 'Analysis of a solar chimney power plant in the Arabian Gulf region', *Renewable Energy*. Elsevier Ltd, pp. 1–6. doi: 10.1016/j.renene.2010.05.002.

Hanna, M. B., Mekhail, T. A., Dahab, O. M., Fathy, M., Esmail, C. and Abdel-rahman, A. R. (2016) 'Experimental and Numerical Investigation of the Solar Chimney Power Plant ' s Turbine', pp. 332–342. doi: 10.4236/ojfd.2016.64025.

Huang, H., Zhang, H., Huang, Y. and Lu, F. (2007) 'Simulation Calculation on Solar Chimney Power Plant System'.

'IEA - Report' (2017).

Kaledin, A. L., Huang, Z., Geletii, Y. V, Lian, T., Hill, C. L. and Musaev, D. G. (2009) 'Computational and Experimental Studies', pp. 0–7.

Kinan, A. and Sidik, N. A. C. (2016) 'Akademia Baru Experimental Studies on Small Scale of Solar Akademia Baru', 22(1), pp. 1–12.

Koonsrisuk, A. and Chitsomboon, T. (2013) 'Mathematical modeling of solar chimney power plants', *Energy*. Elsevier Ltd, 51, pp. 314–322. doi: 10.1016/j.energy.2012.10.038.

Koonsrisuk, A., Lorente, S. and Bejan, A. (2010) 'International Journal of Heat and Mass Transfer Constructal solar chimney configuration', *International Journal of Heat and Mass Transfer*. Elsevier Ltd, 53(1–3), pp. 327–333. doi: 10.1016/j.ijheatmasstransfer.2009.09.026.

Kumar, S. and Mullick, S. C. (2012) 'Glass cover temperature and top heat loss coefficient of a single glazed flat plate collector with nearly vertical configuration', *Ain Shams Engineering Journal*. Faculty of Engineering, Ain Shams University, 3(3), pp. 299–304. doi: 10.1016/j.asej.2012.03.008.

Ming, T. Z., Zheng, Y., Liu, C., Liu, W. and Pan, Y. (2010) 'Simple analysis on thermal performance of solar chimney power generation systems', 83(1), pp. 2–7. doi: 10.1179/014426009X12519696923902.

Ming, T. Z., Zheng, Y., Liu, C., Liu, W., Pan, Y., Ming, T. Z., Zheng, Y., Liu, C., Liu, W. and Pan, Y. (2016) 'Simple analysis on thermal performance of solar chimney power generation systems Simple analysis on thermal performance of solar chimney power generation systems', 9671(December). doi: 10.1179/014426009X12519696923902.

Mustafa, A. T., Al-kayiem, H. H. and Gilani, S. I. U. (2015) 'INVESTIGATION AND EVALUATION OF THE SOLAR AIR COLLECTOR MODEL TO SUPPORT THE SOLAR VORTEX ENGINE', 10(12), pp. 5309–5319.

Ngala, G. M., Sulaiman, A. T. and Garba, I. (2013) 'Review of Solar Chimney Power Technology and Its Potentials in Semi-Arid Region of Nigeria', 3(3), pp. 1283–1289.

Ninic, N. (2006) 'Available energy of the air in solar chimneys and the possibility of its ground-level concentration', 80, pp. 804–811. doi: 10.1016/j.solener.2005.05.010.

'Poor Access to Health Services : Ways Ethiopia is Overcoming it By Nada Chaya' (2007).
Pretorius, J. P. (2007) 'Optimization and Control of a Large-scale Solar Chimney Power Plant by', (March).

Rabadiya, A. V and Kirar, R. (2012) 'Comparative Analysis of Wind Loss Coefficient (Wind Heat Transfer Coefficient) For Solar Flat Plate Collector .', 2(9).

Renewable, I. and Agency, E. (2017) renewable energy statistics 2017 statistiques d ' énergie renouvelable 2017 estadísticas de energía.
Renewable, U., Program, E. and Final, D. (2012) 'Federal Democratic Republic of Ethiopia Ministry of Water and Energy', (January).

Sakir, T., Piash, B. K. and Akhter, S. (2014) 'Design, Construction and Performance Test of a Small SolarChimney Power Plant', 14(1).

To, T. S., Partial, I. N., Of, F., Requirement, T. H. E., Degree, F. O. R., Of, M., In, S. and Engineering, M. (2011) 'Modeling and Simulation of Solar Chimney Power Plant with and without the Effect of Thermal Energy Storage Systems Addis Ababa Institute of Technology School of Graduate Studies Mechanical Engineering Department', (September).

Wetstone, G., Thornton, K., Hinrichs-rahlwes, R., Sawyer, S., Sander, M., Taylor, R., Rodgers, D., Alers, M., Lehmann, H., Eckhart, M. and Hales, D. (2016) *United Arab Emirates*.

Zhou, X., Wang, F., Fan, J. and Ochieng, R. M. (2010) 'Performance of solar chimney power plant in Qinghai-Tibet Plateau', *Renewable and Sustainable Energy Reviews*. Elsevier Ltd, 14(8), pp. 2249–2255. doi: 10.1016/j.rser.2010.04.017.

Zhou, X., Xiao, B., Liu, W., Guo, X., Yang, J. and Fan, J. (2010) 'Comparison of classical solar chimney power system and combined solar chimney system for power generation and seawater desalination', *DES*. Elsevier B.V., 250(1), pp. 249–256. doi: 10.1016/j.desal.2009.03.007.

Zhou, X., Yang, J., Xiao, B., Hou, G. and Xing, F. (2014) 'Analysis of chimney height for solar chimney power plant', (January 2009), pp. 0–8. doi: 10.1016/j.applthermaleng.2008.02.014.

APPENDIX

Annex A: main component geometry of small-scale SCCP using CATIA V5

Annex(A-1): solar collector

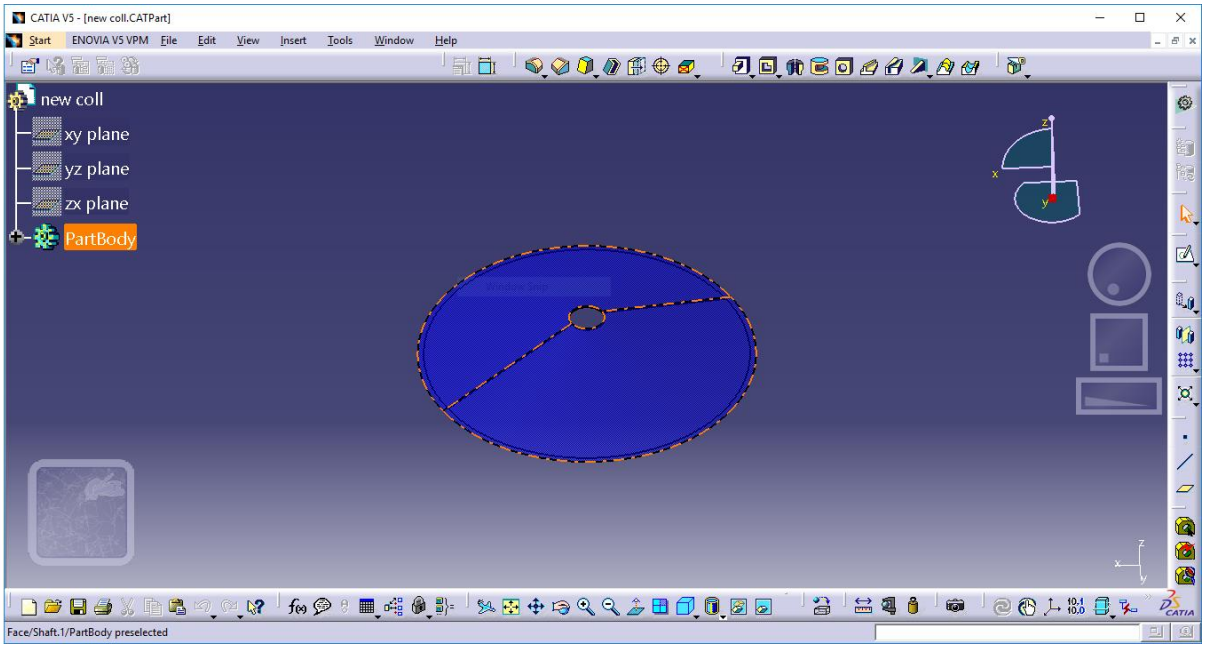

Figure(A-1): Solar collector CATIA model

Annex(A-2): turbine(runner)

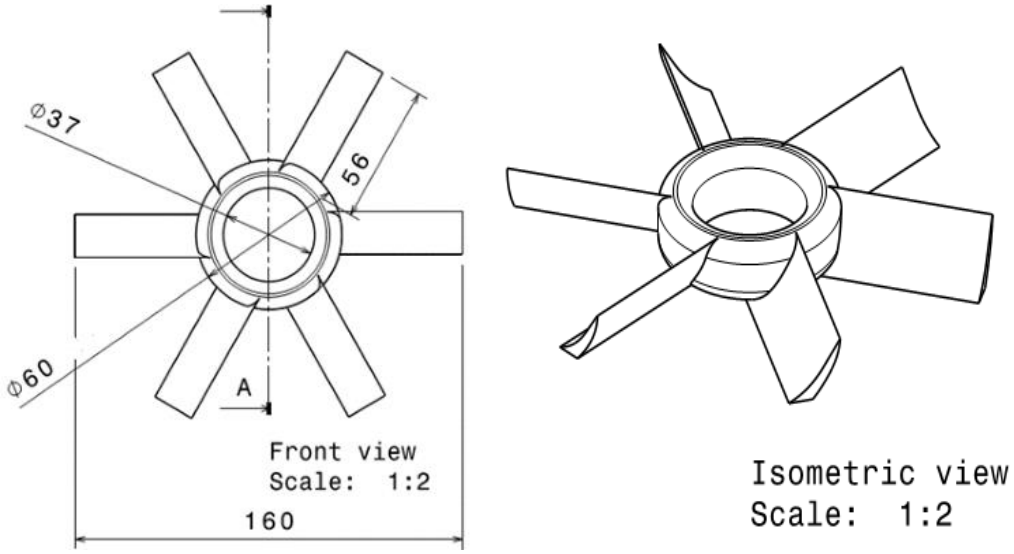

Figure(A-2): Turbine geometry modeling.

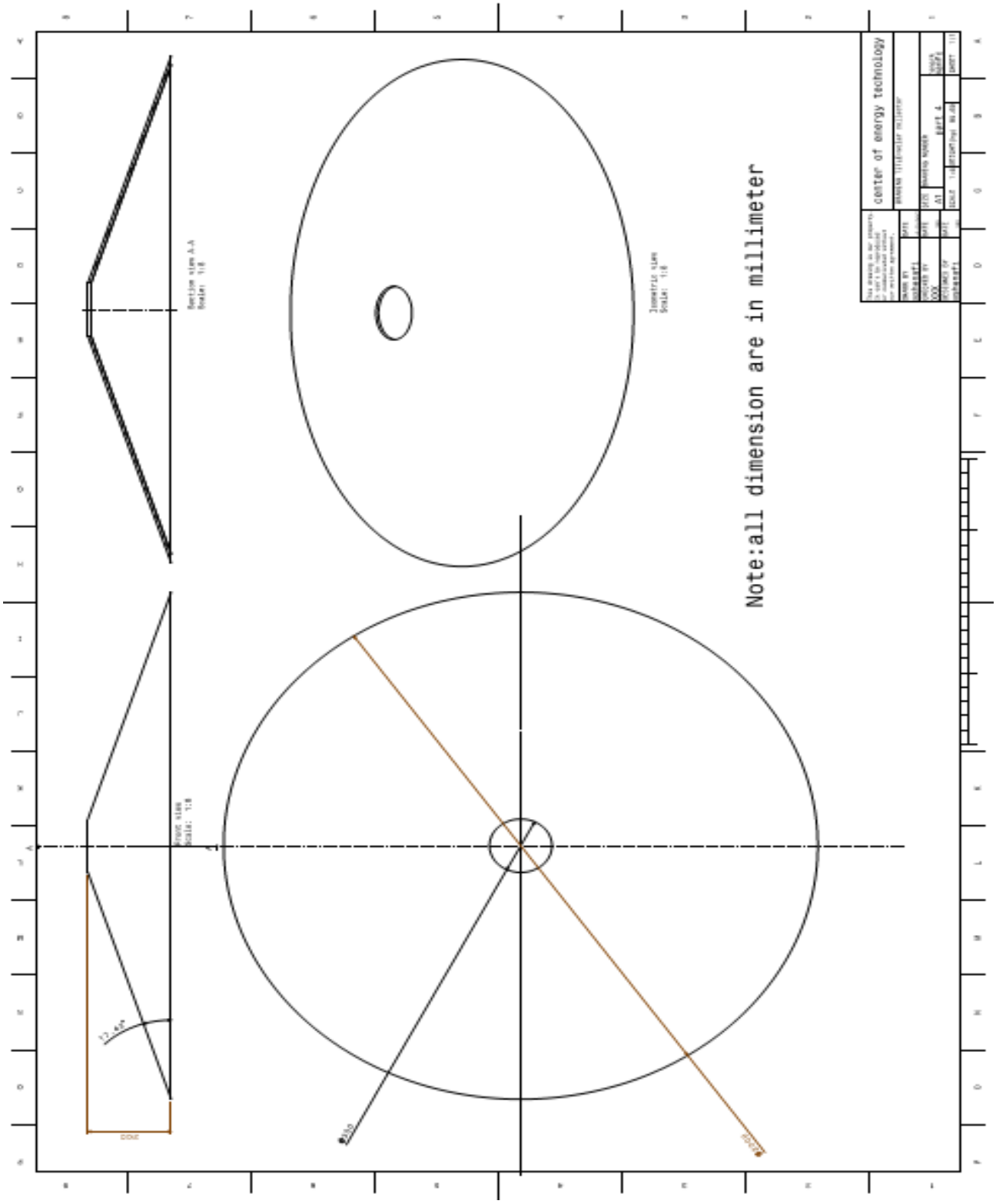

Figure(A-3):Solar collector roof structure

Annex(A-3): Solar chimney

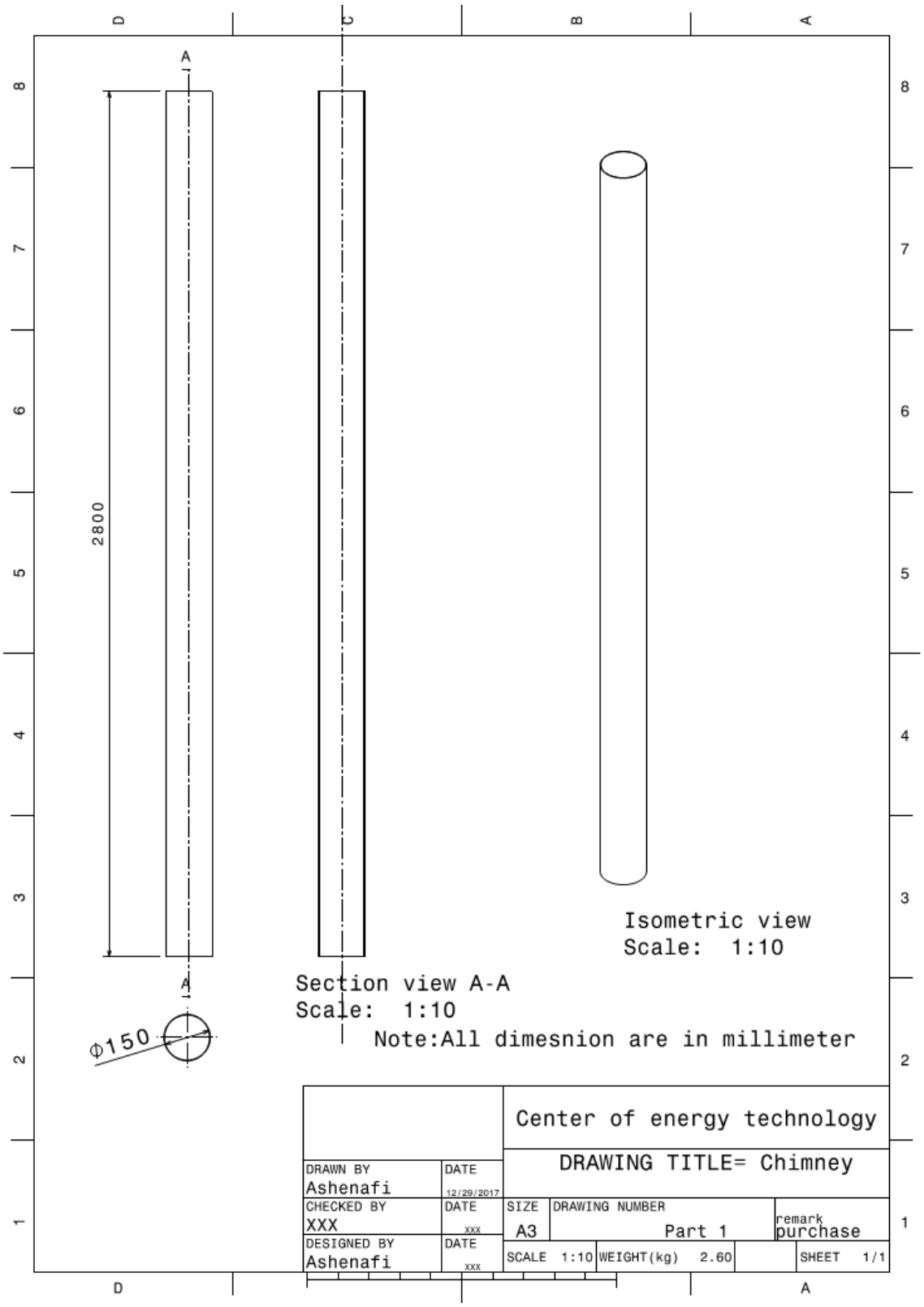

Figure(A-4): solar chimney modeling

Annex(A-4): Model assembly drawing

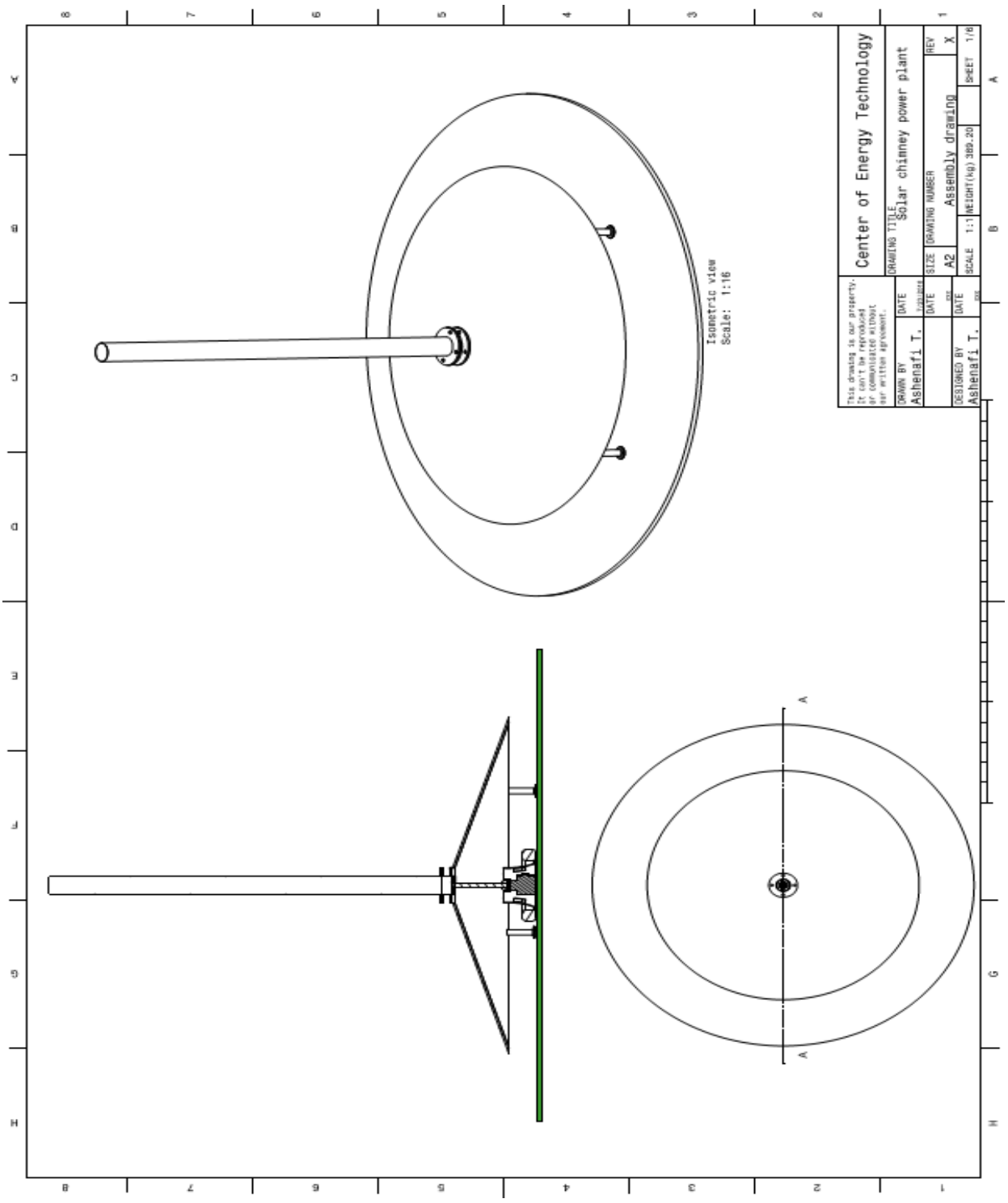

Figure (A-5): CATIA model assembly drawing view

Annex(A-5): Model assembly drawing with bill of material

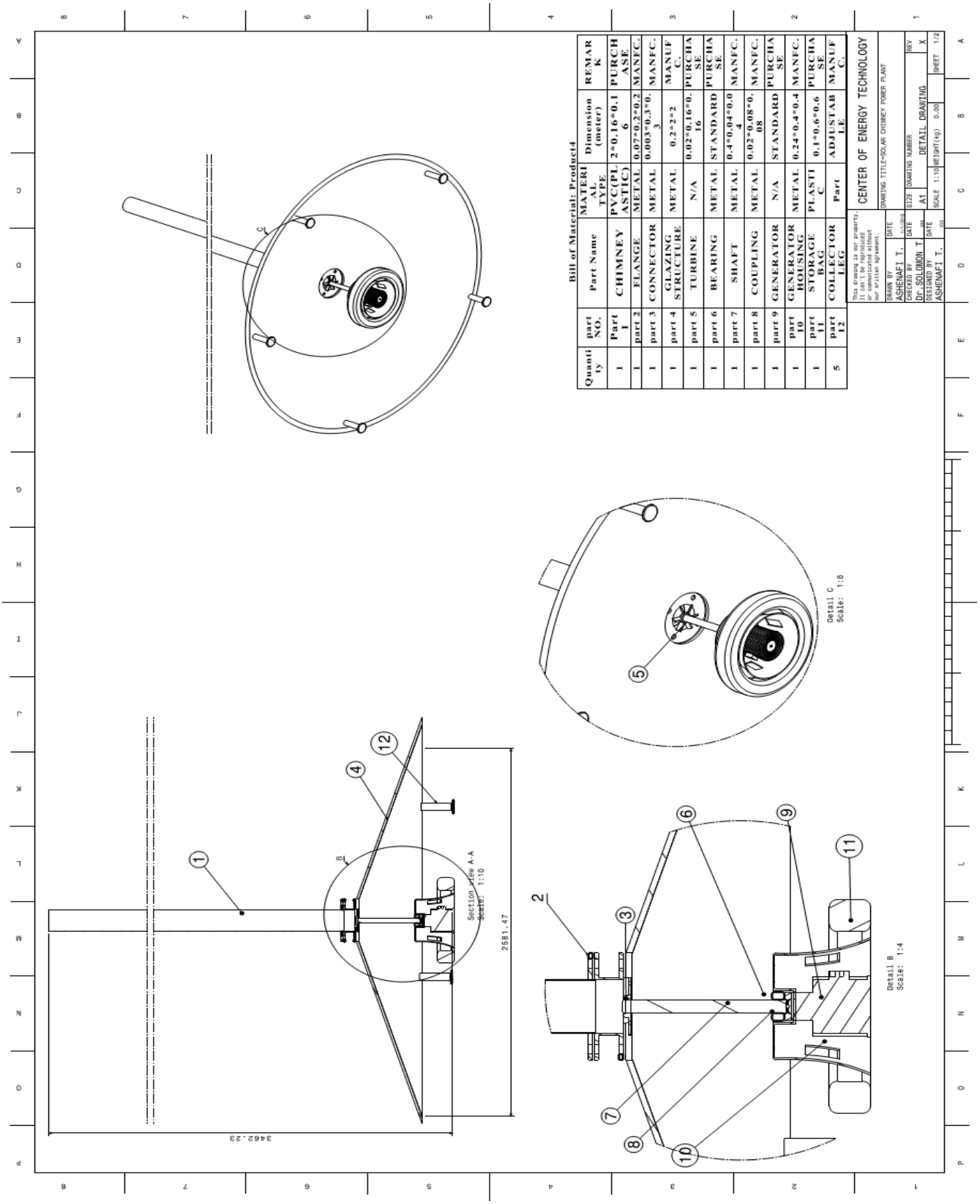

Figure (A-6): CATIA model assembly drawing bill of material

Annex(A-6): 3D Model assembly drawing

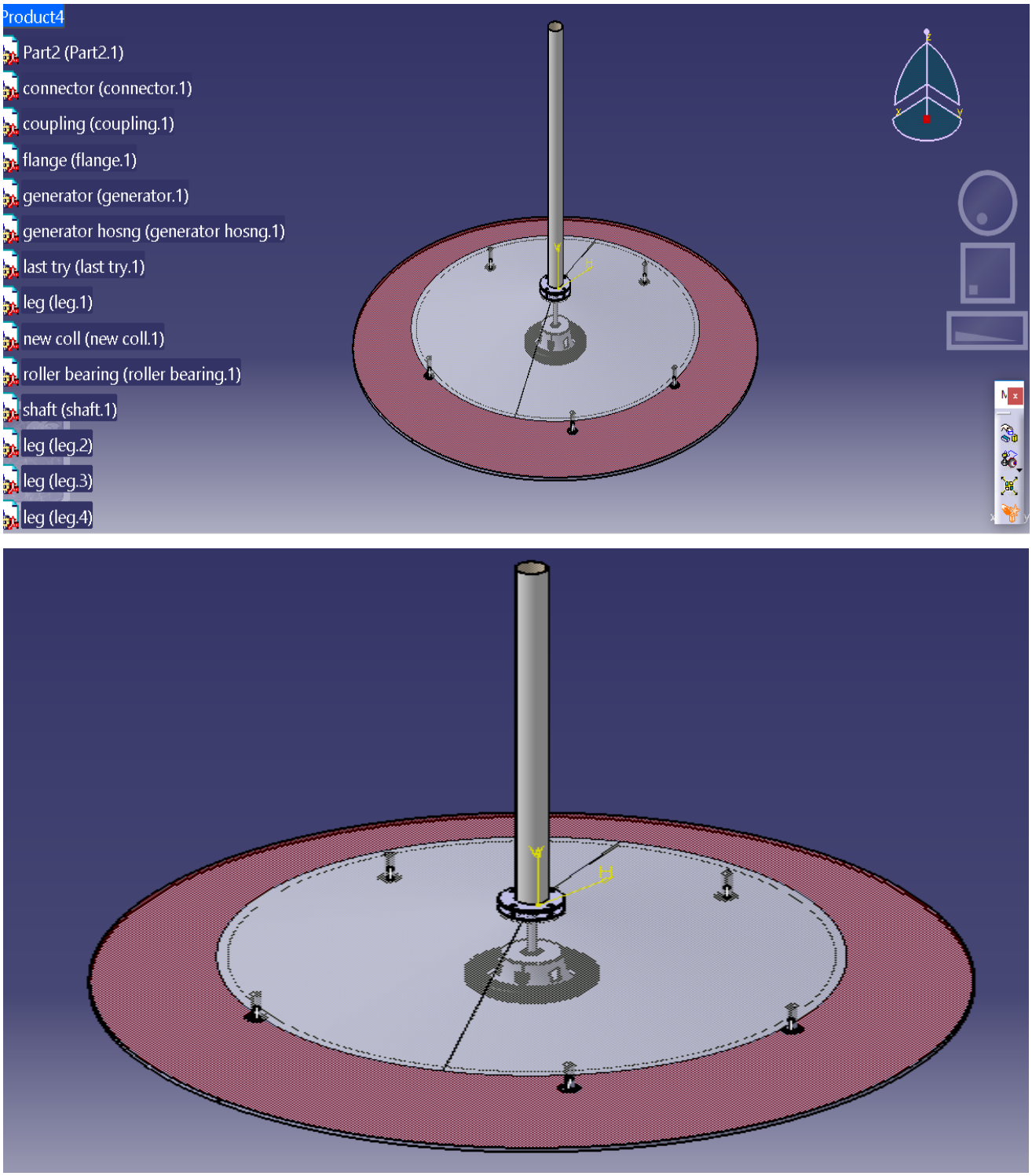

Figure (A-6): CATIA 3 D model assembly drawing

Annex B: ENERGY 2D simulation

Annex (B-1) Temperature modeling@ mid-day

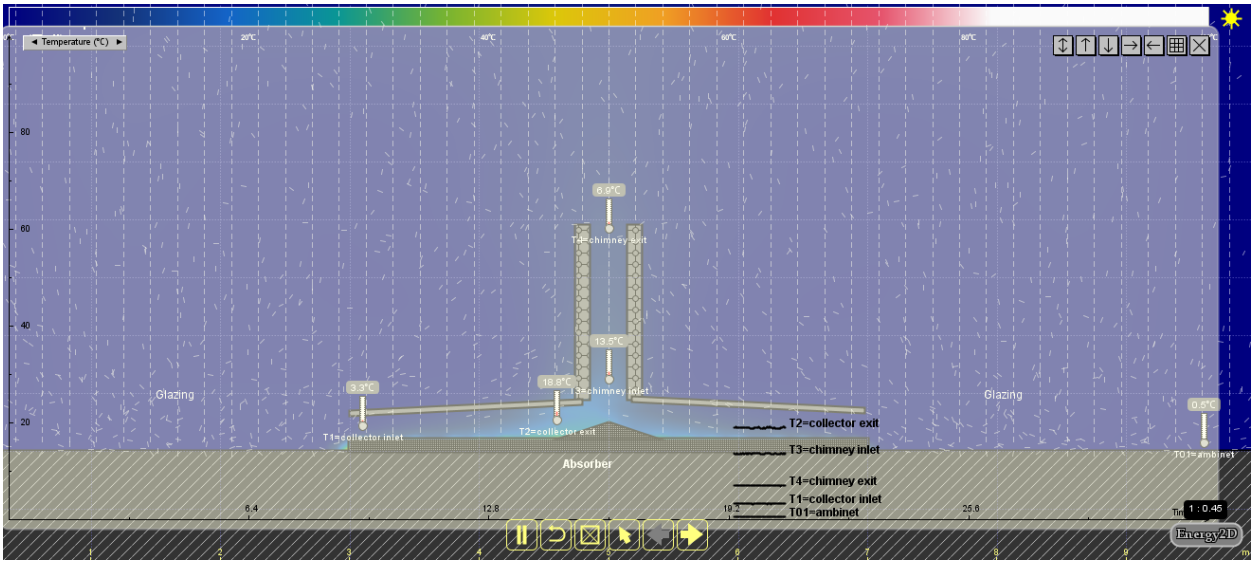

Figure(B-1):mid-day temperature modeling

Annex(B-2): velocity stream line across the plant @Mid-Day

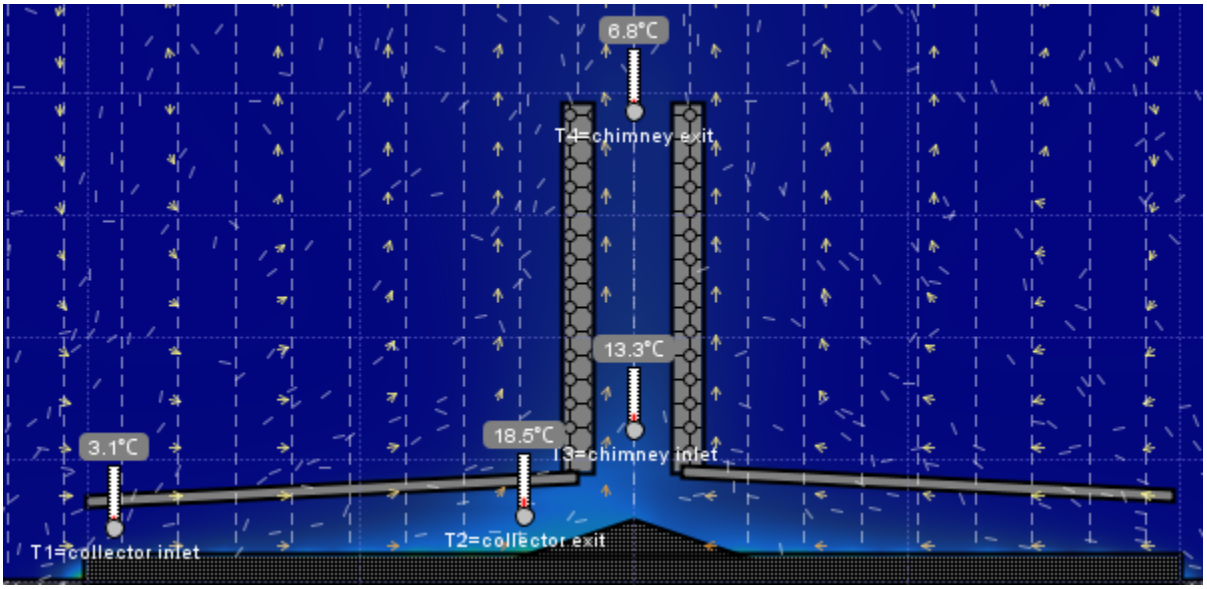

Figure(B-2): velocity stream line

Annex(B-3): air streamline in the surrounding of SCPP

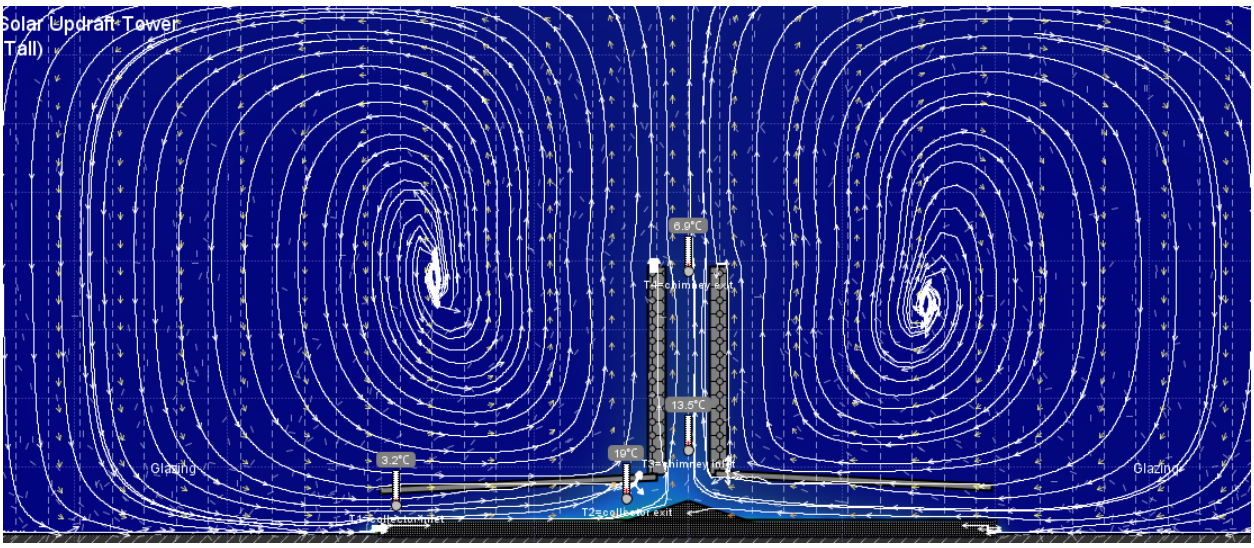

Figure(B-3): Air streamline in the surrounding

Annex(B-4):heat flux on the surface of the SCPP

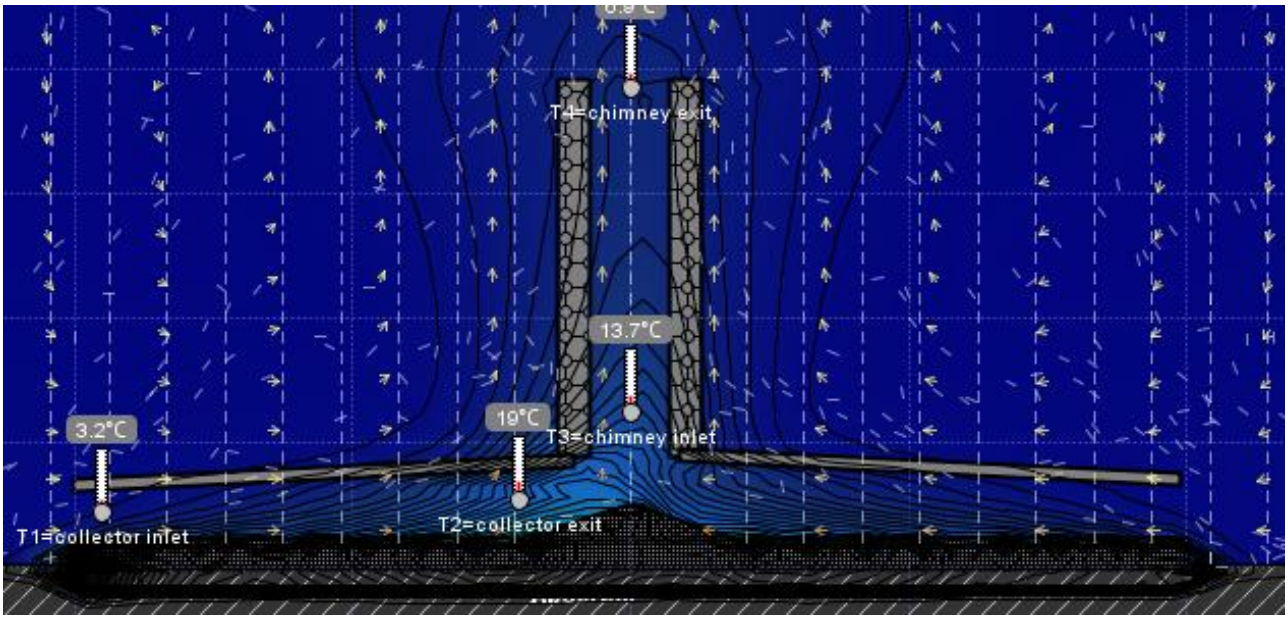

Figure(B-4): Heat flux on the surface of SCPP

ANNEX (C):National instrument(NI) specifications.

Safety Voltages

Connect only voltages that are within the following limits.

Between any two pins	±30 V maximum
Isolation, channel-to-channel	None
Isolation, channel-to-earth ground	
Up to 3,000 m	
Continuous	60 VDC, Measurement Category I
Withstand	1,000 Vrms, verified by a 5 s dielectric withstand test
Up to 5,000 m	
Continuous	60 VDC, Measurement Category I
Withstand	860 Vrms, verified by a 5 s dielectric withstand test

Analog Input

Number of channels	16 differential or 32 single ended
ADC resolution	16 bits
DNL	No missing codes guaranteed
INL	Refer to the *AI Absolute Accuracy* section.
Sample rate	
Single channel maximum	2.00 MS/s
Multichannel maximum (aggregate)	1.00 MS/s
Minimum	No minimum
Timing resolution	10 ns
Timing accuracy	50 ppm of sample rate
Input coupling	DC
Input range	±0.1 V, ±0.2 V, ±0.5 V, ±1 V, ±2 V, ±5 V, ±10 V
Maximum working voltage for analog inputs (signal + common mode)	±11 V of AI GND
CMRR (DC to 60 Hz)	100 dB
Input impedance	
Device on	
AI+ to AI GND	>10 GΩ in parallel with 100 pF
AI- to AI GND	>10 GΩ in parallel with 100 pF

Figure(C-1)National instrument(NI) specifications

ANNEX(D):MATLAB SCRIPT

Annex(D-1):influence of chimney height and collector dimeter on power output

```
%%initial input at coll dia=5 meter
Hchim=0:5:60;%height of chimney,m
Dchim=0.2;%diameter of the chimney,m
Achim=(pi.*Dchim.^2)./4;
Dcoll=5;%diamter of the glazing,m
hc1=0.2;%height of the glazing at inlet from the ground
hc2=0.4;%height of the glazing at oulet from ground to center of chimney
Cp=1005;%specific heat capacity of air j/kg K
phi=0.7;%? transmittance OF GLAZING
reff=0.3;%reflectance of glazing
phiab=0.5;%transmittance of absorber plate
alpha=0.8;%absorbitance of absorber plate
tabs=0.7;%transmittance absorbitance of glazing
U=5;%HEAT LOSS COEFFICENT
G=600;%GLOBAL SOLAR RADIATION
gama=1.4;%isentropic coefficent
T1=298;%AMBIENET temprature
T2=315;%collector exit temprature or design temprature
P1=0.77;%1 bar,atomospheric pressure
P2=0.77;%1 BAR Atomospheric pressure
mf=0.08;%mass flow rate kg/s
P3=0.97.*P2;%turbine exit pressure
Chc1=0.88;%correction factor for height of a chimney from the ground
Agz=(pi.*Dcoll.^2)./4;%glazing area required to produce required power
T22=T1+((G.*phi.*reff.* Agz)./(Cp.*mf)).*Chc1;%temp. at collector exit
T3=T2.*((P3/P2).^((gama-1)./gama));%temprature at the chimney inlet
x=((P2/P3).^((gama-1)./gama));%
q=tabs.*G-U.*(T2-T1);%heat flux
P4=P1.*(1-((g.*Hchim)./(Cp.*T1)).^(R./Cp));%exit pressure at chimney outlet
den1=1.12;,den2=P2./R.*T2;,den3=P3./R.*T3; %density at each state
T4=T3-((g.*Hchim)./Cp);
den4=P4./R.*T4;
%now find the pressure at state 3
P3N=P4+(0.5.*( g.*Hchim.* den3+den4)./100000) +(mf./Agz).*(1./den4 -1/den3);
%assumed value and found value has a variation then iterate until P3=P3N
% calculate every value using the new pressure P3N
T33=T2.*((P3N/P2).^((gama-1)./gama));%temprature at the chimney inlet
P4=P1.*(1-(xx).^(R./Cp));%the exit pressure at the chimney outlet
den33=P3N./R.*T33;
T44=T33-((g.*Hchim)./Cp);
den44=P4./R.*T4;
%the pressure difference
Ptot=g.*(den2-den44).*Hchim;
turbeff=0.9;%turbibne efficency
%VELOCITY AT THE CHIMNEY INLET
V2=sqrt(2.*g.*Hchim.*(T22-T1)./T22);%m/s
Pf=(0.0004.*Hchim.*den2.*(V2.^2))./Dchim;
mff=den1.*Achim.*V2;
Pt=Ptot-Pf;%usefull total pressure
%POWER OUTPUT
Pout1=0.90.*Pt.*V2.*Agz.*0.001;
%%%%%%%%at collector dia 10
Hchim=0:5:60;%height of chimney,m
```

```
Dchim=0.2;%diameter of the chimney,m
rchim=0.75;%radius of the chimney,m
Achim=(pi.*Dchim.^2)./4;
Dcoll=10;%diamter of the glazing,m
rcoll=1;%diameter of the glazing,m
hc1=0.2;%height of the glazing at inlet from the ground
hc2=0.4;%height of the glazing at oulet from ground to center of chimney
Cp=1005;%specific heat capacity of air j/kg K
phi=0.7;%? transmittance OF GLAZING
phiab=0.5;%transmittance of absorber plate
reff=0.3;%reflactance of the glazing
alpha=0.8;%absorbitance of absorber plate
U=5;%HEAT LOSS COEFFICENT
G=600;%GLOBAL SOLAR RADIATION
gama=1.4;%isentropic coefficent
T1=298;%AMBIENET temprature
T2=315;%collector exit temprature or design temprature
P1=0.77;%1 bar,atomospheric pressure
P2=0.77;%1 BAR Atomospheric pressure
mf=0.08;%mass flow rate kg/s
P3=0.82.*P2;%turbine exit pressure
Chc1=0.88;%correction factor for temp. for coll.height above ground=170mm
Agz=(pi.*Dcoll.^2)./4;%glazing area required to produce reqiured power
T22=T1+((G.*phi.*reff.* Agz)./(Cp.*mf)).*Chc1;%temp. at collector exit inlet
T3=T2.*((P3/P2).^((gama-1)./gama));%temprature at the chimney inlet
x=((P2/P3).^((gama-1)./gama));%
q=phi.*G-U.*(T2-T1);%heat flux
P4=P1.*(1-( g.*Hchim)./(Cp.*T1).^(R./Cp));%exit pressure at chimney outlet
den1=1.12;den2=P2./R.*T2;den3=P3./R.*T3; %density at indicated state
T4=T3-((g.*Hchim)./Cp);
den4=P4./R.*T4;
%now find the pressure at state 3
P3N=P4+(0.5.*( g.*Hchim.* den3+den4)./100000) +(mf./Agz).*(1./den4 -1/den3);
%assumed value and found value has a variation
% calculate every value using the new pressure P3N
T33=T2.*((P3N/P2).^((gama-1)./gama));%temprature at the chimney inlet
P4=P1.*(1-(xx).^(R./Cp));%the exit pressure at the chimney outlet
den33=P3N./R.*T33;
T44=T33-((g.*Hchim)./Cp);
den44=P4./R.*T4;
%the pressure difference
Ptot=g.*(den2-den44).*Hchim;
turbeff=0.9;%turbibne efficency
%VELOCITY AT THE CHIMNEY INLET
V2=sqrt(2.*g.*Hchim.*(T22-T1)./T22);%m/s
Pf=(0.0004.*Hchim.*den2.*(V2.^2))./Dchim;
mff=den1.*Achim.*V2;
Pt=Ptot-Pf;
%POWER OUTPUT
Pout2=0.90.*Pt.*V2.*Agz.*0.001;
%%%%% at coll dia=15
Hchim=0:5:60;%height of chimney,m
Dchim=0.2;%diameter of the chimney,m
rchim=0.75;%radius of the chimney,m
Achim=(pi.*Dchim.^2)./4;
Dcoll=15;%diamter of the glazing,m
rcoll=1;%diameter of the glazing,m
```

```
hc1=0.2;%height of the glazing at inlet from the ground
hc2=0.4;%height of the glazing at oulet from ground to center of chimney
Cp=1005;%specific heat capacity of air j/kg K
phi=0.7;%? transmittance OF GLAZING
phiab=0.5;%transmittance of absorber plate
alpha=0.8;%absorbitance of absorber plate
reff=0.3;%reflactance of glazing
U=5;%HEAT LOSS COEFFICENT
G=600;%GLOBAL SOLAR RADIATION
gama=1.4;%isentropic coefficent
T1=298;%AMBIENET temprature
T2=315;%collector exit temprature or design temprature
P1=0.77%1 bar,atomospheric pressure
P2=0.77;%1 BAR Atomospheric pressure
mf=0.08;%mass flow rate kg/s
P3=0.82.*P2;%turbine exit pressure
Chc1=0.88;% for hc1=200mm,temp.correction factor for coll. height from ground
Agz=(pi.*Dcoll.^2)./4;%glazing area required to produce reqiured power
T22=T1+((G.*phi.*reff.* Agz)./(Cp.*mf)).*Chc1;%temprature at collector inlet
T3=T2.*((P3/P2).^((gama-1)./gama));%temprature at the chimney inlet
x=((P2/P3).^((gama-1)./gama));%
q=phi.*G-U.*(T2-T1);%heat flux
P4=P1.*(1-( g.*Hchim)./(Cp.*T1).^(R./Cp));% exit pressure at  chimney outlet
den1=1.12;,den2=P2./R.*T2;,den3=P3./R.*T3; % density at indicated state
T4=T3-((g.*Hchim)./Cp);
den4=P4./R.*T4;
%now find the pressure at state 3
P3N=P4+(0.5.*( g.*Hchim.* den3+den4)./100000) +(mf./Agz).*(1./den4 -1/den3);
%assumed value and found value has a variation
%%%%%%%%%%%%%%%%%%%%%%%%%%%%%%%%%%%%%%%%%%%%%%%%%%%%%%%%%%%%
% calculate every value using the new pressure P3N
T33=T2.*((P3N/P2).^((gama-1)./gama));%temprature at the chimney inlet
P4=P1.*(1-(xx).^(R./Cp));%the exit pressure at the chimney outlet
den33=P3N./R.*T33;
T44=T33-((g.*Hchim)./Cp);
den44=P4./R.*T4;
%the pressure difference
Ptot=g.*(den2-den44).*Hchim;
%the the power output becomes
turbeff=0.9;%turbibne efficency
%VELOCITY AT THE CHIMNEY INLET
V2=sqrt(2.*g.*Hchim.*(T22-T1)./T22);%m/s hc1=170mm,drag coeffient
Pf=(0.0004.*Hchim.*den2.*(V2.^2))./Dchim;
mff=den1.*Achim.*V2;
Pt=Ptot-Pf;
%POWER OUTPUT
Pout3=0.90.*Pt.*V2.*Agz.*0.001;
%%%%%%%%%%%%%%%%%%% at coll dia=20
Hchim=0:5:60;%height of chimney,m
Dchim=0.2;%diameter of the chimney,m
Achim=(pi.*Dchim.^2)./4;
Dcoll=20;%diamter of the glazing,m
rcoll=1;%diameter of the glazing,m
hc1=0.2;%height of the glazing at inlet from the ground
hc2=0.4;%height of the glazing at oulet from ground to center of chimney
Cp=1005;%specific heat capacity of air j/kg K
phi=0.7;%? transmittance OF GLAZING
```

```
phiab=0.5;%transmittance of absorber plate
reff=0.3;%reflactance of the glazing
alpha=0.8;%absorbitance of absorber plate
U=5;%HEAT LOSS COEFFICENT
G=600;%GLOBAL SOLAR RADIATION
gama=1.4;%isentropic coefficent
T1=298;%AMBIENET temprature
T2=315;%collector exit temprature or design temprature
P1=0.77;%1 bar,atomospheric pressure
P2=0.77;%1 BAR Atomospheric pressure
mf=0.08;%mass flow rate kg/s
P3=0.82.*P2;%turbine exit pressure
Chc1=0.88;%for chimney height from the ground hc1=200mm
Agz=(pi.*Dcoll.^2)./4;%glazing area required to produce reqiured power
T22=T1+((G.*phi.*reff.* Agz)./(Cp.*mf)).*Chc1;%temp. at collector exit inlet
T3=T2.*((P3/P2).^((gama-1)./gama));%temprature at the chimney inlet
x=((P2/P3).^((gama-1)./gama));%
q=phi.*G-U.*(T2-T1);%heat flux
P4=P1.*(1-( g.*Hchim)./(Cp.*T1).^(R./Cp));%exit pressure at chimney outlet
den1=1.12;,den2=P2./R.*T2;,den3=P3./R.*T3; %density at the indicated state
T4=T3-((g.*Hchim)./Cp);
den4=P4./R.*T4;
%now find the pressure at state 3
xxx=g.*Hchim;
yy=den3+den4;
P3N=P4+(0.5.*(xxx.*yy)./100000) +(mf./Agz).*(1./den4 -1/den3);
%assumed value and found value has a variation
%%%%%%%%%%%%%%%%%%%%%%%%%%%%%%%%%%%%%%%%%%%%%%%%%%%
% calculate every value using the new pressure P3N
T33=T2.*((P3N/P2).^((gama-1)./gama));%temprature at the chimney inlet
P4=P1.*(1-(xx).^(R./Cp));%the exit pressure at the chimney outlet
den33=P3N./R.*T33;
T44=T33-((g.*Hchim)./Cp);
den44=P4./R.*T4;
%the pressure difference
Ptot=g.*(den2-den44).*Hchim;
%the the power output becomes
turbeff=0.9;%turbibne efficency
%VELOCITY AT THE CHIMNEY INLET
V2=sqrt(2.*g.*Hchim.*(T22-T1)./T22);%m/s
Pf=(0.0004.*Hchim.*den2.*(V2.^2))./Dchim;
mff=den1.*Achim.*V2;
Pt=Ptot-Pf;
%POWER OUTPUT
Pout4=0.90.*Pt.*V2.*Agz.*0.001;
%%%at collector dia=25
Hchim=0:5:60;%height of chimney,m
Dchim=0.2;%diameter of the chimney,m
Achim=(pi.*Dchim.^2)./4;
Dcoll=25;%diamter of the glazing,m
rcoll=1;%diameter of the glazing,m
hc1=0.2;%height of the glazing at inlet from the ground
hc2=0.4;%height of the glazing at oulet from ground to center of chimney
phitlt=8;%collector tilt angle,deg
Cp=1005;%specific heat capacity of air j/kg K
phi=0.9;%? transmittance OF GLAZING
phiab=0.5;%transmittance of absorber plate
```

```
reff=0.3;%reflactance of the glazing
alpha=0.8;%absorbitance of absorber plate
U=5;%HEAT LOSS COEFFICENT
G=600;%GLOBAL SOLAR RADIATION
gama=1.4;%isentropic coefficent
T1=298;%AMBIENET temprature
T2=315;%collector exit temprature or design temprature
P1=0.77;%1 bar,atomospheric pressure
P2=0.77;%1 BAR Atomospheric pressure
mf=0.08;%mass flow rate kg/s
P3=0.82.*P2;%turbine exit pressure
Chc1=0.88;%temprature correction factor for chimney height from ground.
Agz=(pi.*Dcoll.^2)./4;%glazing area required to produce reqiured power
T22=T1+((G.*phi.*reff.* Agz)./(Cp.*mf)).*Chc1;%temp. at collector exit inlet
T3=T2.*((P3/P2).^((gama-1)./gama));%temprature at the chimney inlet
x=((P2/P3).^((gama-1)./gama));%
q=phi.*G-U.*(T2-T1);%heat flux
P4=P1.*(1-( g.*Hchim)./(Cp.*T1).^(R./Cp));%exit pressure at chimney outlet
den1=1.12;,den2=P2./R.*T2;,den3=P3./R.*T3; %density at indicated state
T4=T3-((g.*Hchim)./Cp);
den4=P4./R.*T4;
%now find the pressure at state 3
P3N=P4+(0.5.*( g.*Hchim.* den3+den4)./100000) +(mf./Agz).*(1./den4 -1/den3);
%assumed value and found value has a variation
%%%%%%%%%%%%%%%%%%%%%%%%%%%%%%%%%%%%%%%%%%%%%%%%%%%
% calculate every value using the new pressure P3N
T33=T2.*((P3N/P2).^((gama-1)./gama));%temprature at the chimney inlet
P4=P1.*(1-(xx).^(R./Cp));%the exit pressure at the chimney outlet
den33=P3N./R.*T33;
T44=T33-((g.*Hchim)./Cp);
den44=P4./R.*T4;
%the pressure difference
Ptot=g.*(den2-den44).*Hchim;
turbeff=0.9;%turbibne efficency
%VELOCITY AT THE CHIMNEY INLET
V2=sqrt(2.*g.*Hchim.*(T22-T1)./T22);%m/s
Pf=(0.0004.*Hchim.*den2.*(V2.^2))./Dchim;
mff=den1.*Achim.*V2;
Pt=Ptot-Pf;
%POWER OUTPUT
Pout5=0.90.*Pt.*V2.*Agz.*0.001;
%plot(T22,G)
plot(Hchim,Pout1,'k--o',Hchim,Pout2,'rd--',Hchim,Pout3,'y--',Hchim,Pout4,'kx-
','linewidth',2)
%plot(Hchim,Pout);
hold on
plot(Hchim,Pout5,'g','linewidth',3)
legend('Pout1','Pout2','Pout3','Pout4','Pout5')
xlabel('chimney height')
ylabel('power outpot(kW)')
grid on
```